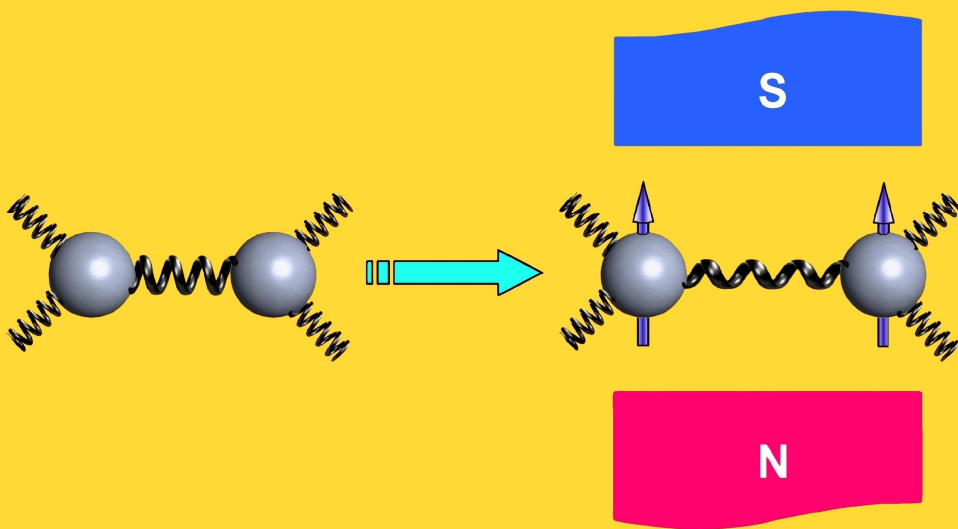


MOMENT FORMATION *and* GIANT MAGNETOCALORIC EFFECTS *in* HEXAGONAL Mn-Fe-P-Si COMPOUNDS



Nguyễn Hữu Dũng

Keywords:

Magnetocaloric effect, magnetic refrigeration, intermetallic compounds, moment formation, first-order, second-order, magnetic transition, structural transformation, entropy change, temperature change, Fe₂P-based compounds.

Cover:

An illustration of the competition between moment formation and chemical bonding. The 3*d* transition-metal atoms are non-magnetic due to strong *d-d* hybridization between them (left). A magnetic field can support the moment formation by enhancing electron localization via increasing the interatomic distance (right). However, this weakens the chemical bonding. The magnetic moments are therefore metastable. This behavior is similar to that happening for the 3*f* sites in Fe₂P-based hexagonal Mn-Fe-P-Si compounds presented in this thesis.

Moment formation and giant magnetocaloric effects in hexagonal Mn-Fe-P-Si compounds

PROEFSCHRIFT

ter verkrijging van de graad van doctor

aan de Technische Universiteit Delft;

op gezag van de Rector Magnificus prof. ir. K.C.A.M. Luyben;

voorzitter van het College voor Promoties

in het openbaar te verdedigen op maandag 03 december 2012 om 15:00 uur

door

NGUYỄN HỮU DŨNG

Master of Science in Materials Science, Hanoi University of Technology

geboren te Thai Binh, Vietnam

Dit proefschrift is goedgekeurd door de promotor:

Prof. dr. E. H. Brück

Copromotor: Dr. ir. N. H. van Dijk

Samenstelling promotiecommissie:

Rector Magnificus	voorzitter
Prof. dr. E. H. Brück	Technische Universiteit Delft, promotor
Dr. ir. N. H. van Dijk	Technische Universiteit Delft, copromotor
Prof. dr. T. T. M. Palstra	Rijksuniversiteit Groningen
Prof. dr. ir. S. van der Zwaag	Technische Universiteit Delft
Prof. dr. K. H. J. Buschow	Universiteit van Amsterdam
Dr. V. Basso	Istituto Nazionale di Ricerca Metrologica, Italy
Dr. K. G. Sandeman	Imperial College London, UK
Prof. dr. F. M. Mulder	Technische Universiteit Delft, reservelid

The work described in this thesis was part of the Industrial Partnership Program I18 of the Dutch Foundation for Fundamental Research on Matter (FOM) and carried out at the section Fundamental Aspects of Materials and Energy, Faculty of Applied Sciences, Delft University of Technology (TU Delft). The Industrial Partnership Program was co-financed by BASF Future Business GmbH.



ISBN/EAN: 978-94-6186-081-1

An electronic version of this thesis is available at: <http://repository.tudelft.nl>

Copyright © 2012 by Nguyễn Hữu Dũng

Printed in the Netherlands by Off Page

Dedicated to my grandmother and my parents

TABLE OF CONTENTS

Acknowledgments	xi
Chapter 1: Introduction	1
1.1. Magnetocaloric effect and magnetic refrigeration.....	1
1.2. Magnetocaloric materials	2
1.3. Active magnetic regenerator	3
1.4. Thesis outline	4
References	
Chapter 2: Theoretical aspects	9
2.1. Thermodynamics	9
2.2. Entropy change of materials with first-order and second-order transition	11
2.3. Contributions to magnetic entropy change	12
2.4. Adiabatic temperature change	12
2.5. The Bean-Rodbell model.....	14
2.6. Mixed magnetism	16
References	
Chapter 3: Experimental	21
3.1. Introduction	21
3.2. Ball-milling system.....	21
3.3. X-ray diffractometer	22
3.4. High-resolution powder neutron diffractometer	23
3.5. Electron probe microanalysis	23
3.6. SQUID magnetometer	23

3.7. Vibrating sample magnetometer	24
3.8. Differential scanning calorimeter	24
References	
Chapter 4: Optimization of hexagonal Mn-Fe-P-Si compounds	27
4.1. Introduction	27
4.2. Experimental details	30
4.3. $Mn_xFe_{2-x}P_{1-y}Si_y$ alloys	30
4.4. Off-stoichiometric $(Mn,Fe)_{2+z}P_{0.50}Si_{0.50}$ alloys	32
4.5. Optimized magnetocaloric effects	34
4.6. Conclusions	37
References	
Chapter 5: From first-order magneto-elastic to magneto-structural transition in $(Mn,Fe)_{1.95}P_{0.50}Si_{0.50}$ compounds	39
5.1. Introduction	39
5.2. Experimental details	40
5.3. First-order magneto-elastic and second-order isostructural transitions	40
5.4. First-order magneto-structural transitions	45
5.5. Phase diagram	45
5.6. Conclusions	47
References	
Chapter 6: High/low-moment phase transition in hexagonal Mn-Fe-P-Si compounds	51
6.1. Introduction	51
6.2. Experimental details	53
6.3. Magnetic structure of the Mn-rich compounds	53
6.4. Low-temperature ferromagnetic phase	58
6.5. High-temperature paramagnetic phase	61
6.6. High/low-moment phase transition	66
6.7. Conclusions	67
References	

Chapter 7: Effects of P:Si ratio on the magnetic and structural properties of hexagonal Mn-Fe-P-Si compounds	71
7.1. Introduction	71
7.2. Experimental details	72
7.3. Magnetic properties	72
7.4. Structural properties	75
7.5. Conclusions	77
References	
Chapter 8: Magneto-elastic coupling and magnetocaloric effect in hexagonal Mn-Fe-P-Si compounds	81
8.1. Introduction	81
8.2. Experimental details	82
8.3. Magneto-elastic coupling and hysteresis	82
8.4. Magneto-elastic coupling and magnetic entropy change	85
8.5. Critical magnetic field for field-induced transition	88
8.6. Role of <i>p</i> -electron element	90
8.7. Conclusions	92
References	
Summary	95
Samenvatting	98
List of publications	101
Curriculum vitae	103

ACKNOWLEDGMENTS

This thesis presents the most interesting results achieved during 4 years of my PhD in Delft. It could not have been completed without direct or indirect contributions from many people to whom I am indebted.

My foremost thank goes to Prof. Ekkes Brück, my promotor, for accepting me as his PhD student. His guidance, valuable suggestions, and appreciation have given me confidence and created great motivations for my studies. I am very grateful to Dr. Niels van Dijk, my copromotor, for his valuable discussions and supporting me in neutron diffraction measurements and data analysis. I would like to express my gratitude to Dr. Lian Zhang for his guidance and valuable discussions.

My gratitude is extended to Prof. K. H. Jürgen Buschow for his careful review and valuable comments on the draft thesis, and to other members of my doctoral examination committee for their time and suggestions.

I wish to extend my thanks to Anton J. E. Lefering, Michel P. Steenvoorde and Bert Zwart for their help in magnetic and structural measurements, and sample preparation, to Dr. Lie Zhao for help in high-temperature magnetic measurements, and to Dr. Jack Voncken for help with electron probe microanalysis. I acknowledge the help I received from Jouke Heringa in computer network-related issues and in the Dutch translation of the thesis summary.

I am thankful to Nicole Banga, Ilse van der Kraaij (FAME, TU Delft), and Annette Bor (FOM) for their kind help in administrative procedures. Thanks are further extended to all members of the section FAME for their company and kind support. Especially,

many thanks to Zhiqiang Ou for helping me to perform the initial experiments of my PhD study. Also, I would like to take the opportunity to thank the former members Dr. Nguyễn Thành Trung and Dr. Đinh T. Cẩm Thanh for sharing their ideas and experiences.

My special thanks go to Prof. Rob de Groot and Dr. Gilles de Wijs (Radboud University) for their collaboration in theoretical calculations, and to all those who contributed to our research at ANSTO, ILL and ISIS for their collaborative support in conducting high-resolution neutron diffraction measurements.

I gratefully acknowledge the financial support from the FOM foundation and the collaboration from BASF Future Business – the industrial partner of our research group.

I wish to express my sincere gratitude to the leaders and staff members of ITIMS for their constant support. Especially, I cannot fail to acknowledge the assistance of the late Prof. Nguyễn Phú Thùy who introduced me to the world of magnetism.

I am sincerely grateful to *chú* Tuyên and *cô* Thọ for their care and encouragement.

My gratitude is extended to all my Vietnamese friends for their support during my PhD time.

Finally, I owe special gratitude to my grandmother, my parents, my young brother and my “extended” family for their care, love, encouragement and constant support over the years.

Delft, 25 Oct 2012

Chapter 1

INTRODUCTION

1.1. Magnetocaloric effect and magnetic refrigeration

Limited resources and the wish for improved prosperity call for efficient use of energy. The UN Advisory Group on Energy and Climate Change recommends a target of 40 % improved efficiency by 2030 [1]. Materials research can contribute significantly to reach this target. Magnetic refrigeration offers potential to achieve a 50 % higher energy-efficiency compared to vapor-compression refrigeration [2]. This makes magnetic refrigeration a technology that attracts growing attention.

Magnetic refrigeration is based on the magnetocaloric effect, i.e., the temperature change of a magnetic material upon the application or removal of a magnetic field in adiabatic conditions. This is due to the entropy transfer between the spin system, the crystal lattice and the conduction electrons.

Apart from the adiabatic temperature change ΔT_{ad} for a magnetic field change as mentioned above, isothermal magnetic entropy change ΔS_{m} for a field change is also a quantity to evaluate the magnetocaloric effect. The term “*magnetic entropy change*” refers to *magnetic field*-induced entropy change. This is not limited to the entropy change of the spin system.

The sketch of an adiabatic demagnetization refrigeration cycle is shown in Figure 1.1. Actually, the basic operating principle of magnetic refrigeration is similar to that of vapor-compression refrigeration. However, the efficiency of magnetic refrigeration can

reach up to 60 %, compared with only 40 % in vapor-compression-refrigeration. Besides, solid magnetic refrigerants are employed instead of gases. Thus, magnetic refrigeration generates less noise, and does not use ozone depleting chemicals (CFCs), hazardous chemicals (NH_3) or greenhouse gases (HCFCs and HFCs). Magnetic refrigeration is therefore a revolutionary, efficient, environmentally friendly cooling technology [3-5].

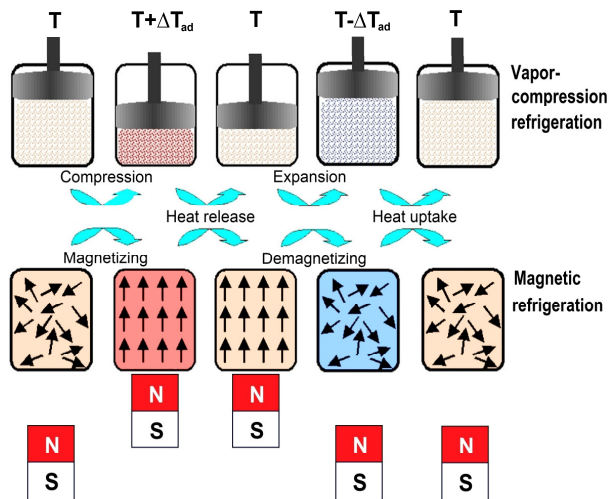


Figure 1.1. Schematic demonstration of magnetic refrigeration. The principle of magnetic refrigeration is similar to that of vapor-compression refrigeration. (After [5])

1.2. Magnetocaloric materials

Magnetocaloric materials play an important role in magnetic refrigeration. A large magnetocaloric effect, which is needed for high cooling power, can only be observed in the vicinity of the point of transition. Many efforts have been made to find magnetic refrigerants which display a large magnetocaloric effect in a proper working temperature span.

The magnetocaloric effect was discovered in pure iron in 1881 by Warburg [6]. Almost half a century later, magnetic refrigeration based on this effect was independently

proposed by Debye [7] and Giauque [8]. It was first demonstrated experimentally to achieve ultra-low temperature (below 1 K) in 1933 by Giauque and MacDougall [9]. Originally suggested refrigerants were paramagnetic salts.

In 1976, the first design of a magnetic refrigerator operating near room temperature was developed by Brown [10]. Then Gd was used as refrigerant.

Searching for magnetocaloric materials for room-temperature magnetic refrigeration has only attracted much attention since Pecharsky and Gschneidner [11] discovered a giant magnetocaloric effect in $\text{Gd}_5(\text{Si,Ge})_4$ with a first-order transition below room temperature in 1997. A number of other magnetocaloric materials with a first-order magnetic phase transition have been intensively explored, such as $\text{MnAs}_x\text{Sb}_{1-x}$ and MnAs-based alloys [12], $\text{La}(\text{Fe}_{1-x}\text{Si}_x)_{13}$ and their hydrides [13,14], $\text{MnFeP}_{1-x}\text{As}_x$ and Fe_2P -based alloys [15-18], $\text{Ni}_{0.50}\text{Mn}_{0.50-x}\text{Sn}_x$ and NiMn-based alloys [19-21], and MnCoGeB_x [22]. In these materials, the first-order phase transition enhances the magnetocaloric effect in the vicinity of the magnetic phase transition. The maximum isothermal entropy change is therefore often significantly greater than that of the benchmark material Gd that presents a second-order magnetic phase transition. However, many other factors still need to be investigated, such as hysteresis, thermal and electrical conductivity, mechanical properties, and corrosion resistance. The hysteresis which is frequently associated with the first-order transition is one of the big drawbacks to magnetic refrigeration applications.

1.3. Active magnetic regenerator

Up to now, over 25 prototypes have been built with different cooling power and working temperature span around room temperature [23,24]. Most of them use Gd as refrigerant which only operates in a limited temperature span. By combining giant magnetocaloric materials with different operating temperatures in series, a higher efficiency and a greater temperature span than that of Gd can be obtained [25]. This concept was introduced in 1982 by Barclay and Steyert [26] and then known as active magnetic regenerator (AMR). Instead of using a separate material as a regenerator to recuperate the heat from the magnetic material, the AMR concept makes use of the

refrigerant itself as the regenerator. A temperature gradient is then established throughout the AMR and a fluid is used to transfer heat from the cold end to the hot end (see Figure 1.2). For optimal performance, the materials used in such a composite regenerator need to have very similar magnetocaloric properties, to achieve a constant entropy change as function of temperature [27]. Some room-temperature AMR refrigerator prototypes have been demonstrated and have generated relatively high cooling powers [2,27-31].

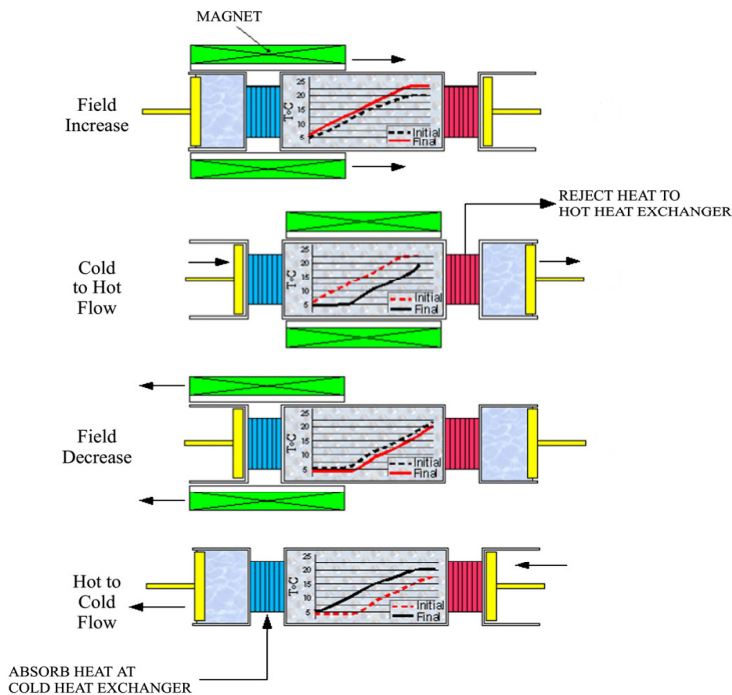


Figure 1.2. Active magnetic regenerator cycle. (After [5])

1.4. Thesis outline

Giant magnetocaloric materials which are globally-abundant, non-toxic and can be industrially-mass-produced via a simple fabrication method are particularly attractive for magnetic refrigeration applications. Fe₂P-based Mn-Fe-P-Si alloys can meet such requirements. The work presented in this thesis is a study of the magnetocaloric effect and related physical properties in the Mn-Fe-P-Si compounds.

Some theoretical aspects of the magnetocaloric effect in general, and the origin of the first-order magneto-elastic transition which enhances the magnetocaloric effect in hexagonal Mn-Fe-P-Si compounds in particular are given in Chapter 2.

In Chapter 3, a short review is presented of the experimental techniques and set-ups that have been employed for the sample preparation and the characterization of the physical properties of the Mn-Fe-P-Si compounds.

Our efforts to optimize the magnetocaloric effect for refrigeration applications are presented in Chapter 4. We show that a giant magnetocaloric effect and a small thermal hysteresis in Mn-Fe-P-Si compounds of hexagonal Fe_2P -type structure can be achieved simultaneously. Furthermore, the working temperature can be controlled over a large interval around room temperature by varying the Mn:Fe and P:Si ratios.

In Chapter 5, we report on various types of transition found in $(\text{Mn,Fe})_{1.95}\text{P}_{0.50}\text{Si}_{0.50}$ when changing the Mn:Fe ratio. Interestingly, we observe a previously unknown first-order magneto-structural transition and a modified first-order magneto-elastic transition favorable for real refrigeration applications.

Using high resolution neutron diffraction, x-ray diffraction and high-temperature magnetic-susceptibility measurements, and based on theoretical calculations, a first-order magneto-elastic transition from high-moment to low-moment in the Mn-Fe-P-Si compounds is presented in Chapter 6. This observation supports our proposal that the competition between moment formation and chemical bonding is at the core of giant magnetocaloric effect displayed in the class of hexagonal Fe_2P -based materials with first-order magneto-elastic transition. The effect of the replacement of Fe by Mn on the magnetic moments is also discussed.

Chapter 7 is devoted to the effects of P:Si ratio on the magnetic and structural properties of the Mn-Fe-P-Si compounds.

In chapter 8, we present magneto-elastic coupling in the Mn-Fe-P-Si compounds. Interestingly, hysteresis and magnetic entropy change are found to be correlated with discontinuous changes of the lattice parameters at the transition temperature. Small thermal hysteresis can be obtained while maintaining the giant magnetocaloric effect.

A preliminary comparison of the magneto-elastic coupling and magnetocaloric effect for Mn-Fe-P-As/Ge/Si is also given.

References

- [1] UN Secretary-General's remarks at Fourth World Future Energy Summit - Abu Dhabi, United Arab Emirates, 17 January 2011, <http://www.un.org/apps/sg/sgstats.asp?nid=5036>
- [2] C. Zimm, A. Jastrab, A. Sternberg, V. Pecharsky, K. Gschneidner, M. Osborne, and I. Anderson, *Adv. Cryog. Eng.* **43**, 1759 (1998).
- [3] E. Brück, *J. Phys. D: Appl. Phys.* **38**, R381 (2005).
- [4] K. A. Gschneidner and V. K. Pecharsky, *J. Rare Earth.* **24**, 641 (2006)
- [5] S. L. Russek and C. B. Zimm, *Int. J. Refrig.* **29**, 1366 (2006).
- [6] E. Warburg, *Ann. Phys. (Leipzig)* **13**, 141 (1881).
- [7] P. Debye, *Ann. Physik* **81**, 1154 (1926).
- [8] W. F. Giaque, *J. Am. Chem. Soc.* **49**, 1864 (1927).
- [9] W. F. Giaque and D. P. MacDougall, *Phys. Rev.* **43**, 768 (1933).
- [10] G. V. Brown, *J. Appl. Phys.* **47**, 3673 (1976).
- [11] V. K. Pecharsky and K. A. Gschneidner, *Phys. Rev. Lett.* **78**, 4494 (1997).
- [12] H. Wada and Y. Tanabe, *Appl. Phys. Lett.* **79**, 3302 (2001).
- [13] F. X. Hu, B. G. Shen, J. R. Sun, Z. H. Cheng, G. H. Rao, and X. X. Zhang, *Appl. Phys. Lett.* **78**, 3675 (2001).
- [14] A. Fujita, S. Fujieda, Y. Hasegawa, and K. Fukamichi, *Phys. Rev. B* **67**, 104416 (2003).
- [15] O. Tegus, E. Brück, K. H. J. Buschow, and F. R. de Boer, *Nature* **415**, 150 (2002).
- [16] N. T. Trung, Z. Q. Ou, T. J. Gortenmulder, O. Tegus, K. H. J. Buschow, and E. Brück, *Appl. Phys. Lett.* **94**, 102513 (2009).
- [17] N. H. Dung, Z. Q. Ou, L. Caron, L. Zhang, D. T. C. Thanh, G. A. de Wijs, R. A. de Groot, K. H. J. Buschow, and E. Brück, *Adv. Energy Mater.* **1**, 1215 (2011).
- [18] N. H. Dung, L. Zhang, Z. Q. Ou, and E. Brück, *Appl. Phys. Lett.* **99**, 092511 (2011).
- [19] T. Krenke, E. Duman, M. Acet, E. F. Wassermann, X. Moya, L. Manosa, and A. Planes, *Nat. Mater.* **4**, 450 (2005).
- [20] E. K. Liu, W. H. Wang, L. Feng, W. Zhu, G. J. Li, J. L. Chen, H. W. Zhang, G. H. Wu, C. B. Jiang, H. B. Xu, and F. de Boer, *Nat. Commun.* **3**, 873 (2012).
- [21] J. Liu, T. Gottschall, K. P. Skokov, J. D. Moore, and O. Gutfleisch, *Nat. Mater.* **11**, 620 (2012).

-
- [22] N. T. Trung, L. Zhang, L. Caron, K. H. J. Buschow and E. Brück, *Appl. Phys. Lett.* **96**, 172504 (2010).
- [23] K. A. Gschneidner, V. K. Pecharsky, and A. O. Tsokol, *Rep. Prog. Phys.* **68**, 1479 (2005).
- [24] J. Tušek, S. Zupan, A. Šarlah, I. Prebil, A. Poredoš, *Int. J. Refrig.* **33**, 294 (2010).
- [25] S. Russek, J. Auringer, A. Boeder, J. Chell, S. Jacobs, and C. Zimm, *Proc. 4th Conference on Magnetic Refrigeration at Room Temperature, Baotou, China* (2010) ISBN 978-2-913149-80-9.
- [26] J. A. Barclay and W. A. Steyert, U.S. Patent, No. 4332135 (1982).
- [27] A. Rowe and A. Tura, *Int. J. Refrig.* **29**, 1286 (2006).
- [28] B. F. Yu, Q. Gao, B. Zhang, X. Z. Meng, and Z. Chen, *Int. J. Refrig.* **26**, 622 (2003).
- [29] M. -A. Richard, A. M. Rowe, and R. Chahine, *J. Appl. Phys.* **95**, 2146 (2004).
- [30] A. Rowe and A. Tura, *J. Magn. Magn. Mater.* **320**, 1357 (2008).
- [31] C. Zimm, A. Boeder, J. Chell, A. Sternberg, A. Fujita, S. Fujieda, and K. Fukamichi, *Int. J. Refrig.* **29**, 1302 (2006).

Chapter 2

THEORETICAL ASPECTS

2.1. Thermodynamics

In thermodynamics, one of the most important thermodynamic potentials is the Gibbs free energy or free enthalpy. The Gibbs free energy of a magnetic material with the magnetization M in an external magnetic field B is defined as:

$$G = U - TS + pV - MB, \quad (2.1)$$

where U represents the internal energy, T the absolute temperature, S the entropy, p the pressure and V the volume. Using the first law of thermodynamics:

$$dU = TdS - pdV + BdM, \quad (2.2)$$

the differential of the Gibbs free energy can be expressed by:

$$dG = -SdT + Vdp - MdB \quad (2.3)$$

Hence, we obtain:

$$S(T, B, p) = -\left(\frac{\partial G}{\partial T}\right)_{B,p} \quad (2.4a)$$

$$M(T, B, p) = -\left(\frac{\partial G}{\partial B}\right)_{T,p} \quad (2.4b)$$

$$V(T, B, p) = \left(\frac{\partial G}{\partial p}\right)_{T,B} \quad (2.4c)$$

The differential of the entropy is given by:

$$dS = \left(\frac{\partial S}{\partial T} \right)_{B,p} dT + \left(\frac{\partial S}{\partial B} \right)_{T,p} dB + \left(\frac{\partial S}{\partial p} \right)_{T,B} dp \quad (2.5)$$

For an isobaric-isothermal process ($dp = 0$, $dT = 0$), Equation (2.5) becomes:

$$dS = \left(\frac{\partial S}{\partial B} \right)_{T,p} dB \quad (2.6)$$

The entropy change ΔS_m for a magnetic field change from B_i to B_f ($\Delta B = B_f - B_i$) can be obtained by using numerical integration of Equation (2.6):

$$\Delta S_m(T, \Delta B) = \int_{B_i}^{B_f} \left(\frac{\partial S}{\partial B} \right)_{T,p} dB \quad (2.7)$$

Furthermore, using the Maxwell relation:

$$\left(\frac{\partial S}{\partial B} \right)_{T,p} = \left(\frac{\partial M}{\partial T} \right)_{B,p}, \quad (2.8)$$

Equation (2.7) can be rewritten as:

$$\Delta S_m(T, \Delta B) = \int_{B_i}^{B_f} \left(\frac{\partial M}{\partial T} \right)_{B,p} dB \quad (2.9)$$

On the other hand, from the second law of thermodynamics, the specific heat C_p is defined by:

$$C_p(T, B) = T \left(\frac{\partial S}{\partial T} \right)_{B,p} \quad (2.10)$$

Combining Equations (2.5) and (2.10), the entropy in magnetic field B and in isobaric condition ($dp = 0$) can be expressed by:

$$S(T, B) = \int_0^T \frac{C_p(T', B)}{T'} dT' + S_0 \quad (2.11)$$

Thus, we obtain:

$$\Delta S_m(T, \Delta B) = \int_0^T \frac{C_p(T', B_f) - C_p(T', B_i)}{T'} dT', \quad (2.12)$$

The entropy change for a magnetic field change can be calculated by using the Maxwell relation [Equation (2.9)], or from the specific heat [Equation (2.12)]. Experimentally, we need to determine the magnetization as a function of temperature and magnetic field, or the specific heat as a function of temperature in initial (B_i) and final (B_f) magnetic fields.

2.2. Entropy change of materials with first-order and second-order transition

From Equation (2.9), it can be seen that the magnitude of ΔS_m is only large near magnetic phase transitions. In general, the phase transitions are categorized into first-order and second-order phase transitions, in which the first and second derivatives of thermodynamic potentials with respect to thermodynamic variables are discontinuous, respectively. Up to now, most magnetic materials exhibit a second-order magnetic phase transition, in which the first derivative of thermodynamic potentials is continuous. Note that the volume, entropy and magnetization are defined as the first derivatives of the Gibbs free energy [see Equation (2.4)]. Hence, there is no jump in magnetization at the point of the second-order transition.

From Equations (2.10) and (2.4a), the specific heat can be rewritten as:

$$C_p(T, B) = -T \left(\frac{\partial^2 G}{\partial T^2} \right)_{B,p} \quad (2.13)$$

Apparently, the specific heat changes discontinuously at the point of the second-order transition. According to the Dulong-Petit law, the specific heat of a mole of a solid above the Debye temperature is approximately $3R$ where R is the molar gas constant.

Concerning Equations (2.9) and (2.12), the continuous change in magnetization and the finite value of the specific heat can give rise to a low ΔS_m . Thus, magnetic materials with a second-order phase transition often display a weak magnetocaloric effect.

If a magnetic material undergoes a first-order transition, the magnetization, lattice parameters and entropy change discontinuously and the specific heat should be infinite at the point of transition. Then the magnetocaloric effect is expected to be much larger. Thus, magnetic materials with a first-order transition are more promising for magnetic refrigeration. Details of the magnetocaloric effect at the first-order and second-order transition have been quantitatively discussed in Ref. [1].

2.3. Contributions to magnetic entropy change

In general, first-order magnetic transitions are often accompanied by structural transitions, which enforce the magnetization change suddenly and, consequently, enhance the magnetocaloric effect.

The entropy of a magnetic material includes contributions from spin (S_{spin}), lattice (S_{lat}) and conduction electrons (S_{el}). Thus, the isothermal field-induced total entropy change can be expressed by:

$$\Delta S_{\text{m}} = \Delta S_{\text{spin}} + \Delta S_{\text{lat}} + \Delta S_{\text{el}} \quad (2.14)$$

It is not straightforward to calculate these contributions. Magnetizing a material in isothermal conditions often increases spin order, and consequently, causes a decrease in the spin contribution to the total entropy. Thus, $\Delta S_{\text{spin}} < 0$. Theoretically, a giant magnetocaloric effect can be obtained if the above contributions have the same sign. However, they may partially cancel each other if they have opposite signs.

2.4. Adiabatic temperature change

By combining Equations (2.5), (2.8) and (2.10), the infinitesimal adiabatic temperature change in adiabatic-isobaric conditions ($dS = 0$, $dp = 0$) is expressed by:

$$dT = -\frac{T}{C_p(T, B)} \left(\frac{\partial M}{\partial T} \right)_{B, p} dB \quad (2.15)$$

Integration of Equation (2.15) yields the adiabatic temperature change for a field change from B_i to B_f :

$$\Delta T_{\text{ad}}(T, \Delta B) = - \int_{B_i}^{B_f} \frac{T}{C_p(T, B)} \left(\frac{\partial M}{\partial T} \right)_{B, p} dB \quad (2.16)$$

The determination of ΔT_{ad} by using Equation (2.16) is very difficult because both the magnetization and specific heat are unknown functions of temperature and magnetic field in the vicinity of the transition. If C_p weakly depends on temperature, the variation of $T/C_p(T, B)$ is small compared to the variation of the magnetization with temperature. Then, Equation (2.16) can be simplified:

$$\Delta T_{\text{ad}}(T, \Delta B) = - \frac{T}{C_p(T, B)} \Delta S_m(T, \Delta B) \quad (2.17)$$

Hence, ΔT_{ad} can be obtained from the specific heat, or combined magnetization and specific heat data. Experimentally, apart from direct measurements, ΔT_{ad} is often determined from the entropy curves (see Figure 2.1). The total entropy as a function of temperature in a constant magnetic field can be derived from the specific heat by using Equation (2.11).

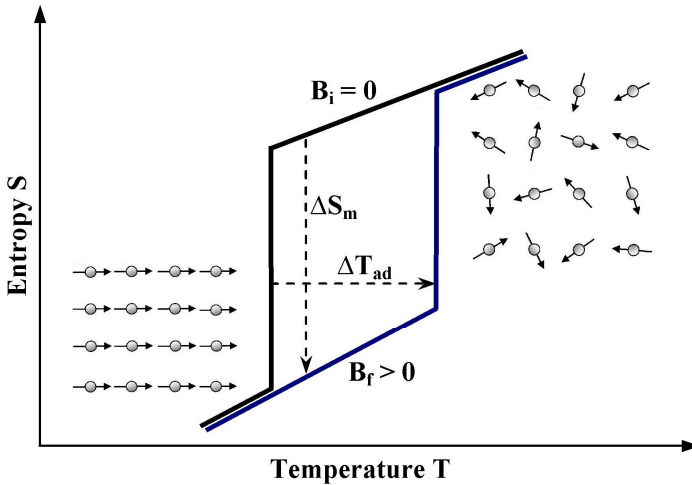


Figure 2.1. Sketch of the total entropy in zero field ($B_i = 0$) and in magnetic field $B_f > 0$ near a first-order phase transition from low-temperature ferromagnetic to high-temperature paramagnetic state.

2.5. The Bean-Rodbell model

Bean and Rodbell proposed a phenomenological model to describe the first-order phase transition observed in MnAs [2]. It is based on the molecular mean field approximation. The framework of the model was extended to explain the first-order transition for $\text{MnFeP}_{1-x}\text{As}_x$ [3,4] and $\text{Gd}_5(\text{Ge}_{1-x}\text{Si}_x)_4$ [5]. The central assumption of the model is that the exchange interaction parameter is a function of the lattice spacing. The dependence of the critical temperature on the volume change is expressed by:

$$T_C = T_0(1 + \beta\omega), \quad (2.18)$$

where $\omega = (V - V_0)/V_0$ represents the cell deformation, V the volume, V_0 the equilibrium volume obtained in the absence of magnetic interaction, T_0 the Curie temperature in the absence of deformation. The parameter β represents the slope of the dependence of the Curie temperature (T_C) on the cell deformation.

In the molecular field approximation, the Gibbs free energy for a ferromagnetic system with contributions from the exchange interaction, the Zeeman energy, the elastic energy is given by:

$$G = \frac{3}{2} \frac{J}{J+1} N k_B T_C \sigma^2 - B g \mu_B J N \sigma + \frac{1}{2K} \omega^2 + p\omega - TS \quad (2.19)$$

where J is the total angular momentum of the ion, N the number of magnetic ions per unit volume, k_B the Boltzmann's constant, μ_B the Bohr magneton, $\sigma = M / g\mu_B J N$ the normalized magnetization, g the Landé factor, B the external magnetic field, K the compressibility and S the entropy. Minimizing G with respect to the deformation, we obtain:

$$\omega = -\frac{3}{2} \frac{J^2}{J(J+1)} N k_B K T_0 \beta \sigma^2 - pK \quad (2.20)$$

By substituting (2.20) into (2.19) and minimizing G with respect to σ , the magnetic state equation can be written as:

$$\sigma = B_J(Y) = \frac{2J+1}{2J} \coth\left(\frac{2J+1}{2J} Y\right) - \frac{1}{2J} \coth\left(\frac{1}{2J} Y\right), \quad (2.21)$$

where $B_J(Y)$ is the Brillouin function and

$$Y = \frac{1}{T} \left\{ 3T_0 \frac{J}{J+1} \sigma + \frac{g\mu_B J}{k_B} B + \frac{9(2J+1)^4 - 1}{5 [2(J+1)]^4} T_0 \eta \sigma^3 - 3 \frac{J\beta p K}{J+1} T_0 \sigma \right\}.$$

Note that the parameter η controlling the order of magnetic phase transition is given by:

$$\eta = \frac{5 [4J(J+1)]^2}{2 (2J+1)^4 - 1} N k_B K T_0 \beta^2 \quad (2.22)$$

If $\eta > 1$, the magnetic system undergoes a first-order phase transition. Otherwise, a second-order magnetic phase transition occurs if $\eta < 1$ [5]. Figure 2.2 shows the relative magnetization of $\text{MnFeP}_{0.45}\text{As}_{0.55}$ as a function of temperature which is calculated for different values of the parameter η [6]. The value $\eta = 1$ separates the first-order and second-order transition. When $\eta > 1$, the transition is of first-order and there is a discontinuous change in the magnetization as indicated by dashed vertical lines.

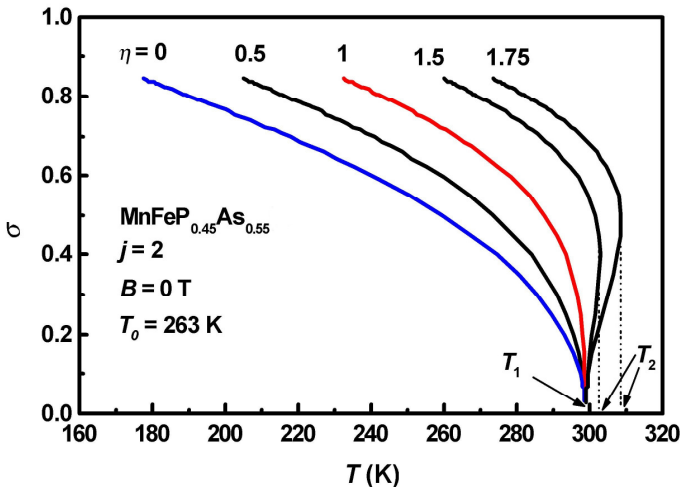


Figure 2.2. Temperature dependence of the relative magnetization of $\text{MnFeP}_{0.45}\text{As}_{0.55}$ calculated in zero field with different values of parameter η . (After [6])

2.6. Mixed magnetism

The Bean-Rodbell model gives a good phenomenological description of magnetic materials with first-order transition, however it fails to explain the origin of the first-order transition. For this a more microscopic approach is needed. With the aid of modern supercomputers one may be able to elucidate the origin of the observed magnetocaloric effect. Recently, electronic structure calculations for hexagonal Fe₂P-based MnFe(P,Si) (space group $P\bar{6}2m$) were performed on the ferromagnetic ground-state, while the behavior at the Curie temperature was modeled by a supercell obtained by doubling the unit cell (allowing for antiferromagnetic configurations) [7].

These first-principle theoretical calculations have revealed the coexistence of strong and weak magnetism in alternate atomic layers. These atomic layers are formed by the preferential occupation of Mn and Fe on the $3g$ and $3f$ sites, respectively. The calculations show that layers occupied by manganese are strongly magnetic; implying that the magnetic order only is lost at the Curie temperature. The size of the Mn moment is reduced from $2.8 \mu_B$ in the ferromagnetic phase to $2.6 \mu_B$ in the paramagnetic phase. By contrast, the iron-layers show weak itinerant magnetism: here the Fe moment in the ferromagnetic phase is $1.54 \mu_B$, while in the paramagnetic phase it vanishes ($\sim 0.003 \mu_B$).

This implies that the electron density around the Fe sites changes drastically at the phase transition. This change is especially significant within the Fe layer as illustrated in Figure 2.3. In this figure we show the difference in electron density between the ferromagnetic and the paramagnetic state. The dominant changes occur close to the Fe sites while near the P/Si sites the electron density is hardly affected. In the ferromagnetic state high electron density forms a dumbbell pointing into the empty space between adjacent P/Si atoms, while in the paramagnetic state high electron density forms a clover four pointing towards the nearest neighbors in the layer. This redistribution of electron density means that non-bonding electron density at the Fe site below T_C changes into a distribution which is hybridized with the nearest neighbors

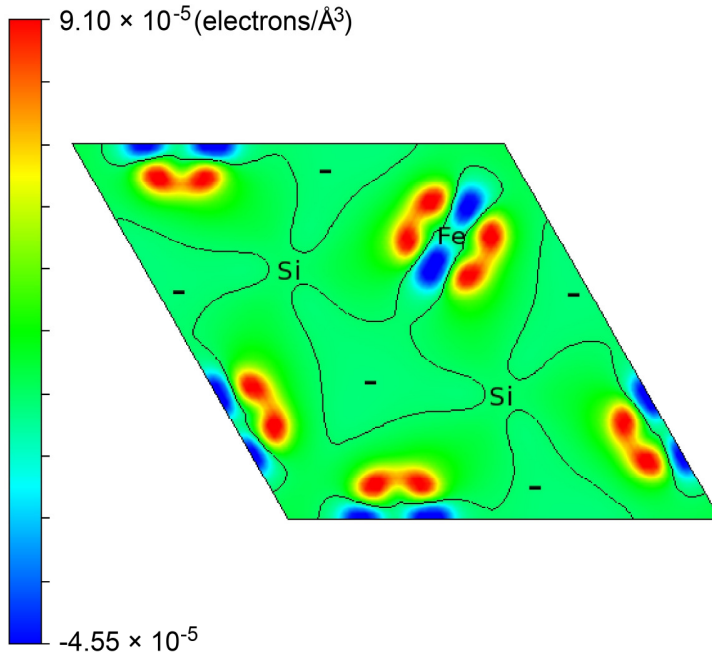


Figure 2.3. Difference between the electron densities calculated for situations above and below the Curie temperature in the iron-silicon/phosphorous plane [ferromagnetic density (-) subtracted from the paramagnetic one]. This results locally in negative electron densities where the highest ferromagnetic density was. The dark lines indicate no change in electron densities. (After [7])

above T_C . This change in hybridization causes the distinct change in c/a ratio observed experimentally in the magneto-elastic transition at T_C .

The loss of moments on the iron site is also clear from the partial density of states as function of energy shown in Figure 2.4. It shows identical curves for the two spin directions for iron above the Curie temperature, in sharp contrast with manganese that maintains its moment.

Such a combination of strong and weak magnetism is directly related to the giant magnetocaloric effect, because in solids the existence of magnetic moments competes with chemical bonding. This is best illustrated in case of a half-filled d -shell: the non-magnetic case allows a maximum in chemical bonding (like all half-filled shells), but

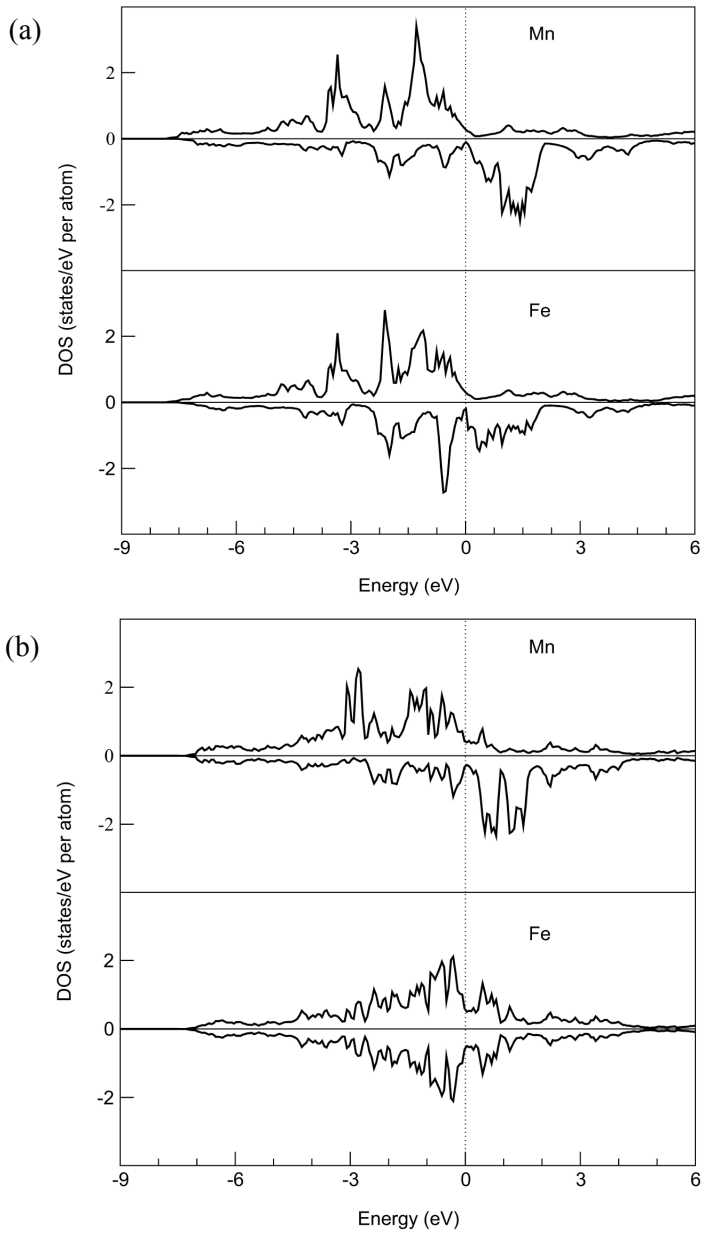


Figure 2.4. Partial local densities of states for the magnetic atoms in (a) the ferromagnetic state and (b) the paramagnetic state representing the state above the Curie point. Note the identical densities of state for the iron above the Curie temperature. (After [7])

the high-spin state does not show bonding, since the majority and minority subbands are completely filled and empty, respectively. The loss of the orientation of the moments at the Curie temperature does not change this situation. The vanishing of the moments is needed to enable the d electrons to participate in chemical bonding. The loss of the magnetic moments of iron enables the strong coupling to the lattice above the Curie temperature resulting in the discontinuity of the c/a ratio leading to the first-order phase transition. On the other hand, the strong magnetism of the manganese layers ensures a Curie temperature near room temperature. Combining weak and strong magnetism in a single material opens the possibility to effectively couple spin, lattice and conduction-electron degrees of freedom. Exploring the conditions for the occurrence of this novel phenomenon shall give us a handle to design new magnetocaloric materials.

References

- [1] A. M. Tishin and Y. I. Spichkin, *The magnetocaloric effect and its applications* (Institute of Physics Publishing, Bristol, 2003).
- [2] C. P. Bean and D. S. Rodbell, *Phys. Rev.* **126**, 104 (1962).
- [3] R. Zach, M. Guillot and J. Tobola, *J. Appl. Phys.* **83**, 7237 (1998).
- [4] O. Tegus, G. X. Lin, W. Dagula, B. Fuquan, L. Zhang, E. Brück, F. R. de Boer and K. H. J. Buschow, *J. Magn. Magn. Mater.* **290-291**, 658 (2005).
- [5] P. J. von Ranke, N. A. de Oliveira and S. Gama, *J. Magn. Magn. Mater.* **277**, 78 (2004).
- [6] O. Tegus, *Novel materials for magnetic refrigeration*, University of Amsterdam (2003), PhD thesis, Chapter 5.
- [7] N. H. Dung, Z. Q. Ou, L. Caron, L. Zhang, D. T. C. Thanh, G. A. de Wijs, R. A. de Groot, K. H. J. Buschow, and E. Brück, *Adv. Energy Mater.* **1**, 1215 (2011).

Chapter 3

EXPERIMENTAL

3.1. Introduction

The materials presented in this thesis were prepared at the section Fundamental Aspects of Materials and Energy (FAME), Faculty of Applied Sciences, Delft University of Technology (TU Delft). Most experimental measurements were also conducted at FAME, such as x-ray diffraction (XRD), magnetization measurements using Superconducting Quantum Interference Device (SQUID) magnetometer, specific heat measurements. Some other measurements were carried out outside FAME. In this chapter, we briefly introduce these measurements and the sample preparation.

3.2. Ball-milling system

Ball-milling technique is used extensively not only for grinding but also for cold welding with the purpose of producing alloys from powders. Compared with common mills, planetary ball-mills are smaller and mainly used in laboratories for grinding sample material down to very small sizes.

Mn-Fe-P-Si compounds were prepared by using a planetary mill PULVERISETTE 5 *classic line* with 4 grinding bowl fasteners. Each grinding bowl (80 ml volume) contains 15 grinding balls (10 mm diameter) and 10 grams of the starting materials with appropriate proportions including binary Fe₂P and red-P powder, Mn and Si chips. Both the bowl and ball are made of tempered steel. Figure 3.1 shows the x-ray diffraction patterns for as-milled powder with different milling times. The rotation

speed was fixed at 360 rpm. It can be seen that the diffraction peaks become lower and broader with increasing milling time. The solid-state reaction occurs after milling for over 40 hours.

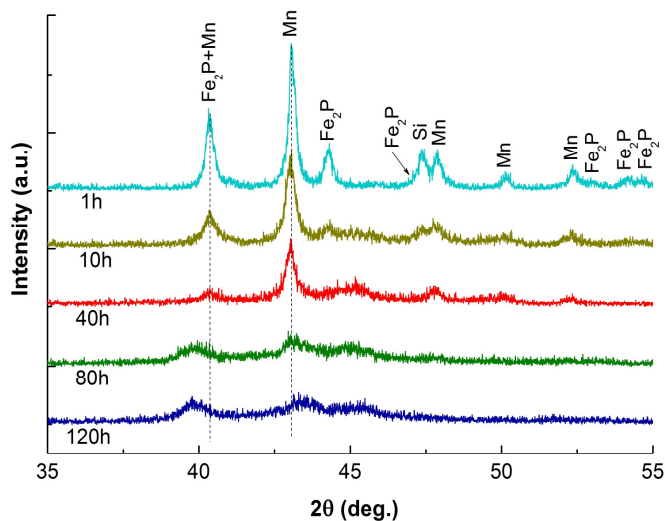


Figure 3.1. X-ray diffraction patterns at room temperature for as-milled powder with different milling times.

For the samples presented in this thesis, the starting materials were ball-milled for 10 hours with a constant rotation speed of 400 rpm. X-ray diffraction measurement for as-milled powder indicated that the solid-state reaction did not occur in the ball-milling process. The fine powder was pressed into small tablets and sealed in quartz ampoules in an Ar atmosphere of 200 mbar. Then, the samples were sintered at 1373 K for 2 hours and annealed at 1123 K for 20 hours before being oven cooled to room temperature.

3.3. X-ray diffractometer

X-ray diffraction patterns were collected using a PANalytical X-pert Pro diffractometer with $\text{Cu K}\alpha$ radiation, a secondary-beam flat-crystal monochromator and a multichannel X'celerator detector. For temperature-dependent x-ray diffraction

measurements, the sample powder was put in an Anton Paar TTK450 low-temperature chamber. The temperature can be varied from 80 to 720 K by using a liquid nitrogen controller and a heater. A thermocouple is used to measure the temperature inside the sample holder. To improve heat transfer between the sample holder and the sample powder, the sample powder was measured in nitrogen or argon gases, or mixed with vacuum grease and measured in vacuum. The characteristic diffraction peaks of the vacuum grease only occur below 240 K and below 30 degrees of 2θ . The x-ray diffraction patterns were analyzed using the Fullprof program [1].

3.4. High-resolution powder neutron diffractometer

Neutron diffraction data were collected at the Bragg Institute of the Australian Nuclear Science and Technology Organization (ANSTO) on the ECHIDNA high-resolution powder diffractometer [2] with an incident wavelength of 1.622 Å and at the Institut Laue-Langevin (ILL) on the D2B high-resolution powder diffractometer [3] with an incident wavelength of 1.595 Å. The sample powder was contained in a vanadium can which is mounted in a cryostat. The measurements were carried out at fixed temperatures from 5 K to 400 K in zero field. The Rietveld refinement was carried out using the FullProf program [4].

3.5. Electron probe microanalysis

The phase homogeneity and the stoichiometry of the samples were investigated with electron probe microanalysis (EPMA). The EPMA measurements were carried out using a JEOL 8800-JXA Superprobe equipped with Wavelength Dispersive Spectrometers (WDS) at the Department of Geoscience and Engineering, TU Delft. Thin slices of the materials were polished using diamond paste to make the surface smooth before they were used for the measurement.

3.6. SQUID magnetometer

Magnetic measurements were carried out using a Quantum Design SQUID MPMS-XL magnetometer. A proper amount of the sample is inserted in a gelatin capsule and

mounted in a plastic straw with a diamagnetic contribution of the order of 10^{-5} emu in 1 T. The sensitivity of the equipment is as high as 10^{-8} emu. Temperatures can be set from 1.7 to 400 K, and a magnetic field up to 5 T is generated by a superconducting magnet surrounding the sample space.

In this thesis, isofield magnetization measurements (M - T curves) were conducted with a sweep rate of 1 K/min upon cooling and heating. The magnetic entropy change (ΔS_m) for a field change is calculated from magnetic isotherms (M - B curves) measured at different temperatures in increasing field from $B_i = 0$ to B_f by using the following formula:

$$\Delta S_m(T, \Delta B) = \sum_j \frac{M(T + \Delta T / 2, B_j) - M(T - \Delta T / 2, B_j)}{\Delta T} \Delta B_j, \quad (3.1)$$

where $M(T \pm \Delta T / 2, B_j)$ is the magnetization in a magnetic field B_j at the temperature $T \pm \Delta T / 2$ and ΔB_j is the step of the field increase. This formula is derived approximately from Equation (2.9) in Chapter 2 for numerical evaluation. Each M - B curve was measured after the sample was zero-field cooled from the paramagnetic state at high temperature in order to remove the history effect [5].

3.7. Vibrating sample magnetometer

High-temperature magnetic measurements were carried out using a vibrating sample magnetometer (VSM) (model LakeShore 7307) equipped with a high-temperature oven (model 73034) at the Department of Materials Science and Engineering, TU Delft. The sensitivity of the VSM is 5×10^{-6} emu. The magnetization versus temperature data were collected in a low magnetic field upon heating with a sweep rate of 5 K/min.

3.8. Differential scanning calorimeter

The differential scanning calorimetry (DSC) measurements were carried out using a TA-Q2000 DSC instrument equipped with a liquid nitrogen cooling system. Employing the so-called Tzero™ DSC technology, this equipment allows to measure the heat capacity directly with a high precision. For a measurement, the temperature

range can vary from 90 K up to 820 K with different temperature sweep rates. Our measurements were conducted with a sweep rate of 10 K/min.

References

- [1] See <http://www.ill.eu/sites/fullprof/index.html>
- [2] K. D. Liss, B. Hunter, M. Hagen, T. Noakes, and S. Kennedy, *Physica B* **385-386**, 1010 (2006).
- [3] A.W. Hewat, *Mater. Sci. Forum* **9**, 69 (1986).
- [4] J. Rodriguez-Carvajal, *Physica B* **192**, 55 (1993).
- [5] L. Caron, Z. Q. Ou, T. T. Nguyen, D. T. Cam Thanh, O. Tegus, and E. Brück, *J. Magn. Magn. Mater.* **321**, 3559 (2009).

Chapter 4

OPTIMIZATION OF HEXAGONAL Mn-Fe-P-Si COMPOUNDS

4.1. Introduction

Magnetocaloric materials are the key to eco-friendly magnetic refrigeration technology [1-3]. Until recently, research on magnetocaloric materials was concentrated on rare-earth-containing alloys. This is because rare-earth-based compounds exhibit large moments compared with transition-metal-based intermetallic compounds and the magnetocaloric effect scales with the size of magnetic moment. However, a serious drawback of these materials for room-temperature refrigeration applications is the ever increasing high price and the limited availability of rare-earth-based magnetic material. Mn-containing compounds should be a good alternative because Mn is a transition metal of high abundance and may display a magnetic moment as large as $5 \mu_B$.

Amongst magnetic materials exhibiting a giant magnetocaloric effect near room temperature [1-6], hexagonal Fe_2P -based materials have been emerging as promising magnetic refrigerants since Tegus *et al.* [7] discovered a giant magnetocaloric effect in $\text{MnFe}(\text{P},\text{As})$ alloys with limited thermal hysteresis ΔT_{hys} of about 2 K and an operating temperature tunable from 220 K to 340 K [8]. These compounds are obtained from Fe_2P by partially replacing Fe and P with Mn and As, respectively. Although solid $\text{MnFe}(\text{P},\text{As})$ compounds are insoluble and non-toxic, the toxic ingredient As hampers the application of this material in household appliances. The toxicity of As also raises the cost of the materials due to the need of coating or encapsulation in order to avoid

releasing As to surrounding environment. Some efforts have been made to replace As with Ge [9,10], but the limited availability of Ge cannot meet the needs of mass-industrial production for real-life refrigeration applications. Recently, a giant magnetocaloric effect has been found in MnFe(P,Si) compounds [11,12]. However, a large amount of the impurity phase $(\text{Mn,Fe})_3\text{Si}$ (about 18 vol%) was also observed for the $\text{MnFeP}_{0.5}\text{Si}_{0.5}$ compound (see Figure 4.1). Furthermore, the thermal hysteresis

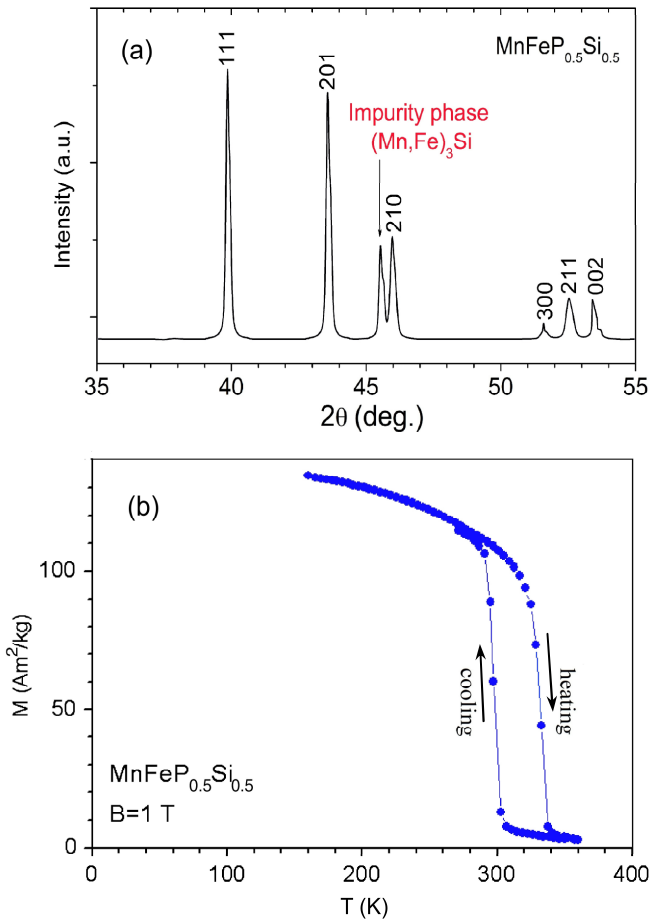


Figure 4.1. (a) X-ray diffraction pattern at room temperature and (b) magnetization as a function of temperature measured in a magnetic field of 1 T on heating and cooling. (After [11,12])

ΔT_{hys} , which is detrimental to the refrigeration cycle efficiency [13], was found to be very large, up to 35 K.

A schematic representation of the structure of hexagonal Fe_2P -based $\text{MnFe}(\text{P},\text{X})$ ($\text{X} = \text{As}, \text{Ge}, \text{Si}$) (space group $P\bar{6}2m$) is shown in Figure 4.2. Mn and Fe preferentially occupy the $3g$ and $3f$ sites, respectively while P and X are randomly distributed on the $1b$ and $2c$ sites [14-16]. Mn coplanar with P/X($1b$) and Fe coplanar with P/X($2c$) form natural multilayers alternating along the c direction. Each Mn atom is surrounded by five P/X nearest neighbors, while the Fe atom has only four P/X nearest neighbors, forming a tetrahedron. Since the Mn-P/X distance is larger than the Fe-P/X and the Mn $3d$ electrons are more localized than the Fe $3d$ electrons, the chemical bonding between Fe and P/X is much stronger than that between Mn and P/X. Mn is therefore surrounded loosely by P/X while the electron density is spatially extended over Fe and P/X. In the Mn-rich compounds, excess Mn enters into the $3f$ site.

In this chapter, we demonstrate optimized magnetocaloric effects in the Mn-Fe-P-Si compounds for refrigeration applications. By varying the composition, both the

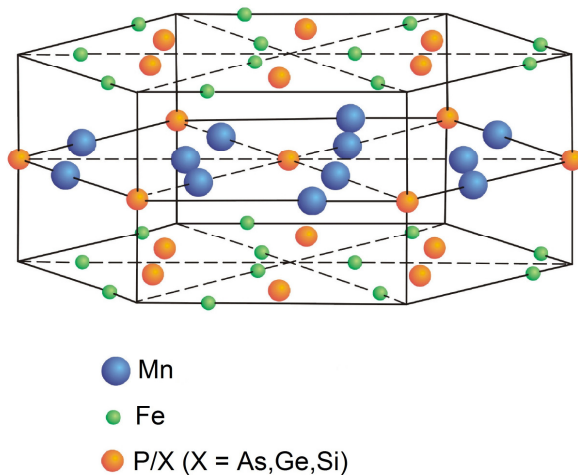


Figure 4.2. Schematic representation of the crystal lattice structure of the hexagonal $\text{MnFe}(\text{P},\text{X})$ ($\text{X} = \text{As}, \text{Ge}, \text{Si}$) compounds.

hysteresis and the operating temperature are simultaneously tunable, and the amount of the impurity phase can be reduced.

4.2. Experimental details

Mn-Fe-P-Si compounds were prepared as described in Chapter 3. A SQUID magnetometer (Quantum Design MPMS 5XL) with the Reciprocating Sample Option (RSO) mode was employed for magnetic measurements. X-ray diffraction patterns were collected at various temperatures in zero field using a PANalytical X-pert Pro diffractometer with Cu $K\alpha$ radiation, a secondary-beam flat-crystal monochromator, a multichannel X'celerator detector and an Anton Paar TTK450 low-temperature camera. The phase homogeneity and the stoichiometry of the samples were investigated with electron probe microanalysis (EPMA). The EPMA measurements were carried out using a JEOL 8800-JXA Superprobe equipped with Wavelength Dispersive Spectrometers (WDS).

4.3. $\text{Mn}_x\text{Fe}_{2-x}\text{P}_{1-y}\text{Si}_y$ alloys

Figure 4.3 shows the partial phase diagram for $\text{Mn}_x\text{Fe}_{2-x}\text{P}_{1-y}\text{Si}_y$ ($x = 1.10-1.30$, $y = 0.50-0.58$) compounds with hexagonal Fe_2P -type structure (space group $P\bar{6}2m$) which display a ferro- to paramagnetic first-order transition around room temperature. It can be seen that both the substitution of Fe with Mn and the substitution of P with Si lead to a reduction in ΔT_{hys} . However, they make the magnetic ordering temperature T_C change in opposite sense. The substitution of Fe with Mn reduces T_C , but the substitution of P with Si increases T_C . These behaviors are similar to those observed in $(\text{Mn,Fe})_2(\text{P,As})$ [17] and $(\text{Mn,Fe})_2(\text{P,Ge})$ [18]. Details of the influence of the substitutions on ΔT_{hys} and T_C are discussed in Chapters 5 and 7.

X-ray diffraction measurements detect a considerable amount of the impurity phase $(\text{Mn,Fe})_3\text{Si}$. Although it is not relevant for the magnetic response, it sets hurdles for preparing single-phase samples, causing difficulty in optimizing the magnetocaloric effect.

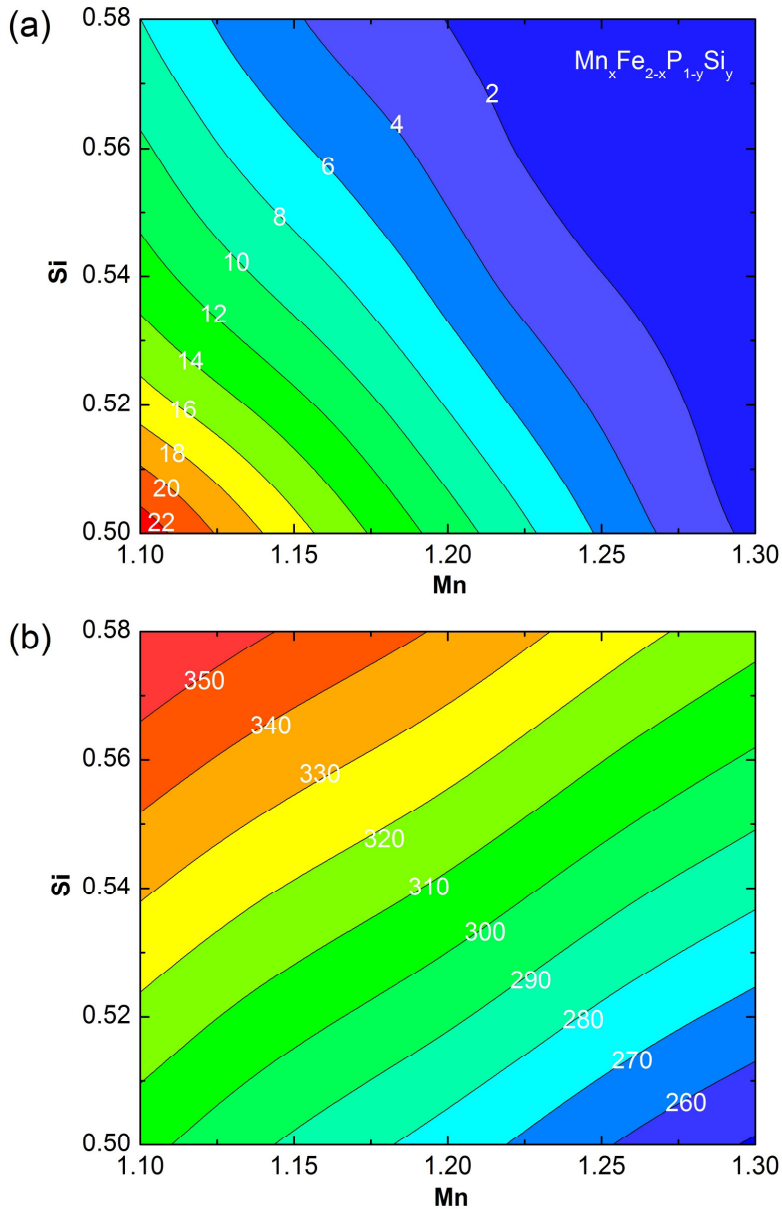


Figure 4.3. Partial phase diagram of the quaternary (MnFePSi) system illustrating (a) the composition dependence of the thermal hysteresis ΔT_{hys} (K) and (b) the composition dependence of the magnetic ordering temperature T_C (K) for $Mn_xFe_{2-x}P_{1-y}Si_y$ compounds.

4.4. Off-stoichiometric $(\text{Mn,Fe})_{2+z}\text{P}_{0.50}\text{Si}_{0.50}$ alloys

Figure 4.4 shows the x-ray diffraction patterns measured at room temperature for the off-stoichiometric $\text{Mn}_{1.30}\text{Fe}_{0.70+z}\text{P}_{0.50}\text{Si}_{0.50}$ ($z = -0.1, -0.08, -0.05, 0, 0.05$) compounds. The main phase is of hexagonal Fe_2P -type structure. For $z \geq -0.05$ the cubic impurity phase $(\text{Mn,Fe})_3\text{Si}$ (space group $Fm\bar{3}m$) emerges and increases with z . The sample with $z = -0.05$ contains a very minute amount of this secondary phase. This is confirmed by x-ray diffraction patterns measured at low temperatures (see Figure 4.5). For the samples with $z < -0.05$, we observe the hexagonal phase $(\text{Mn,Fe})_5\text{Si}_3$ (space group $P6_3/mcm$) as main impurity phase.

The slight deficiency in metal in the $z = -0.05$ sample results in a small amount of impurities in phase composition and the matrix composition is thus quite close to the nominal one. The electron probe microanalysis (EPMA) further confirmed the metal deficiency in the matrix phase of the sample with $z = -0.05$. The metal to metalloid ratio $(\text{Mn,Fe}):(\text{P,Si})$ is 1.92:1 rather than 1.95:1 as indicated by the nominal

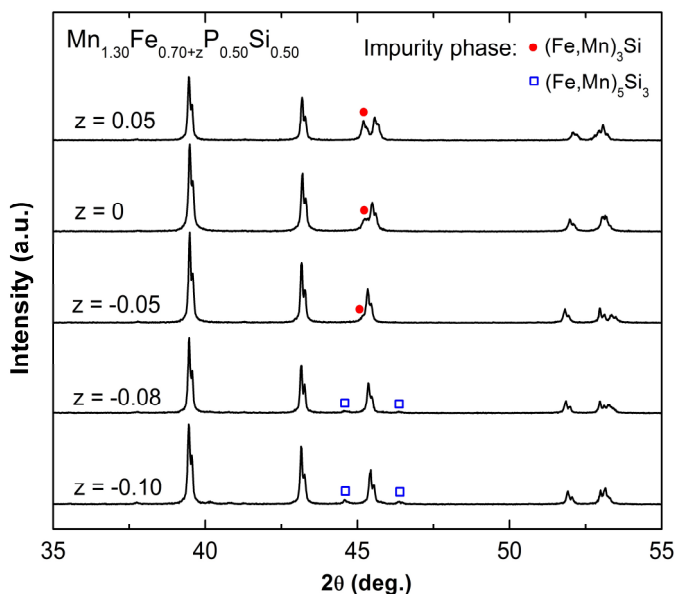


Figure 4.4. X-ray diffraction patterns measured at room temperature for the off-stoichiometric $\text{Mn}_{1.30}\text{Fe}_{0.70+z}\text{P}_{0.50}\text{Si}_{0.50}$ compounds.

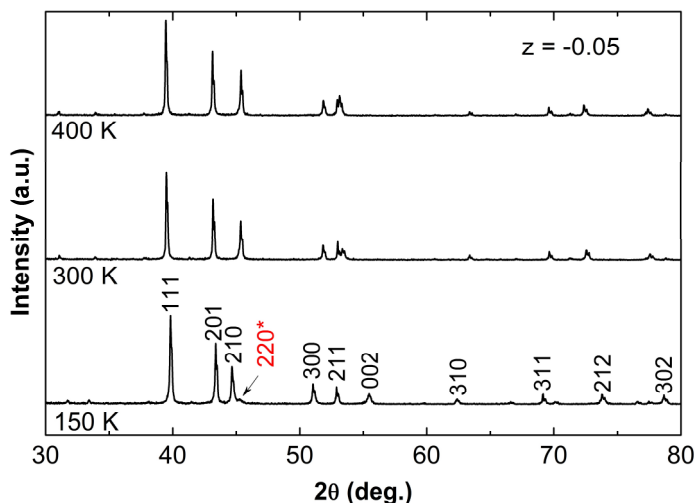


Figure 4.5. X-ray diffraction patterns at 150, 300 and 400 K for the $\text{Mn}_{1.30}\text{Fe}_{0.65}\text{P}_{0.50}\text{Si}_{0.50}$ compound measured upon heating. A very small amount of the impurity phase $(\text{Mn,Fe})_3\text{Si}$ is detected [hkl Miller index with asterisk (*)]. Above room temperature the peak of the impurity phase overlaps with that of the main phase.

composition. This is due to the fact that the occurrence of a small amount of metal-rich $(\text{Mn,Fe})_3\text{Si}$ phase further increased the metal deficiency.

Two different types of impurity occur depending on the value of z . The cubic impurity phase has metal to metalloid ratio $(\text{Mn,Fe}):\text{Si} = 3:1$. Compared to the ratio $(\text{Mn,Fe}):(\text{P,Si}) = 2:1$, it is metal-rich and tends to occur when there is excessive metal in the compounds. The hexagonal impurity phase with $(\text{Mn,Fe}):\text{Si} = 5:3$ is metal-poor and tends to occur if the metal is deficient.

Figure 4.6 shows the temperature dependence of the magnetization for the off-stoichiometric $\text{Mn}_{1.30}\text{Fe}_{0.70+z}\text{P}_{0.50}\text{Si}_{0.50}$ ($z = -0.10, -0.08, -0.05, 0, 0.05$) compounds. The sample with $z = -0.05$ exhibits not only the steepest transition but also the smallest ΔT_{hys} of about 1 K. Both the T_C and the magnetization are the highest for this composition. As for magnetic refrigeration application, the desired sample is the one with $z = -0.05$. Apparently, the transition becomes broader and ΔT_{hys} is larger for

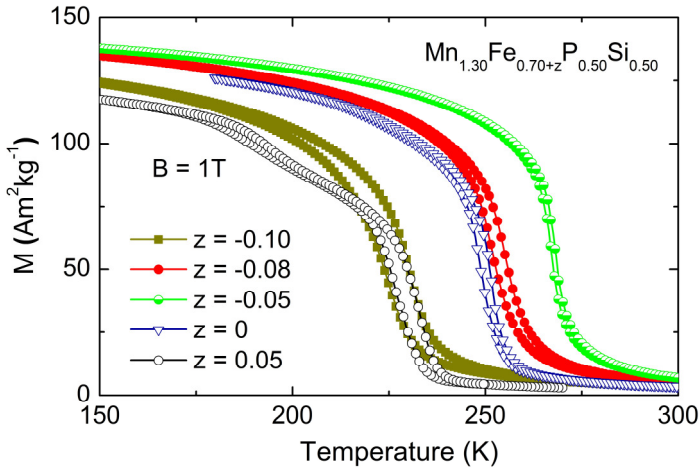


Figure 4.6. Magnetization as a function of temperature measured in 1 T upon heating and cooling for the off-stoichiometric $\text{Mn}_{1.30}\text{Fe}_{0.70+z}\text{P}_{0.50}\text{Si}_{0.50}$ compounds.

increasing z above or for decreasing z below $z = -0.05$. Especially, we observe a double first-order transition for the $z = 0.05$ samples, indicating that the sample with excessive metal seems to have a phase segregation of the main phase. The same behavior may also happen to the $z = 0$ sample but it is less pronounced.

Our extended experimental investigation for $(\text{Mn,Fe})_{2+z}(\text{P,Si})$ with different Mn:Fe and P:Si ratios indicates that the value $z = -0.05$ is also appropriate to reduce impurity phase and obtain a sharp transition.

4.5. Optimized magnetocaloric effects

As mentioned in Section 4.3, the substitutions of Fe and P with Mn and Si, respectively, are beneficial in that they give rise to a decrease in ΔT_{hys} . Furthermore, T_C can be tuned by changing the Mn:Fe and P:Si ratios simultaneously to keep a small ΔT_{hys} . These trends also hold for slightly off-stoichiometric compounds. As seen in Figure 4.7 and Table 4.1, by concurrently changing the Mn:Fe and P:Si ratios in $\text{Mn}_x\text{Fe}_{1.95-x}\text{P}_{1-y}\text{Si}_y$ compounds, the operating temperature can be controlled between 220 and 320 K for $x = 1.34$, $y = 0.46$ and $x = 1.24$, $y = 0.54$, respectively, while the transition remains steep and the ΔT_{hys} remains small (1-2 K). Note that the instrument

thermal lag of about 0.5 K with 1 K/min sweep rate around room temperature was obtained by measuring a Gd sample mounted in the same way as the other samples mentioned above. This instrument thermal lag is not subtracted from the experimental data. The actual thermal hysteresis is therefore somewhat smaller than that displayed in the figures and described in the text.

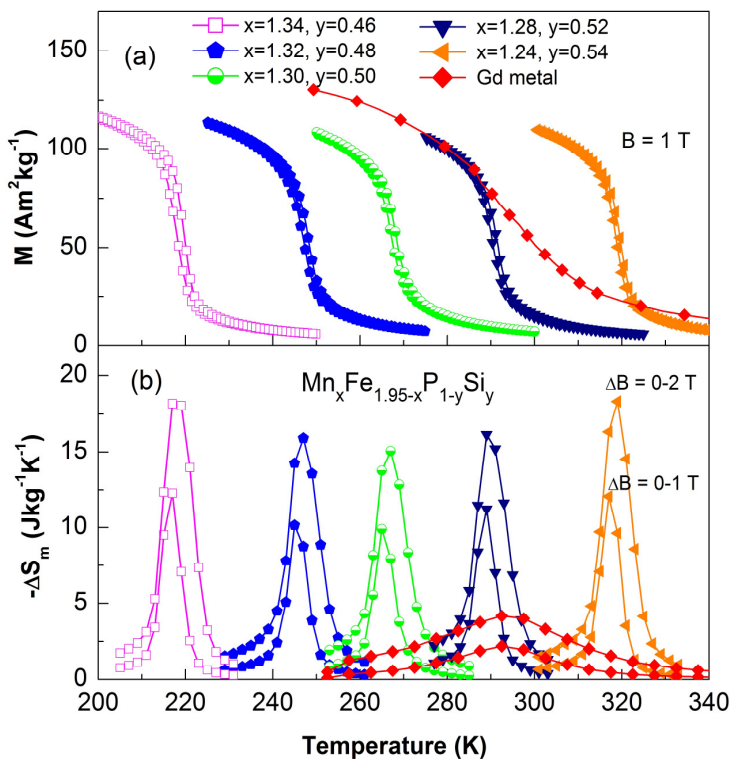


Figure 4.7. (a) Magnetization as a function of temperature measured in 1 T upon heating and cooling, and (b) isothermal magnetic entropy change for a field change of 0-1 T (lower curves) and 0-2 T (upper curves) for some typical $\text{Mn}_x\text{Fe}_{1.95-x}\text{P}_{1-y}\text{Si}_y$ compounds. The data of Gd metal are included.

M - B measurements in the vicinity of T_C show reversible magnetic isotherms with negligible magnetic hysteresis (see Figure 4.8 for a representative sample). The extremely small magnetic hysteresis is in line with the observed small ΔT_{hys} , indicating

Table 4.1. Magnetic-ordering temperature (T_C) derived from the magnetization curves measured in 1 T on heating, magnetic entropy change (ΔS_m) for a magnetic field change of 0-2 T, and thermal hysteresis (ΔT_{hys}) derived from the magnetization curves measured in 1 T on cooling and heating for the $\text{Mn}_x\text{Fe}_{1.95-x}\text{P}_{1-y}\text{Si}_y$ compounds.

Composition	T_C (K)	$ \Delta S_m $ ($\text{Jkg}^{-1}\text{K}^{-1}$)	ΔT_{hys} (K)
$x=1.24, y=0.54$	320	18	1
$x=1.28, y=0.52$	292	16	1
$x=1.30, y=0.50$	269	15	1
$x=1.32, y=0.48$	248	16	1
$x=1.34, y=0.46$	220	18	2

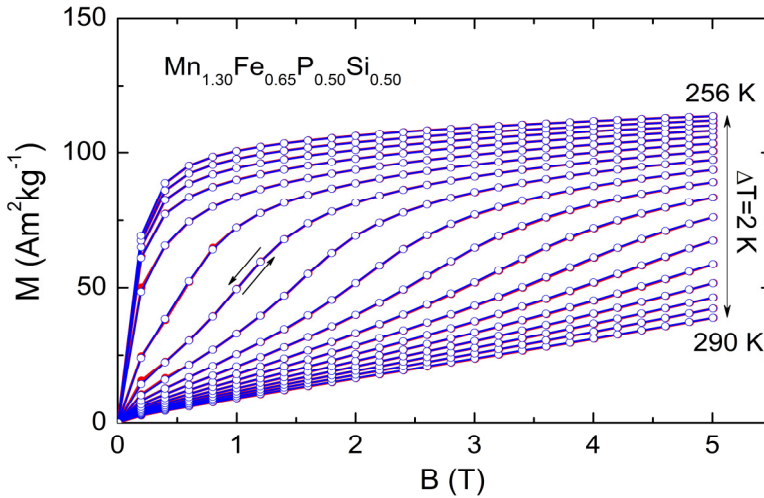


Figure 4.8. Magnetic isotherms measured in increasing and decreasing field for $\text{Mn}_{1.30}\text{Fe}_{0.65}\text{P}_{0.50}\text{Si}_{0.50}$ in the vicinity of the magnetic ordering temperature. The reversible magnetic isotherms indicate a negligible hysteresis.

a low energy barrier for nucleation of the first-order magnetic transition. From the magnetic isotherms, the entropy changes as function of temperature were derived through the Maxwell relations [1,2,19]. The absolute value of ΔS_m reaches $18 \text{ Jkg}^{-1}\text{K}^{-1}$

around both 220 and 320 K, under a magnetic field change of 0-2 T. The peak values are rather stable (between 15-18 $\text{Jkg}^{-1}\text{K}^{-1}$) throughout the whole temperature range from 220 to 320 K. These values are about 4 times greater than that of Gd (see the data included in Figure 4.7) for tunable temperatures. Note that the observed entropy change is already large in a field change of 0-1 T. Thus, with the current materials magnetic refrigerators using permanent magnets that often produce a magnetic field of less than 2 T can work efficiently. Because the large effect is observed over a broad range of compositions, one can achieve an equally large magnetocaloric effect over a wide temperature interval by cascading several alloys with slightly different compositions in one active magnetic regenerator [20]. In this way, the cooling power can be enhanced and, simultaneously, the operating temperature span is enlarged and flexible.

4.6. Conclusions

A giant magnetocaloric effect and a small thermal hysteresis in Mn-Fe-P-Si compounds of hexagonal Fe_2P -type structure have been achieved simultaneously by varying the Mn:Fe and P:Si ratios. We demonstrate that the operating temperature can be controlled between 220 and 320 K by concurrently changing the Mn:Fe and P:Si ratios. The combination of several alloys with slightly different compositions in one active magnetic regenerator will allow for efficient magnetic refrigeration with large temperature span. The fact that we use materials that are not only globally-abundant and non-toxic but also able to be industrially-mass-produced via a simple powder-metallurgical method makes Mn-Fe-P-Si compounds particularly attractive. The discovery of these high-performance low-cost magnetic refrigerants paves the way for commercialization of magnetic refrigeration.

References

- [1] E. Brück, *J. Phys. D: Appl. Phys.* **38**, R381 (2005).
- [2] K. A. Gschneidner, V. K. Pecharsky, and A. O. Tsokol, *Rep. Prog. Phys.* **68**, 1479 (2005).
- [3] V. Franco, J. S. Blazquez, B. Ingale, and A. Conde, *Annu. Rev. Mater. Res.* **42**, 305 (2012).

-
- [4] V. K. Pecharsky and K. A. Gschneidner, *Phys. Rev. Lett.* **78**, 4494 (1997).
- [5] T. Krenke, E. Duman, M. Acet, E. F. Wassermann, X. Moya, L. Manosa, and A. Planes, *Nat. Mater.* **4**, 450 (2005).
- [6] N. T. Trung, L. Zhang, L. Caron, K. H. J. Buschow, and E. Brück, *Appl. Phys. Lett.* **96**, 172504 (2010).
- [7] O. Tegus, E. Brück, K. H. J. Buschow, and F. R. de Boer, *Nature* **415**, 150 (2002).
- [8] O. Tegus, E. Brück, L. Zhang, Dagula, K. H. J. Buschow, and F. R. de Boer, *Physica B* **319**, 174 (2002).
- [9] N. T. Trung, Z. Q. Ou, T. J. Gortenmulder, O. Tegus, K. H. J. Buschow, and E. Brück, *Appl. Phys. Lett.* **94** (2009).
- [10] E. Brück, N. T. Trung, Z. Q. Ou, and K. H. J. Buschow, *Scripta Mater.* **67**, 590 (2012).
- [11] D. T. C. Thanh, E. Brück, N. T. Trung, J. C. P. Klaasse, K. H. J. Buschow, Z. Q. Ou, O. Tegus, and L. Caron, *J. Appl. Phys.* **103**, 07B318 (2008).
- [12] D. T. C. Thanh, *Magnetocalorics and magnetism in MnFe(P,Ge,Si) materials*, University of Amsterdam (2009), PhD thesis, Chapter 5.
- [13] A. M. Tishin and Y. I. Spichkin, *The magnetocaloric effect and its applications* (Institute of Physics Publishing, Bristol, 2003).
- [14] M. Bacmann, J.-L. Soubeyroux, R. Barrett, D. Fruchart, R. Zach, S. Niziol, and R. Fruchart, *J. Magn. Magn. Mater.* **134**, 59 (1994).
- [15] D. M. Liu, Q. Z. Huang, M. Yue, J. W. Lynn, L. J. Liu, Y. Chen, Z. H. Wu, and J. X. Zhang, *Phys. Rev. B* **80**, 174415 (2009).
- [16] L. Zhang, O. Moze, K. Prokes, O. Tegus, and E. Brück, *J. Magn. Magn. Mater.* **290**, 679 (2005).
- [17] O. Tegus, *Novel materials for magnetic refrigeration*, University of Amsterdam (2003), PhD thesis, Chapters 5 and 6.
- [18] N. T. Trung, *First-order phase transitions and giant magnetocaloric effect*, Delft University of Technology (2010), PhD thesis, Chapter 4.
- [19] E. Brück, O. Tegus, L. Zhang, X. W. Li, F. R. de Boer, and K. H. J. Buschow, *J. Alloy. Compd.* **383**, 32 (2004).
- [20] A. Rowe and A. Tura, *Int. J. Refrig.* **29**, 1286 (2006).

Chapter 5

FROM FIRST-ORDER MAGNETO-ELASTIC TO MAGNETO-STRUCTURAL TRANSITION IN (Mn,Fe)_{1.95}P_{0.50}Si_{0.50} COMPOUNDS

5.1. Introduction

Nowadays, advanced magnetocaloric materials often undergo a first-order magnetic transition [1-4], because the first-order magnetic transition is associated with an abrupt change in crystal lattice which enhances magnetocaloric effects via a spin - lattice coupling. The first-order transition can be divided into first-order magneto-structural transition which exhibits a structure change coupled with a magnetic transition as observed for Gd₅(Ge_xSi_{1-x})₄ [5,6], Ni_{0.50}Mn_{0.50-x}Sn_x [7] and MnCoGeB_x [8]; or first-order magneto-elastic transition for which the crystal structure remains unchanged but the lattice constants suddenly change at the magnetic transition, as observed for MnFeP_{1-x}As_x [9] and La(Fe_{1-x}Si_x)₁₃ [10,11].

Fe₂P-based compounds are known as giant magnetocaloric materials with a first-order magneto-elastic transition. Most studies have recently focused on (Mn,Fe)₂(P,As,Ge) compounds [1-3,9,12,13]. However, the limited availability of Ge and toxicity of As hold these materials back from real refrigeration applications. Substitution of As and Ge with Si becomes one of the most prominent studies towards making a high performance room-temperature magnetic refrigerant. In Chapter 4, we demonstrate that a giant magnetocaloric effect and a small thermal hysteresis in hexagonal Mn-Fe-P-Si

compounds with tunable operating temperatures can be achieved simultaneously by varying the Mn:Fe and P:Si ratios. Here we report on $(\text{Mn,Fe})_{1.95}\text{P}_{0.50}\text{Si}_{0.50}$ compounds when changing the Mn:Fe ratio with emphasis on the coupling between magnetic and structural transitions. We observe a previously unknown first-order magneto-structural transition and a modified first-order magneto-elastic transition favorable for real refrigeration applications.

5.2. Experimental details

The $(\text{Mn,Fe})_{1.95}\text{P}_{0.50}\text{Si}_{0.50}$ alloys were prepared by ball-milling as described in Chapter 3. Magnetic measurements were carried out using the Reciprocating Sample Option (RSO) mode in a Superconducting Quantum Interference Device (SQUID) magnetometer (Quantum Design MPMS 5XL). X-ray diffraction patterns were obtained by a PANalytical X-pert Pro diffractometer equipped with an Anton Paar TTK450 low-temperature chamber using Cu $K\alpha$ radiation, a secondary-beam flat-crystal monochromator and a multichannel X'celerator detector. Each x-ray pattern was recorded at a constant temperature and the following one was recorded at a higher temperature. A differential scanning calorimeter equipped with a liquid nitrogen cooling system was employed to measure the specific heat.

5.3. First-order magneto-elastic and second-order isostructural transitions

The room-temperature x-ray diffraction measurements pointed out that all the samples crystallize in the hexagonal Fe_2P -type structure (space group $\overline{P6}2m$). The temperature dependence of the magnetization for the $\text{Mn}_x\text{Fe}_{1.95-x}\text{P}_{0.50}\text{Si}_{0.50}$ compounds measured in a field of 1 T is shown in Figure 5.1. For $x < 1.40$, the M - T curves show very sharp ferro- to paramagnetic transitions. A clear ΔT_{hys} confirms the first-order nature of these transitions. The ΔT_{hys} can be tuned from 5 K, 2 K to 1 K by varying the Mn:Fe ratio from $x = 1.20, 1.25$ to 1.30, respectively. Figure 5.2a shows the isothermal magnetic entropy change (ΔS_{m}) as a function of temperature under a field change ΔB of 0-1 T and 0-2 T for the $x = 1.20, 1.25, 1.30, 1.40$ and 1.50 samples. Here the ΔS_{m} is calculated using magnetic isotherms through the Maxwell relations [4]. Apparently, the

absolute value of ΔS_m is lower in the sample with more Mn. However, it should be noted that the $x = 1.30$ sample which has a very small ΔT_{hys} still displays a large $|\Delta S_m|$ of $15 \text{ J kg}^{-1} \text{ K}^{-1}$ under a 2 T field change. This value is 4 times higher than that of the benchmark material Gd [14].

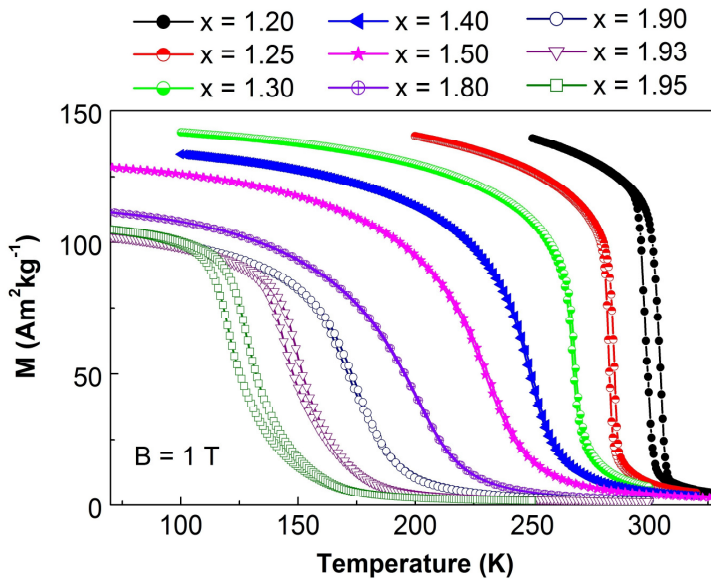


Figure 5.1. Temperature dependence of the magnetization in a field of 1 T upon cooling and heating for the $\text{Mn}_x\text{Fe}_{1.95-x}\text{P}_{0.50}\text{Si}_{0.50}$ compounds.

Figure 5.2b illustrates Arrot plots derived from the magnetic isotherms in the vicinity of the transition temperature for the $x = 1.20, 1.25, 1.30, 1.40$ and 1.50 samples. The S-shaped magnetization curves revealing relevant high-order terms in the Landau free energy expansion [13] prove a first-order transition for $x < 1.40$. However, neither a negative slope nor an inflection point is observed for the $x = 1.40$ and 1.50 samples, confirming a second-order magnetic transition. Thus, replacing some Fe with Mn can lower the energy barrier in the first-order magnetic transition, and the first-order magnetic transition gradually changes into a second-order magnetic transition when the energy barrier becomes lower and finally vanishes.

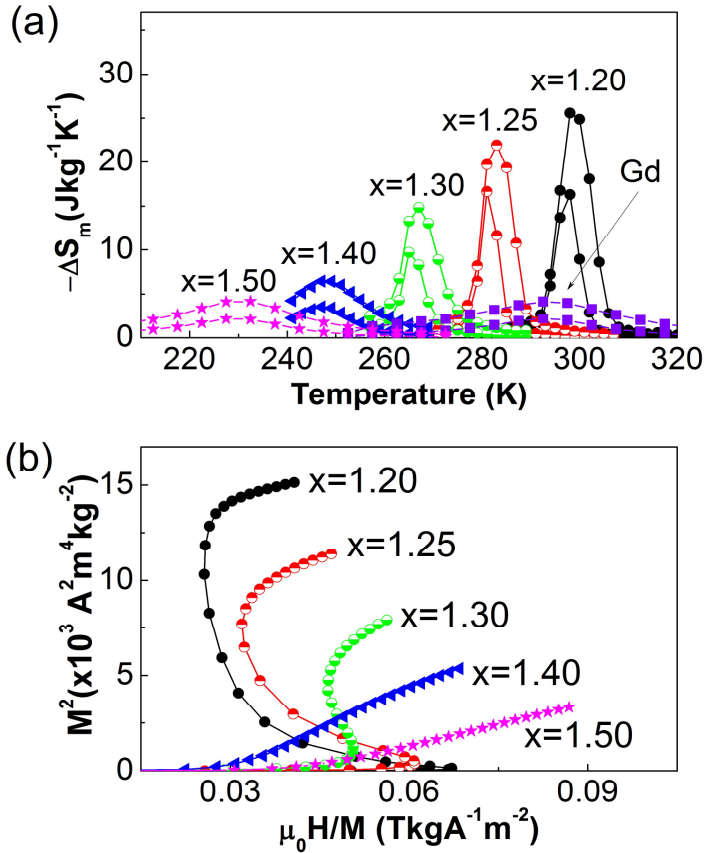


Figure 5.2. (a) Magnetic entropy change as a function of temperature for a field change of 0-1 T (lower curves) and 0-2 T (upper curves), and (b) Arrot plots obtained from magnetic isotherms measured in increasing field in the vicinity of the transition temperature for the $\text{Mn}_x\text{Fe}_{1.95-x}\text{P}_{0.50}\text{Si}_{0.50}$ compounds. The magnetic entropy change of the benchmark material Gd is added for comparison.

The x-ray diffraction patterns at various temperatures confirm a stable hexagonal Fe_2P -type structure for $x = 1.20, 1.25, 1.30, 1.40, 1.50$ and 1.80 samples. The thermal evolution of the x-ray diffraction patterns is illustrated in Figure 5.3a for $x = 1.20, 1.30, 1.40$ and 1.50 . For the $x = 1.20$ and 1.30 samples, a discontinuity of the diffraction peaks at the transition temperature indicates a jump of lattice constants. Note that the samples with a larger magnetocaloric effect exhibit a stronger peak shift at the critical

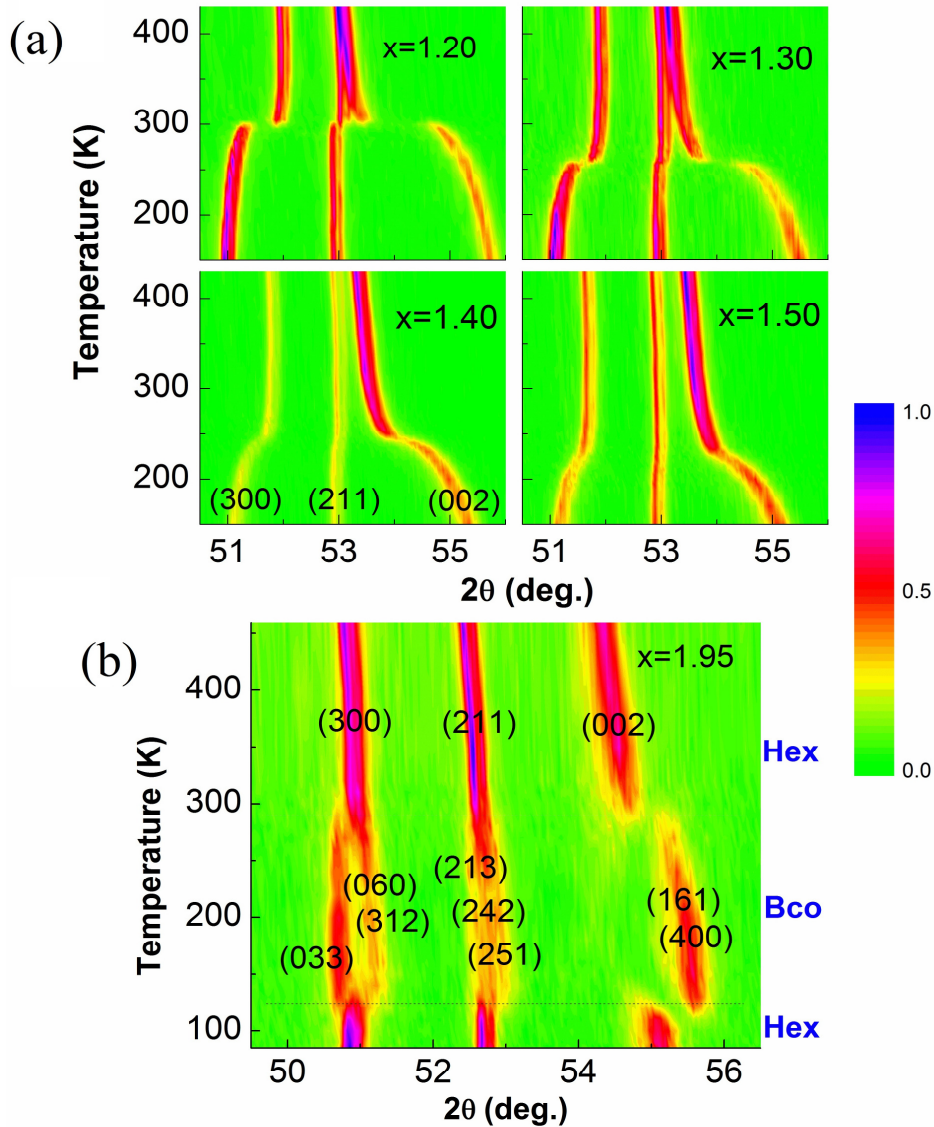


Figure 5.3. Contour plots of the x-ray diffraction patterns for the $\text{Mn}_x\text{Fe}_{1.95-x}\text{P}_{0.50}\text{Si}_{0.50}$ compounds: (a) $x = 1.20, 1.30, 1.40, 1.50$ and (b) $x = 1.95$ collected using Cu $K\alpha$ radiation in zero field upon heating. Only a small range of 2θ is shown for clarity. The bar on the right represents the normalized intensity scale.

temperature. Additionally, the (300) and (002) peaks are shifted in opposite direction which implies that the lattice constants a and c change in opposite sense. The steep change of lattice constants coupled with the magnetic transition confirms a first-order magneto-elastic transition. On the other hand, a continuity of the peaks with respect to temperature is observed for the $x = 1.40$ and 1.50 samples, demonstrating a second-order magnetic transition. This observation is in good agreement with the results from the Arrot plots. It can also be realized based on the characteristic of the specific heat at first-order and second-order transitions (see Figure 5.4).

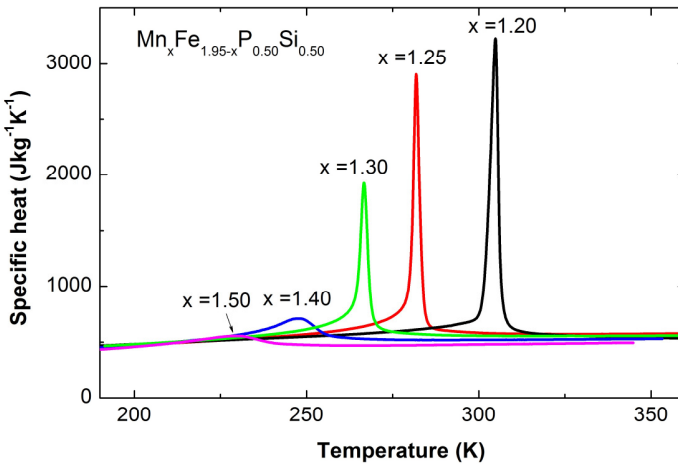


Figure 5.4. Specific heat as a function of temperature for the $\text{Mn}_x\text{Fe}_{1.95-x}\text{P}_{0.50}\text{Si}_{0.50}$ compounds measured in zero field upon heating.

From the above behaviors, it is found that a small ΔT_{hys} can be achieved by changing the chemical composition when the magnetic transition is controlled to be close to the border separating the first-order and second-order transition regimes. This still holds for other first-order transition materials, such as hydrogen absorption [15] or addition of transition metals [16,17] for the pseudo-binary system $\text{Gd}_5(\text{Ge}_x\text{Si}_{1-x})_4$; or addition of carbon and boron [18] for $\text{La}(\text{Fe},\text{Si})_{13}$. Therefore, modification in chemical composition can play a very important role in optimizing the magnetocaloric performance of advanced materials that can be used for magnetic refrigerators.

5.4. First-order magneto-structural transitions

The ferromagnetic order of the $\text{Mn}_x\text{Fe}_{1.95-x}\text{P}_{0.50}\text{Si}_{0.50}$ compounds remains until Fe is completely replaced by Mn (see Figure 5.1). Note that the existence of the ΔT_{hys} for $x \geq 1.90$ indicates the reoccurrence of a first-order transition. However structural measurements show that these samples have a different type of first-order transition. On cooling below room temperature we find that the paramagnetic hexagonal phase is transformed into a paramagnetic body-centered orthorhombic (Bco) phase (space group *Imm2*). Further cooling makes this orthorhombic structure transform back into the hexagonal structure in a first-order magneto-structural transition. The orthorhombic structure is similar to that found in $\text{Fe}_2(\text{P},\text{Si})$ compounds [19,20]. The re-entrant hexagonal structure in the first-order magneto-structural transition points to a preference of the ferromagnetism for the hexagonal rather than the orthorhombic structure. Figure 5.3b illustrates the structural transformation based on x-ray diffraction patterns measured on heating for the $x = 1.95$ sample without Fe. The orthorhombic phase exists over a temperature range from 125 K to 290 K between low-temperature ferromagnetic and high-temperature paramagnetic hexagonal phases. A quite large structural transition zone at which both the hexagonal and orthorhombic phases exist explains why we could not see a sharp magnetic transition in the first-order magneto-structural transition (see Figure 5.1). The magnetocaloric effect of the $\text{Mn}_{1.95}\text{P}_{0.50}\text{Si}_{0.50}$ compound at the first-order magneto-structural transition is, therefore, not so large with $|\Delta S_{\text{m}}| \sim 6 \text{ Jkg}^{-1}\text{K}^{-1}$ for a field change of 0-2 T (see Figure 5.5).

Since hexagonal $\text{Mn}_x\text{Fe}_{2-x}\text{P}$ ($x > 1.35$) is antiferromagnetic [21], this study indicates that the Si addition supports a ferromagnetic order. The enhancement of the ferromagnetism by replacing P with Si was also observed in $\text{Fe}_2(\text{P},\text{Si})$ [19,20].

5.5. Phase diagram

Because of a strong coupling between the crystal and magnetic structure, the magnetic-ordering temperature (T_{C}) can be defined as the temperature at which we see a very clear change in the tendency of the thermal evolution of the lattice constants or the structure. It can also be determined from the specific heat curves or, in some cases of

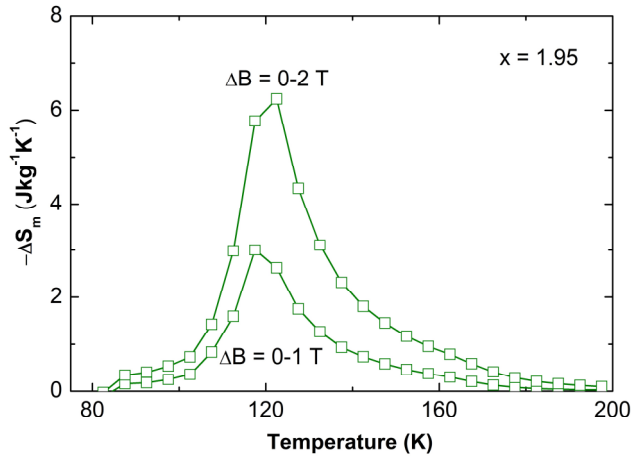


Figure 5.5. Entropy change for a field change of 0.1 T (lower curve) and 0.2 T (upper curve) for the $\text{Mn}_{1.95}\text{P}_{0.50}\text{Si}_{0.50}$ compound.

the first-order phase transition, from extremes of the first derivative of the isofield magnetization with respect to temperature. Figure 5.6 shows the phase diagram of the $\text{Mn}_x\text{Fe}_{1.95-x}\text{P}_{0.50}\text{Si}_{0.50}$ compounds illustrating the composition dependence of the phase transition temperatures. It is found that the temperature range over which the orthorhombic phase exists becomes narrower and disappears as x is lower than a critical value which is extrapolated to be about $x = 1.88$. T_C decreases almost linearly with Mn:Fe ratio for the first-order magneto-elastic transition, gradually for the second-order magnetic transition and drops faster in a very narrow composition range of the first-order magneto-structural transition. The Mn(3g)-Fe(3f) interlayer exchange coupling is believed to be responsible for a ferromagnetic order in MnFe(P,Si) compounds [22]. For the Mn-rich compounds, since the Mn and Fe atoms favor the 3g and 3f sites, respectively, excess Mn atoms enter into the 3f sites. The replacement of Fe by Mn may weaken the Mn(3g)-Fe/Mn(3f) interlayer exchange coupling, leading to the reduction of T_C . When Mn is replaced by Fe on the 3g site in the Fe-rich compounds, the Mn/Fe(3g)-Fe(3f) exchange coupling will be stronger than that of the Mn-rich compounds. Therefore, the ferromagnetism will be enhanced and T_C of hexagonal $\text{Fe}_2\text{P}_{0.8}\text{Si}_{0.2}$ with even less Si content (about 510 K) was found to exceed that of the Mn-rich compounds [19,20].

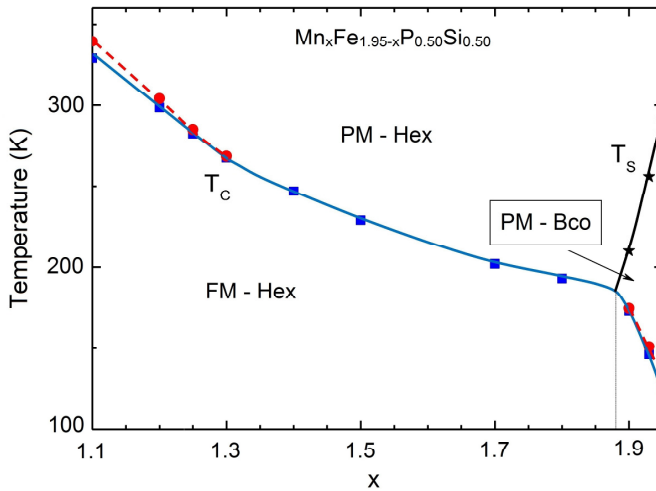


Figure 5.6. Phase diagram of the $\text{Mn}_x\text{Fe}_{1.95-x}\text{P}_{0.50}\text{Si}_{0.50}$ compounds illustrating the composition dependence of the phase transition temperatures: magnetic ordering temperature (T_C) upon heating (solid circles) and cooling (solid squares), and paramagnetic orthorhombic to paramagnetic hexagonal transition temperature (T_S) upon heating (solid stars).

5.6. Conclusions

In summary, by varying the Mn:Fe ratio the $(\text{Mn,Fe})_{1.95}\text{P}_{0.50}\text{Si}_{0.50}$ compounds change from a first-order magneto-elastic transition into a first-order magneto-structural transition through a second-order isostructural magnetic transition. The study also shows the preference of the hexagonal Fe_2P -type structure for the ferromagnetic order and a strong coupling between the crystal and magnetic structure. Although the magnetocaloric effect from the first-order magneto-structural transition is not so large, the existence of the first-order magneto-structural transition with the re-entrant hexagonal structure is very interesting for further study on exchange coupling in Fe_2P -based materials. Moreover, a small ΔT_{hys} and a giant magnetocaloric effect, which are favorable for real magnetic refrigeration applications, can be achieved when the magnetic transition is controlled to be close to the border separating the first-order and second-order transition regimes.

References

- [1] E. Brück, *J. Phys. D: Appl. Phys.* **38**, R381 (2005).
- [2] E. Brück, O. Tegus, D. T. C. Thanh, N. T. Trung, and K. H. J. Buschow, *Int. J. Refrig.* **31**, 763 (2008).
- [3] E. Brück, O. Tegus, D. T. C. Thanh, and K. H. J. Buschow, *J. Magn. Magn. Mater.* **310**, 2793 (2007).
- [4] K. A. Gschneidner, V. K. Pecharsky, and A. O. Tsokol, *Rep. Prog. Phys.* **68**, 1479 (2005).
- [5] V. K. Pecharsky and K. A. Gschneidner, *Phys. Rev. Lett.* **78**, 4494 (1997).
- [6] F. Casanova, A. Labarta, X. Batlle, F. J. Perez-Reche, E. Vives, L. Manosa, and A. Planes, *Appl. Phys. Lett.* **86**, 262504 (2005).
- [7] T. Krenke, E. Duman, M. Acet, E. F. Wassermann, X. Moya, L. Manosa, and A. Planes, *Nat. Mater.* **4**, 450 (2005).
- [8] N. T. Trung, L. Zhang, L. Caron, K. H. J. Buschow, and E. Brück, *Appl. Phys. Lett.* **96**, 162507 (2010).
- [9] O. Tegus, E. Brück, K. H. J. Buschow, and F. R. de Boer, *Nature (London)* **415**, 150 (2002).
- [10] S. Fujieda, A. Fujita, and K. Fukamichi, *Appl. Phys. Lett.* **81**, 1276 (2002).
- [11] A. Fujita, S. Fujieda, Y. Hasegawa, and K. Fukamichi, *Phys. Rev. B* **67**, 104416 (2003).
- [12] O. Gutfleisch, M. A. Willard, E. Brück, C. H. Chen, S. G. Sankar, and J. P. Liu, *Adv. Mater.* **23**, 821 (2011).
- [13] N. T. Trung, Z. Q. Ou, T. J. Gortenmulder, O. Tegus, K. H. J. Buschow, and E. Brück, *Appl. Phys. Lett.* **94**, 102513 (2009).
- [14] K. A. Gschneidner and V. K. Pecharsky, *Int. J. Refrig.* **31**, 945 (2008).
- [15] A. M. G. Carvalho, C. S. Alves, C. C. Colucci, M. A. Bolanho, A. A. Coelho, S. Gama, F. C. Nascimento, and L. P. Cardoso, *J. Alloy. Compd.* **432**, 11 (2007).
- [16] T. Zhang, Y. Chen, Y. Tang, H. J. Du, T. Ren, and M. Tu, *J. Alloy. Compd.* **433**, 18 (2007).
- [17] V. Provenzano, A. J. Shapiro, and R. D. Shull, *Nature* **429**, 853 (2004).
- [18] H. Zhang, B. G. Shen, Z. Y. Xu, X. Q. Zheng, J. Shen, F. X. Hu, J. R. Sun, and Y. Long, *J. Appl. Phys.* **111**, 07A909 (2012).
- [19] L. Häggström, L. Severin, and Y. Andersson, *Hyperfine Interact.* **94**, 2075 (1994).

- [20] E. K. Delczeg-Czirjak, L. Delczeg, M. P. J. Punkkinen, B. Johansson, O. Eriksson, and L. Vitos, *Phys. Rev. B* **82**, 085103 (2010).
- [21] S. Nagase, H. Watanabe and T. Shinohara, *J. Phys. Soc. Jpn.* **34**, 908 (1973).
- [22] X. B. Liu and Z. Altounian, *J. Appl. Phys.* **105**, 07A902 (2009).

Chapter 6

HIGH/LOW-MOMENT PHASE TRANSITION IN HEXAGONAL Mn-Fe-P-Si COMPOUNDS

6.1. Introduction

The interplay between crystal structure and magnetism, which is often very pronounced in first-order magnetic transition materials, is proposed to be at the core of giant magnetocaloric effect. Up to now, giant magnetocaloric effect has been discovered in several materials which are promising for room-temperature magnetic refrigeration applications [1-7]. Although a magnetic phase transition coupled with a change in crystal structure can be observed clearly in these materials, pinpointing the microscopic mechanism for the coupling between magnetism and crystal structure is not easy. By using x-ray magnetic circular dichroism and density functional theory, the mechanism of first-order bond-breaking magneto-structural transition in $\text{Gd}_5\text{Ge}_{4-x}\text{Si}_x$ was clarified with emphasis on the role of Ge in bridging ferromagnetism [8]. Spin-dependent hybridization between Ge $4p$ and Gd $5d$ conduction states enables long-range Ruderman-Kittel-Kasuya-Yosida (RKKY) ferromagnetic interactions between Gd $4f$ moments in adjacent Gd slabs connected by Ge/Si - Ge/Si bonds. Hence, ferromagnetic order will be destroyed if the RKKY interactions are weakened above the Ge/Si - Ge/Si bond-breaking transition. The chemical bonding between Ge/Si atoms plays an important role in first-order magneto-structural transition for this class of materials. For $\text{LaFe}_{13-x}\text{Si}_x$, electronic structure calculations indicated the existence of several shallow minima and maxima in the total energy versus the spin-moment curve,

resulting in a ferro- to paramagnetic transition that involves a series of consecutive transitions [9]. The extremes in the theoretical total energy profile are very sensitive to the lattice parameter of the cubic $\text{LaFe}_{13-x}\text{Si}_x$ phase. Although a peculiar series of consecutive field-induced transitions were realized in $\text{La}(\text{Fe},\text{Si})_{13}\text{H}_x$ under pressure [10], a microscopic mechanism is still lacking for the first-order magnetic transition in this class of materials. Similarly, for $\text{Ni}_{0.50}\text{Mn}_{0.50-x}\text{Sn}_x$ with an inverse magnetocaloric effect, the first-order magnetic transition is often ascribed to a change in atomic distance at the martensitic transition that modifies magnetic properties of the alloy [5]. However, *ab initio* electronic structure calculations still need to be done for a microscopic interpretation of the first-order magnetic transition [5].

Recently, first-principle electronic-structure calculations for hexagonal $\text{MnFe}(\text{P},\text{Si})$ revealed the coexistence of strong and weak magnetism in alternate atomic layers [7]. These atomic layers are formed by the preferential occupation of Mn and Fe on the $3g$ and $3f$ sites, respectively. While the first-order magnetic transition only causes a small reduction in the Mn moments on the $3g$ sites, the Fe moments vanish in the paramagnetic state. This implies that the electron density around the Fe sites changes drastically at the phase transition. The redistribution of electron density means that non-bonding electron density at the Fe site below T_C changes into a distribution which is hybridized with the nearest neighbors. Therefore, the competition between chemical bonding and moment formation was proposed to be at the basis of the first-order magnetic transition. A detailed study of the magnetic moments on different sites is needed to clarify the origin of the first-order magneto-elastic transition.

In this chapter, we focus on the determination of the magnetic structure and magnetic moments using neutron diffraction measurements on Mn-rich hexagonal $\text{Mn}_x\text{Fe}_{1.95-x}\text{P}_{0.50}\text{Si}_{0.50}$ compounds ($x > 1.0$) with special attention paid to compounds ($x < 1.4$) displaying a first-order magneto-elastic transition [11]. The reduction of the moment caused by the first-order magneto-elastic transition is discussed based on a sudden change in the interatomic distances at the transition temperature (T_C), an anomalous thermal expansion of the lattice parameters in the paramagnetic state and high-temperature magnetic-susceptibility measurement. We show a general physical

picture of high-moment to low-moment phase transition in the hexagonal Mn-Fe-P-Si compounds.

6.2. Experimental details

The Mn-rich $\text{Mn}_x\text{Fe}_{1.95-x}\text{P}_{0.50}\text{Si}_{0.50}$ compounds were prepared as described in Chapter 3. To make the samples more homogeneous, they were reannealed at 1373 K for 20 hours before being quenched in cold water. A Superconducting Quantum Interference Device (SQUID) magnetometer (Quantum Design MPMS 5XL) with the Reciprocating Sample Option (RSO) mode was employed for magnetic measurements below 400 K. High-temperature magnetic measurements were carried out using a vibrating sample magnetometer (VSM) (model LakeShore 7307) equipped with a high-temperature oven (model 73034). The neutron diffraction data were collected at the Bragg Institute of the Australian Nuclear Science and Technology Organization (ANSTO) on the ECHIDNA high-resolution powder diffractometer [12] with an incident wavelength of 1.622 Å for the $x = 1.20, 1.25, 1.30$ samples and at the Institut Laue-Langevin (ILL) on the D2B high-resolution powder diffractometer [13] with an incident wavelength of 1.595 Å for the $x = 1.95$ sample. The sample powder was contained in a vanadium can which is mounted in a cryostat. The measurements were carried out at fixed temperatures from 5 K to 400 K in zero field. X-ray diffraction patterns were collected at various temperatures in zero field using a PANalytical X-pert Pro diffractometer equipped with an Anton Paar TTK450 low-temperature chamber using Cu $K\alpha$ radiation, a secondary-beam flat-crystal monochromator and a multichannel X'celerator detector. Starting at 150 K each x-ray pattern was recorded at a constant temperature and the following one was recorded at a higher temperature, up to 500 K.

6.3. Magnetic structure of the Mn-rich compounds

All the samples studied display a para- to ferromagnetic transition. Figure 6.1 shows the neutron diffraction patterns for the $x = 1.30$ sample at 285 K in the paramagnetic state and 5 K in the ferromagnetic state. The Rietveld refinement carried out using the FullProf program [14] confirms hexagonal Fe_2P -type of structure (space group $P\bar{6}2m$).

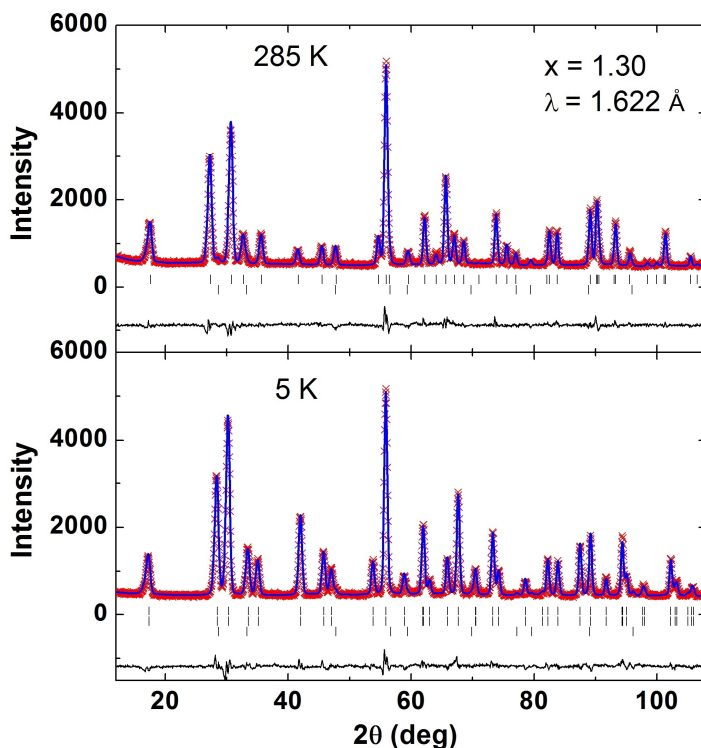


Figure 6.1. Observed (crosses), calculated (continuous lines) neutron diffraction patterns for hexagonal $\text{Mn}_{1.30}\text{Fe}_{0.65}\text{P}_{0.50}\text{Si}_{0.50}$ ($\lambda = 1.622 \text{ \AA}$) in the para- (upper plot) and ferromagnetic (lower plot) state. Differences are shown in the low part of the plots. The low-temperature diffraction patterns were fitted with the magnetic moments aligned in the a - b plane. The refined parameters are listed in Table 6.1. A very small amount of cubic $(\text{Mn,Fe})_3\text{Si}$ impurity phase is detected. Vertical lines indicate the diffraction peaks for the nuclear (top) and magnetic (middle, if any) structure of the main phase, and the impurity phase $(\text{Mn,Fe})_3\text{Si}$ (bottom).

The results listed in Table 6.1 show that Mn prefers the $3g$ sites while Fe favors the $3f$ sites. In the Mn-rich compounds some Mn will occupy the $3f$ sites (see Figure 6.2). The refinement also indicates that P and Si are randomly distributed on the $2c$ and $1b$ sites. Earlier studies on $\text{MnFe}(\text{P,Si})$ have pointed out that the magnetic moments prefer to be in the a - b plane rather than in the c direction as observed in Fe_2P [15,16]. In the present study, the low-temperature diffraction pattern fits well when the magnetic moments are

Table 6.1. Structural parameters of hexagonal $\text{Mn}_{1.30}\text{Fe}_{0.65}\text{P}_{0.50}\text{Si}_{0.50}$ and $\text{Mn}_{1.95}\text{P}_{0.50}\text{Si}_{0.50}$ in the paramagnetic and ferromagnetic state. Space group: $\overline{P}62m$. Atomic positions: $3g$ ($x_1, 0, 1/2$); $3f$ ($x_2, 0, 0$); $2c$ ($1/3, 2/3, 0$) and $1b$ ($0, 0, 1/2$). These parameters are derived from neutron diffraction patterns in Figures 6.1 and 6.3.

Refined parameters		$x = 1.30$		$x = 1.95$	
		285 K	5 K	400 K	10 K
		Paramagnetic	Ferromagnetic	Paramagnetic	Ferromagnetic
Unit cell	a (Å)	6.11390(4)	6.20611(4)	6.21889(4)	6.2145(1)
	c (Å)	3.42997(4)	3.29842(4)	3.38478(3)	3.3400(1)
	V (Å ³)	111.034(2)	110.021(2)	113.367(1)	111.709(4)
$3g$	x_1	0.5918(3)	0.5971(3)	0.5948(3)	0.5968(3)
	$n(\text{Mn})/n(\text{Fe})$	0.249/0.001(1)	0.249/0.001(1)	0.25/0	0.25/0
	B (Å ²)	0.83(4)	0.44(3)	0.89(4)	0.11(3)
	M (μ_B)	-	2.74(4)	-	2.61(3)
$3f$	x_2	0.2562(2)	0.2585(2)	0.2531(4)	0.2531(4)
	$n(\text{Fe})/n(\text{Mn})$	0.168/0.082(1)	0.168/0.082(1)	0/0.25	0/0.25
	B (Å ²)	0.81(3)	0.48(2)	1.14(3)	0.35(3)
	M (μ_B)	-	1.20(4)	-	0.36(3)
$2c$	$n(\text{P})/n(\text{Si})$	0.066/0.101(2)	0.066/0.101(2)	0.064/0.103(6)	0.064/0.103(6)
	B (Å ²)	0.39(4)	0.42(4)	0.59(5)	0.05(3)
$1b$	$n(\text{P})/n(\text{Si})$	0.059/0.024(2)	0.059/0.024(2)	0.061/0.022(6)	0.061/0.022(6)
	B (Å ²)	0.85(6)	0.53(4)	1.21(8)	0.30(4)
	R_p (%)	3.75	4.27	5.61	6.19
	wR_p (%)	4.92	5.52	7.31	7.99
	χ^2	3.42	4.16	4.15	4.99

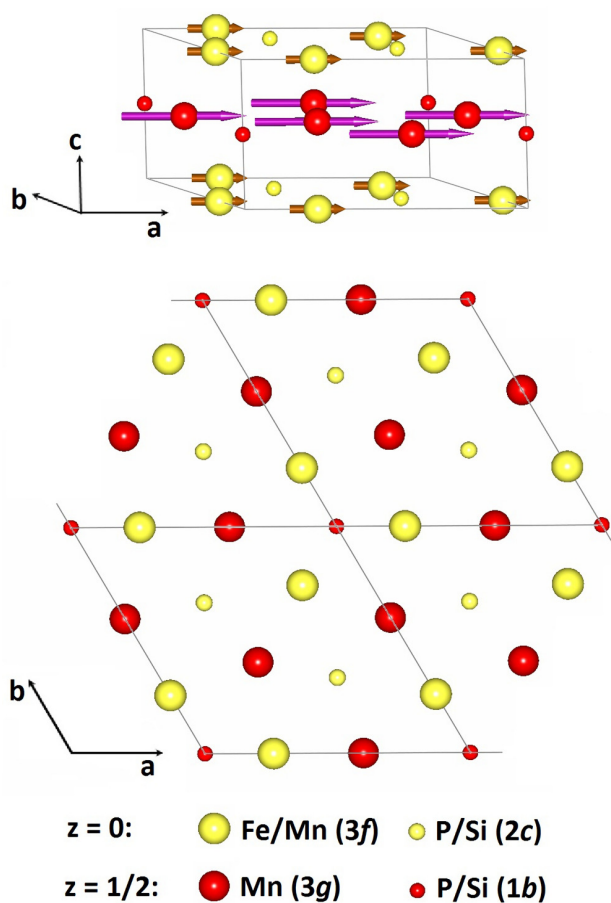


Figure 6.2. Atomic and spin arrangement within the unit cell of the Mn-rich $(\text{Mn,Fe})_2(\text{P,Si})$ compounds.

aligned in the a - b plane, indicating that replacing some Fe with Mn on the $3f$ sites does not affect the preferential alignment of the magnetic moments.

In the previous chapter, we have shown that for the Mn-rich $\text{Mn}_x\text{Fe}_{1.95-x}\text{P}_{0.50}\text{Si}_{0.50}$ compounds with increasing Mn/Fe ratios, the first-order magneto-elastic transition ($x < 1.40$) changes into a first-order magneto-structural transition via a second-order isostructural magnetic transition ($x \geq 1.40$) [11]. However, the hexagonal structure is stable in the ferromagnetic state at low temperature for all Mn/Fe ratios. By using neutron diffraction, we find that the alignment of the magnetic moments in the a - b

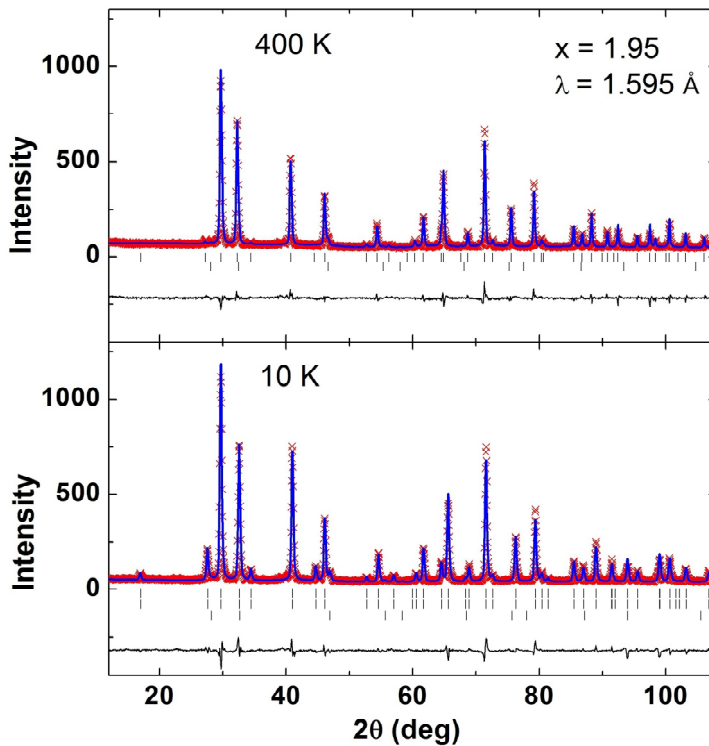


Figure 6.3. Observed (crosses), calculated (continuous lines) neutron diffraction patterns for hexagonal $\text{Mn}_{1.95}\text{P}_{0.50}\text{Si}_{0.50}$ ($\lambda = 1.595 \text{ \AA}$) in the para- (upper plot) and ferromagnetic (lower plot) state. Differences are shown in the low part of the plots. The low-temperature diffraction patterns were fitted with the magnetic moments aligned in the a - b plane. The refined parameters are listed in Table 6.1. A very small amount of cubic Mn_3Si impurity phase is detected. Vertical lines indicate the diffraction peaks for the nuclear (top) and magnetic (middle, if any) structure of the main phase, and the impurity phase Mn_3Si (bottom).

plane is also maintained until Fe is completely replaced by Mn on the $3f$ sites (see Figure 6.3 and Table 6.1). Interestingly, the $\text{Mn}(3g)$ moments remain constant at about $2.6 \mu_{\text{B}}$, while the $\text{Fe}/\text{Mn}(3f)$ moments decrease linearly from $1.5 \mu_{\text{B}}$ for $x = 1.20$ down to $0.4 \mu_{\text{B}}$ for $x = 1.95$ (see Figure 6.4). The total moments obtained from macroscopic measurements of the low-temperature saturation magnetization are very close to those derived from the neutron diffraction patterns at 3-10 K. The linear reduction of the

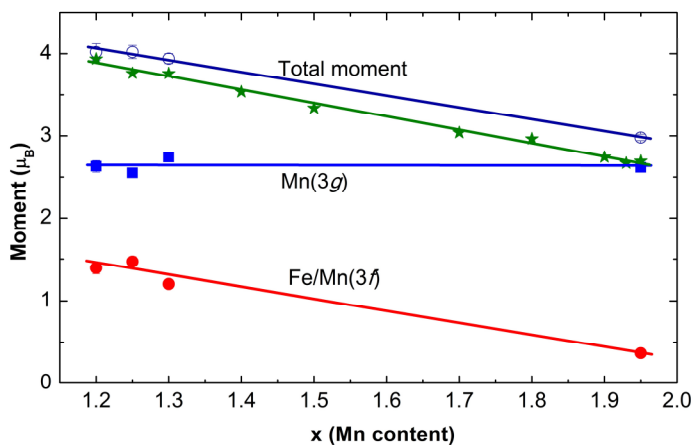


Figure 6.4. Composition dependence of the magnetic moments derived from the neutron diffraction patterns measured at 3-10 K for $\text{Mn}_x\text{Fe}_{1.95-x}\text{P}_{0.50}\text{Si}_{0.50}$. The total magnetic moments per formula unit (empty circles) are very close to those obtained from saturation magnetization measurements at 5 K (solid stars).

Fe/Mn(3f) moments for increasing x indicates that the Mn atom may develop a much lower magnetic moment than the Fe atom on the 3f sites.

6.4. Low-temperature ferromagnetic phase

To investigate the thermal evolutions of the magnetic and structural properties, neutron diffraction measurements were performed at different temperatures for the $x = 1.25$ sample exhibiting a first-order magneto-elastic transition. At 280 K, coexistence of the ferro- and paramagnetic phases was detected (see Figure 6.5). The fraction of the ferro- to paramagnetic phase is estimated to be 33:67. While the Mn(3g) moments show almost no change for increasing temperature, the Fe/Mn(3f) moments rapidly decrease near T_C (see Figure 6.6). This behavior is similar to that observed for $\text{Mn}_{1.1}\text{Fe}_{0.9}\text{P}_{0.8}\text{Ge}_{0.2}$ by Liu *et al.* [17]. This may be the signature for the reduction of magnetic moments, especially on the 3f sites, at T_C which we proposed based on theoretical calculations [7].

Figure 6.7 illustrates the temperature dependence of the lattice parameters and the distances between the magnetic atoms and the nearest neighbors for the $x = 1.25$

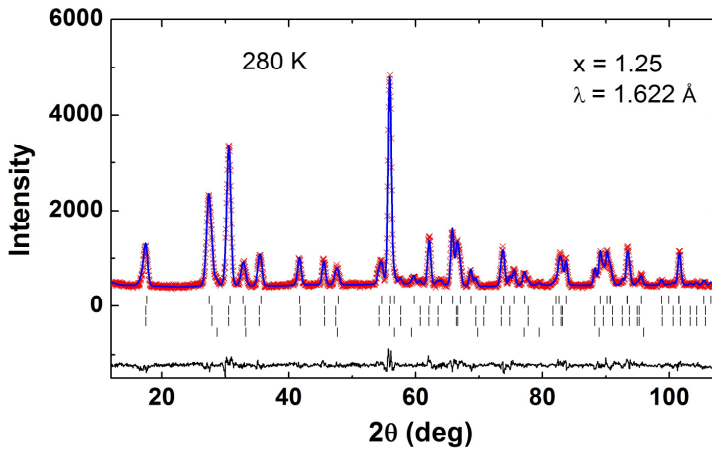


Figure 6.5. Observed (crosses) and calculated (continuous lines) neutron diffraction patterns for $\text{Mn}_{1.25}\text{Fe}_{0.70}\text{P}_{0.50}\text{Si}_{0.50}$ ($\lambda = 1.622 \text{ \AA}$) at 280 K at which the ferro- and paramagnetic phases are coexistent. The lattice parameters and interatomic distances between the magnetic atoms and their nearest neighbors are listed in Table 6.2. From top to bottom, vertical lines indicate the diffraction peaks for the nuclear structure of the paramagnetic phase, the nuclear and magnetic structure of the ferromagnetic phase, and the impurity phase $(\text{Mn,Fe})_3\text{Si}$.

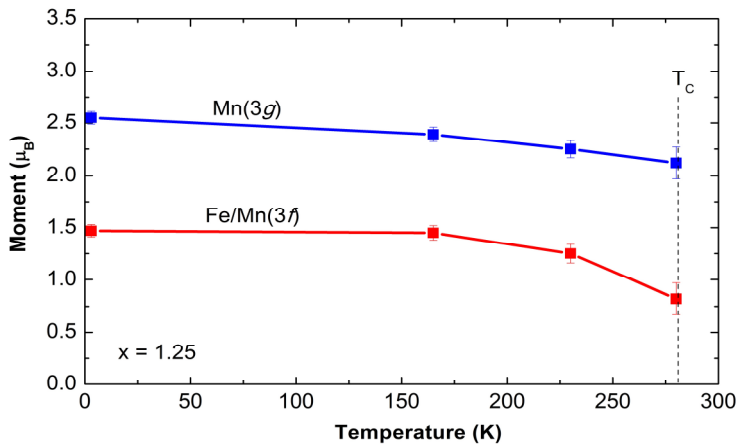


Figure 6.6. Ordered magnetic moments as a function of temperature derived from neutron diffraction patterns measured at fixed temperatures upon heating for $\text{Mn}_{1.25}\text{Fe}_{0.70}\text{P}_{0.50}\text{Si}_{0.50}$.

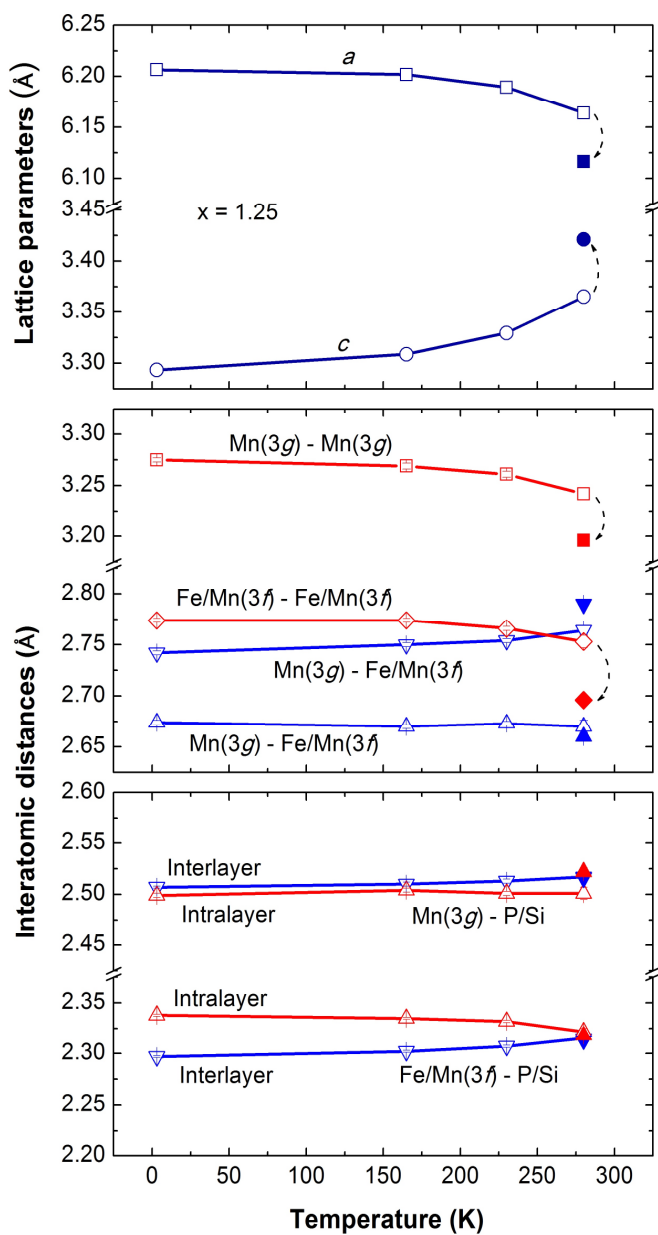


Figure 6.7. Lattice parameters and interatomic distances as a function of temperature derived from neutron diffraction patterns measured at fixed temperatures upon heating for $\text{Mn}_{1.25}\text{Fe}_{0.70}\text{P}_{0.50}\text{Si}_{0.50}$ in the ferromagnetic (empty symbols) and the paramagnetic (solid symbols) state.

sample. At temperatures below T_C , the lattice parameters change in opposite sense, i.e., the a parameter decreases while the c parameter increases with increasing temperature. This happens gradually near and below T_C and abruptly at the transition. The interatomic distances of the ferro- and paramagnetic phases at T_C are listed in Table 6.2. The mean Mn(3g)-P/Si and Fe/Mn(3f)-P/Si distances show almost no change at the transition temperature while sudden changes in the mean distances between the magnetic atoms are observed. It should be noted that the distances between the intralayer magnetic atoms drop strongly, enhancing the overlap between the $3d$ states and resulting in an abrupt reduction of the magnetic moments. However, the relative displacement of the Mn(3g) atoms during the transition is smaller than that of the Fe/Mn(3f) atoms. Furthermore, the intralayer Mn(3g)-Mn(3g) distance is larger than the intralayer Fe/Mn(3f)-Fe/Mn(3f) distance, and the Mn $3d$ electrons are more localized. Thus, the reduction of the Mn(3g) moments is much smaller than that of the Fe/Mn(3f) moments. In terms of mean distances, the reduction of the distances between the intralayer magnetic atoms makes the main contribution to the decrease in the magnetic moments, especially for the Fe/Mn(3f) layers. This may be a common feature for all other hexagonal Fe₂P-based materials exhibiting a first-order magneto-elastic transition [17]. The above arguments confirm our proposal for the competition between chemical bonding and moments. The observed behaviors of the moments and the lattice parameter below T_C indicate that the competition between chemical bonding and moments becomes stronger when T_C is approached.

6.5. High-temperature paramagnetic phase

The value of the lattice parameters obtained from the neutron diffraction measurements is in good agreement with that derived from x-ray diffraction patterns by using the Fullprof refinement program (see Figure 6.8). It should be noted that above T_C we observe non-linear temperature variations of the lattice parameters up to a certain temperature T_O while the volume increases linearly with temperature. It seems that the competition between chemical bonding and moments does not affect the volume because there is only a small volume change of about 0.1 % at T_C and a linear variation

Table 6.2. Lattice parameters and interatomic distances of $\text{Mn}_{1.25}\text{Fe}_{0.70}\text{P}_{0.50}\text{Si}_{0.50}$ at 280 K at which the ferro- and paramagnetic phases are coexistent. These data are derived from neutron diffraction pattern in Figure 6.5.

			280 K	
			Ferromagnetic	Paramagnetic
Lattice parameters				
a (Å)			6.1638(1)	6.1163(1)
c (Å)			3.3653(1)	3.4212(1)
V (Å ³)			110.726(4)	110.837(3)
Interatomic distances: Mn(3g)-nearest neighbors (Å)				
Mn(3g)-Mn(3g)	Intralayer	× 4	3.242(6)	3.196(4)
Mn(3g)-Fe/Mn(3f)	Interlayer	× 2	2.670(7)	2.660(3)
	Interlayer	× 4	2.764(6)	2.790(3)
	Mean distance		2.733(4)	2.747(2)
Mn(3g)-P/Si	Interlayer	× 4	2.517(3)	2.516(3)
	Intralayer	× 1	2.501(6)	2.522(4)
	Mean distance		2.514(2)	2.517(1)
Interatomic distances: Fe/Mn(3f)-nearest neighbors (Å)				
Fe/Mn(3f)-Fe/Mn(3f)	Intralayer	× 2	2.753(6)	2.696(3)
Fe/Mn(3f)-Mn(3g)	Interlayer	× 2	2.670(7)	2.660(3)
	Interlayer	× 4	2.764(6)	2.790(3)
	Mean distance		2.733(4)	2.747(2)
Fe/Mn(3f)-P/Si	Intralayer	× 2	2.322(3)	2.318(2)
	Interlayer	× 2	2.315(3)	2.313(2)
	Mean distance		2.319(2)	2.316(1)

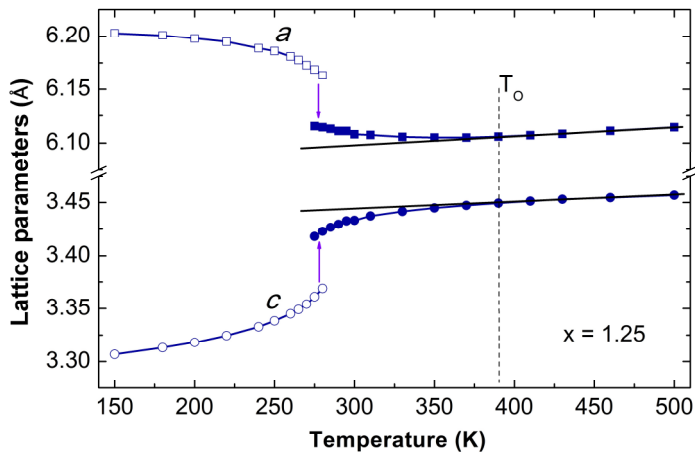


Figure 6.8. Lattice parameters as a function of temperature derived from x-ray diffraction patterns measured at fixed temperatures upon heating for $\text{Mn}_{1.25}\text{Fe}_{0.70}\text{P}_{0.50}\text{Si}_{0.50}$. The error bar is smaller than the size of the symbols.

of the volume is also observed at temperatures well below T_C . The value of T_O is determined to be about 390 K for the $x = 1.25$ sample. The non-linear variations of the lattice parameters imply that the competition between chemical bonding and moments still continues above T_C . Thus, for the Mn-rich compounds the Fe/Mn(3f) moments do not actually disappear at T_C , but their size significantly drops to a lower value. With further increasing temperature, the Fe/Mn(3f) moments gradually decrease and vanish at T_O while the Mn(3g) moments prevail above T_O . The evolution of these moments leads to the non-linear variations of the lattice parameters via the magneto-elastic coupling. Thus, T_O represents the onset of the moment formation on the 3f site.

In Figure 6.9 the magnetic susceptibility at temperatures above T_C is shown for the $x = 1.25$ sample. In the paramagnetic state, the magnetic susceptibility deviates from the Curie-Weiss law, up to $T^* \sim 630$ K. The paramagnetic Curie temperature (θ_p) is estimated to be about 400 K. The deviation of the susceptibility from the Curie-Weiss law is a general feature for hexagonal Fe_2P -based compounds and is often ascribed to short-range magnetic order [18-20]. We suggest that the decrease in the magnetic moments upon heating also contributes to the non-linear variation of the inverse

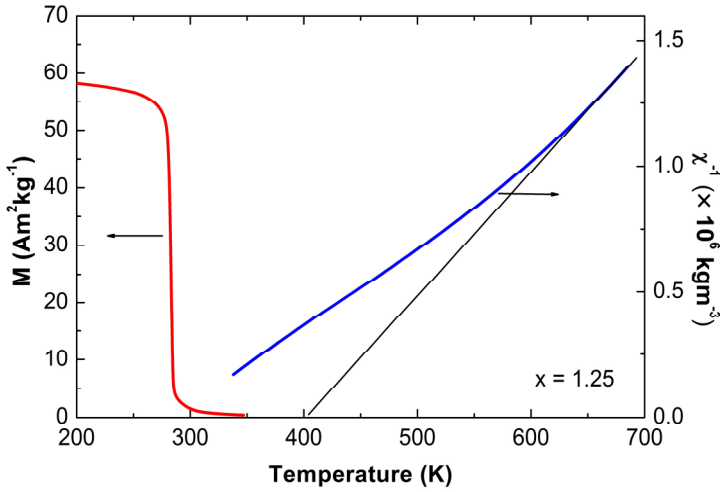


Figure 6.9. Magnetization and inverse susceptibility as a function of temperature measured in 0.1 T upon heating for $\text{Mn}_{1.25}\text{Fe}_{0.70}\text{P}_{0.50}\text{Si}_{0.50}$.

susceptibility at temperatures below T_0 . Using the Curie-Weiss law, the effective moment per formula unit (μ_{eff}) can be derived from the Curie constant (C) by:

$$C = \frac{\mu_0 N \mu_{\text{eff}}^2}{3k_B}, \quad (6.1)$$

where C is taken as inverse slope of the χ^{-1} - T curve, N is the number of formula units per mass unit, μ_0 is the magnetic constant and k_B is the Boltzmann constant. The Curie-Weiss fit above 630 K leads to a μ_{eff} of about $4.2 \mu_B$ for the $x = 1.25$ sample.

The Rhodes-Wohlfarth ratio q_c/q_s [21,22] is frequently used to distinguish between local moment and itinerant-electron ferromagnetism. Here, q_c and q_s are deduced from the Curie constant and from the low-temperature saturation magnetization, respectively, by using the formulas:

$$\mu_{\text{eff}}^2 = N_{\text{at}} q_c (q_c + 2) \mu_B^2 \quad (6.2)$$

and

$$\mu_s = q_s \mu_B, \quad (6.3)$$

where N_{at} is the number of magnetic atoms per formula unit and μ_s is the average ordered moment per magnetic atom at low temperature. For the $x = 1.25$ sample, the magnetization data and neutron diffraction measurements at 5 K give values for μ_s of $1.9 \mu_B$ and $2.1 \mu_B$, respectively. Assuming magnetic moments on the $3g$ and $3f$ sites, we obtain a q_c of 2.1 from Equation (6.2). The ratio q_c/q_s of about 1 seems to give an indication of localized magnetism [21,22]. Our calculation for $\text{MnFeP}_{0.85}\text{Ge}_{0.15}$ using the data reported by Yabuta *et al.* [20] also leads to the ratio q_c/q_s of 1. These results are in contradiction with the generally agreed description of the hexagonal Fe_2P -based alloys as itinerant-electron magnetic compounds. We propose that this deviation from the Rhodes-Wohlfarth plot may arise from the large difference between the high-moment and low-moment phase at low and high temperature, respectively (see Figure 6.10).

The low-moment phase which has only magnetic moments on the $3g$ sites only exists in the paramagnetic state at high temperature. It would become ferromagnetic at the para- to ferromagnetic transition temperature of the low-moment phase (T_C^{LM}) in the vicinity of θ_p . However, the ferromagnetic state of the low-moment phase is apparently not energetically preferred which indicates that the high-moment phase possesses a

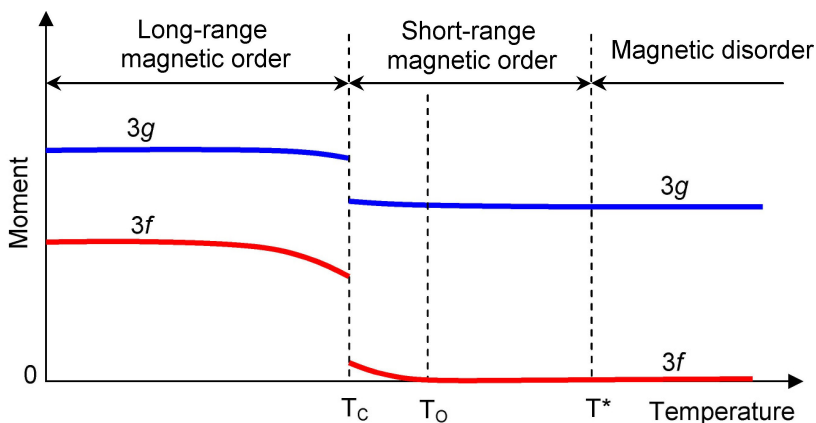


Figure 6.10. Sketch of the magnetic moments near the first-order magneto-elastic transition in hexagonal Mn-Fe-P-Si compounds. The itinerant moments are not to scale.

lower free energy under the same condition. From the Rhodes-Wohlfarth plot [21], q_c/q_s of an itinerant-electron ferromagnetic system with $T_C = 400$ K is roughly estimated to be about 1.7. For the $x = 1.25$ sample, since the low-moment phase has T_C^{LM} somewhat lower than 400 K, we may assume that the ratio q_c/q_s of the low-moment phase is 1.7. On the other hand, when we assume for the low-moment phase only magnetic moments on the $3g$ sites, q_c is found to be about 3.3. We therefore deduce $q_s \sim 1.9$, and $\mu_s \sim 1.9 \mu_B$. This value of μ_s reflects the magnitude of the ordered Mn($3g$) moments of the low-moment phase at low temperature. Hence, the first-order magneto-elastic transition for the $x = 1.25$ sample produces the Fe/Mn($3f$) moments of $1.5 \mu_B$ and the Mn($3g$) moments of $2.6 \mu_B$.

6.6. High/low-moment phase transition

The following physical picture evolves from our results: At high temperatures above T_O , Mn on the $3g$ sites carries magnetic moments and the $3f$ sites are predominantly in the bonding state. At lower temperatures, due to ferromagnetic exchange interaction between the Mn($3g$) moments the Fe/Mn($3f$) moments experience a local field that supports the non-bonding high-moment state. Furthermore, it can be seen that magnetic order is enhanced upon cooling. The high-temperature magnetic disorder at $T > T^*$ changes into a short-range magnetic order in the range of $T^* > T > T_C$ before developing into a long-range magnetic order at $T < T_C$ (see Figure 6.10). The enhanced magnetic order which gives rise to an increase in the exchange field therefore supports the formation and evolution of the Fe/Mn($3f$) moments. The exchange fields are critical for the moment formation and for the development of ferromagnetic order which occur at T_O and T_C , respectively. The short-range magnetic order therefore plays an important role in the mechanism of the first-order magneto-elastic transition in the hexagonal Mn-Fe-P-Si compounds. An external magnetic field can also support the non-bonding high-moment state and make the transition shift to higher temperature (see Figure 6.11). The value of dT_C/dB is estimated to be about 3.0-3.5 K/T for the $x = 1.25$ sample.

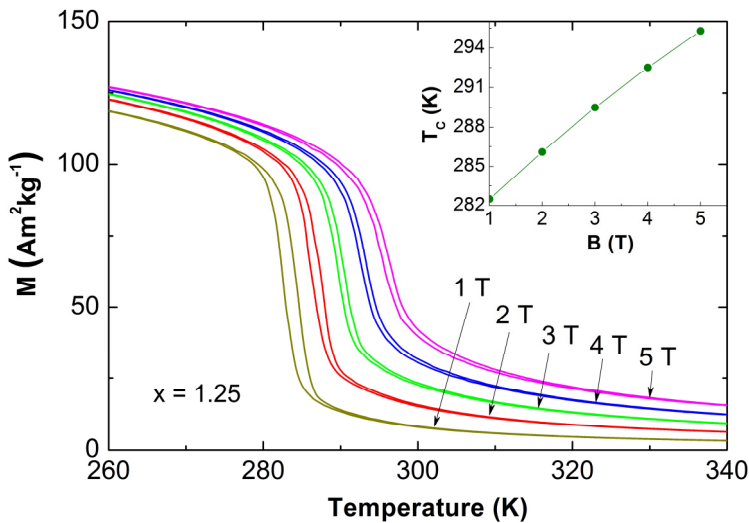


Figure 6.11. Temperature dependence of the magnetization measured in different magnetic fields (from 1 to 5 T) upon cooling and heating for $\text{Mn}_{1.25}\text{Fe}_{0.70}\text{P}_{0.50}\text{Si}_{0.50}$. The inset shows the field dependence of the transition temperature derived from the M - T curves measured upon cooling.

6.7. Conclusions

In summary, a general physical picture of the evolution of the magnetic moments has been put forward for the Mn-rich hexagonal Mn-Fe-P-Si compounds with first-order magneto-elastic transition. The substitution of Fe with Mn on the $3f$ sites does not cause a change in the Mn($3g$) magnetic moments but results in a linear decrease in the magnitude of the Fe/Mn($3f$) magnetic moments. The reduction of the magnetic moments with increasing temperature below the transition temperature has been observed by using neutron diffraction. The sudden change in the interatomic distances validates our description of high/low-moment phase transition which leads to the deviation from the Rhodes-Wohlfarth plot. The formation and gradual development of the magnetic moment on the $3f$ sites upon cooling give rise to anomalous thermal expansion in the paramagnetic state. By exploiting high-temperature magnetic-susceptibility measurement, we demonstrate the difference of the magnitude of the magnetic moments at low and high temperatures. This work also reveals the role of

short-range magnetic order in the development of the first-order magneto-elastic transition. These results support our proposal that the competition between the moments and chemical bonding is at the core of giant magnetocaloric effect displayed in the class of hexagonal Fe₂P-based materials with first-order magneto-elastic transition.

References

- [1] E. Brück, *J. Phys. D: Appl. Phys.* **38**, R381 (2005).
- [2] V. K. Pecharsky and K. A. Gschneidner, *Phys. Rev. Lett.* **78**, 4494 (1997).
- [3] A. Fujita, S. Fujieda, Y. Hasegawa, and K. Fukamichi, *Phys. Rev. B* **67**, 104416 (2003).
- [4] N. T. Trung, L. Zhang, L. Caron, K. H. J. Buschow, and E. Brück, *Appl. Phys. Lett.* **96**, 172504 (2010).
- [5] T. Krenke, E. Duman, M. Acet, E. F. Wassermann, X. Moya, L. Manosa, and A. Planes, *Nat. Mater.* **4**, 450 (2005).
- [6] O. Tegus, E. Brück, K. H. J. Buschow, and F. R. de Boer, *Nature* **415**, 150 (2002).
- [7] N. H. Dung, Z. Q. Ou, L. Caron, L. Zhang, D. T. C. Thanh, G. A. de Wijs, R. A. de Groot, K. H. J. Buschow, and E. Brück, *Adv. Energy Mater.* **1**, 1215 (2011).
- [8] D. Haskel, Y. B. Lee, B. N. Harmon, Z. Islam, J. C. Lang, G. Srajer, Y. Mudryk, K. A. Gschneidner, and V. K. Pecharsky, *Phys. Rev. Lett.* **98**, 247205 (2007).
- [9] M. D. Kuz'min and M. Richter, *Phys. Rev. B* **76**, 092401 (2007).
- [10] J. Lyubina, K. Nenkov, L. Schultz, and O. Gutfleisch, *Phys. Rev. Lett.* **101**, 177203 (2008).
- [11] N. H. Dung, L. Zhang, Z. Q. Ou, and E. Brück, *Appl. Phys. Lett.* **99**, 092511 (2011).
- [12] K. D. Liss, B. Hunter, M. Hagen, T. Noakes, and S. Kennedy, *Physica B* **385-386**, 1010 (2006).
- [13] A.W. Hewat, *Mater. Sci. Forum* **9**, 69 (1986).
- [14] J. Rodriguez-Carvajal, *Physica B* **192**, 55 (1993).
- [15] V. Hoglin, M. Hudl, M. Sahlberg, P. Nordblad, P. Beran, and Y. Andersson, *J. Solid State Chem.* **184**, 2434 (2011).
- [16] L. Zhang, O. Moze, K. Prokes, O. Tegus, and E. Brück, *J. Magn. Magn. Mater.* **290**, 679 (2005).
- [17] D. M. Liu, Q. Z. Huang, M. Yue, J. W. Lynn, L. J. Liu, Y. Chen, Z. H. Wu, and J. X. Zhang, *Phys. Rev. B* **80**, 174415 (2009).

-
- [18] O. Beckman and L. Lundgren, in *Handbook of Magnetic Materials*, edited by K. H. J. Buschow (Elsevier, Amsterdam 1991), Vol. 6, pp. 181.
- [19] R. Zach, M. Guillot, and R. Fruchart, *J. Magn. Magn. Mater.* **89**, 221 (1990).
- [20] H. Yabuta, K. Umeo, T. Takabatake, K. Koyama, and K. Watanabe, *J. Phys. Soc. Jpn.* **75**, 113707 (2006).
- [21] P. Rhodes and E. P. Wohlfarth, *Proc. R. Soc. A* **273**, 247 (1963).
- [22] E. P. Wohlfarth, *J. Magn. Magn. Mater.* **7**, 113 (1978).

Chapter 7

EFFECTS OF P:SI RATIO ON THE MAGNETIC AND STRUCTURAL PROPERTIES OF HEXAGONAL Mn-Fe-P-Si COMPOUNDS

7.1. Introduction

Replacing some Fe and P in Fe_2P , which displays a first-order isostructural magnetic transition from ferro- to paramagnetic state at 215 K [1,2], modifies the magnetic and structural properties, forming a family of promising magnetocaloric materials. Up to now, most studies have concentrated on hexagonal Mn-Fe-P-X ($X = \text{As}, \text{Ge}, \text{Si}$) compounds which can be obtained by partially replacing Fe and P with Mn and X, respectively, in Fe_2P [3-8]. In these compounds, Mn and Fe preferentially occupy the $3g$ and $3f$ sites, respectively, while P and X are randomly distributed on the $1b$ and $2c$ sites.

The partial replacement of P by Si in Fe_2P [9,10] results in a steep increase in the magnetic transition temperature T_C . 10 at% Si addition gives rise to an 60 % increase in T_C with an almost-linear change up to 35 at% Si.

On replacing Fe with Mn in Fe_2P , the ferromagnet is rapidly changed into an antiferromagnet and the hexagonal crystal lattice is transformed into an orthorhombic one before being changed back into the hexagonal structure in Mn-rich $(\text{Mn,Fe})_2\text{P}$ compounds [11]. Then, the substitution of P with Si not only enhances the ferromagnetic order but also stabilizes the hexagonal structure (see Chapter 5).

In this chapter, we show the effect of P:Si ratio on the magnetic and structural properties of the hexagonal Mn-Fe-P-Si compounds. The interplay between the magnetic and structural properties is also discussed.

7.2. Experimental details

$\text{Mn}_{1.25}\text{Fe}_{0.70}\text{P}_{1-y}\text{Si}_y$ ($y = 0.40\text{-}0.55$) compounds were prepared as described in Chapter 3. A SQUID magnetometer (Quantum Design MPMS 5XL) with the Reciprocating Sample Option (RSO) mode was employed for magnetic measurements. The x-ray diffraction patterns were collected at various temperatures in zero field using a PANalytical X-pert Pro diffractometer equipped with an Anton Paar TTK450 low temperature camera using Cu $K\alpha$ radiation, a secondary-beam flat-crystal monochromator and a multichannel X'celerator detector. Structure determination and refinement using the FullProf program show that all the samples crystallize in the hexagonal Fe_2P -type structure (space group $P\bar{6}2m$).

7.3. Magnetic properties

As seen in Figure 7.1a, the $\text{Mn}_{1.25}\text{Fe}_{0.70}\text{P}_{1-y}\text{Si}_y$ compounds display a sharp first-order magnetic transition. This is confirmed by the presence of thermal hysteresis ΔT_{hys} which is intrinsic to a first-order transition [12]. The ΔT_{hys} is reduced from 22 to 1 K when increasing y from 0.40 to 0.55. Note that the $y = 0.55$ sample exhibits a small thermal hysteresis ($\Delta T_{\text{hys}} \sim 1$ K) which is in line with a very small magnetic hysteresis as observed in Figure 7.2. A negative slope and an inflection point are observed from the Arrot plots in Figure 7.1b, indicating the first-order nature of the transitions. It can be seen that the observed features of the first-order phase transition become weaker on increasing y . This is supported by weakened characteristic of the first-order transition in specific heat curves (see Figure 7.3), i.e., the peak at T_C becomes lower and broader when y increases. These observations provide an indication that the magnetic transition is controlled to be close to the border between first-order and second-order transition. Then, a small ΔT_{hys} can be obtained as mentioned in Chapter 5. Details of the behavior of the isothermal magnetic field-induced entropy changes are discussed in Chapter 8.

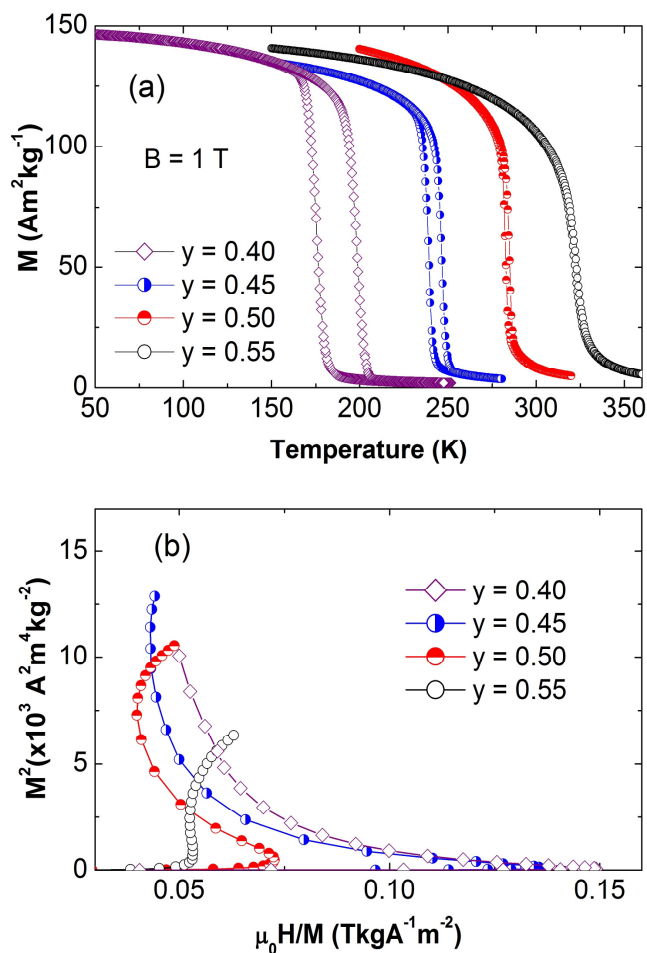


Figure 7.1. (a) Magnetization curves measured on heating and cooling in a magnetic field of 1 T and (b) Arrot plots in the vicinity of T_C for the $\text{Mn}_{1.25}\text{Fe}_{0.70}\text{P}_{1-y}\text{Si}_y$ compounds.

The magnetic ordering temperature T_C derived from the isofield magnetization curves and the saturation moments measured at 5 K are shown in Figure 7.4. It can be seen that T_C on heating increases almost linearly when increasing y . This was also found for substitution series of $\text{MnFe}(\text{P},\text{As})$ and $\text{Mn}_{1.1}\text{Fe}_{0.9}(\text{P},\text{Ge})$ [7,13,14]. In this study, 10 at% Si addition leads to an increase of about 80 K in T_C for the $\text{Mn}_{1.25}\text{Fe}_{0.70}(\text{P},\text{Si})$ compounds. This value is higher than that of $\text{MnFe}(\text{P},\text{As})$ (about 40 K for 10 at% As

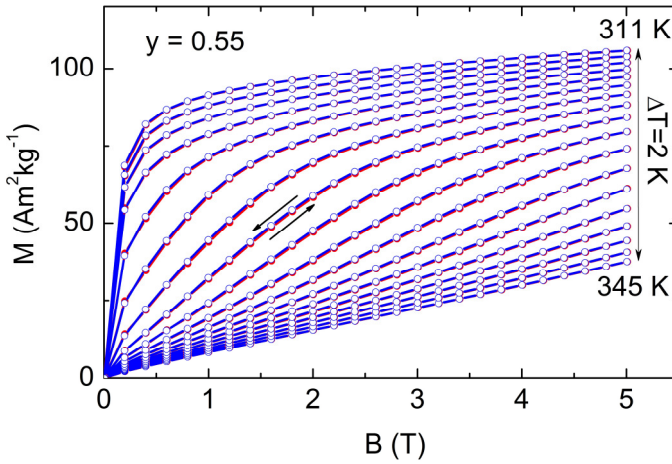


Figure 7.2. Magnetic isotherms measured in increasing and decreasing field for $\text{Mn}_{1.25}\text{Fe}_{0.70}\text{P}_{0.45}\text{Si}_{0.55}$ in the vicinity of the magnetic ordering temperature. The reversible magnetic isotherms indicate a negligible hysteresis.

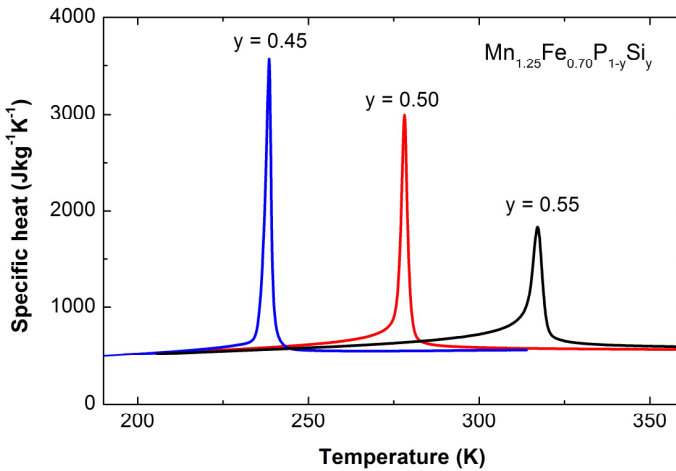


Figure 7.3. Specific heat of the $\text{Mn}_{1.25}\text{Fe}_{0.70}\text{P}_{1-y}\text{Si}_y$ compounds measured in zero field upon cooling.

addition) [13] and smaller than that of $\text{Mn}_{1.1}\text{Fe}_{0.9}(\text{P},\text{Ge})$ (120 K for 10 at% Ge addition) [7,14].

Although T_C rises with increasing Si content, the total magnetic moment is almost constant. For the $\text{Mn}_{1.25}\text{Fe}_{0.70}(\text{P},\text{Si})$ compounds, the value of the magnetic moment is

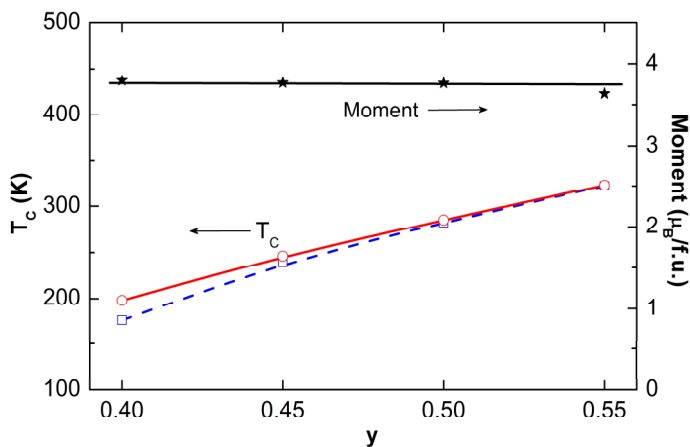


Figure 7.4. Magnetic ordering temperature on cooling (empty squares) and heating (empty circles), and total magnetic moment per formula unit (solid stars) of the $\text{Mn}_{1.25}\text{Fe}_{0.70}\text{P}_{1-y}\text{Si}_y$ compounds.

about $3.8 \mu_{\text{B}}$. In $\text{MnFe}(\text{P},\text{As})$, the total magnetic moment was also found to be independent of As content and is $4.1 \mu_{\text{B}}$ [15]. Neutron diffraction and low-temperature saturation magnetization measurements for $\text{MnFeP}_{0.5}\text{Si}_{0.5}$ [16,17] show that the value of the total moment is $4.4 \mu_{\text{B}}$. This value is very close to the value of $4.3 \mu_{\text{B}}$ extrapolated from the total moment versus Mn content curve for $\text{Mn}_x\text{Fe}_{1.95-x}\text{P}_{0.50}\text{Si}_{0.50}$ (see Figure 6.4, Chapter 6). Hence, the total magnetic moment of $\text{MnFe}(\text{P},\text{As})$ may be somewhat lower than that of $\text{MnFe}(\text{P},\text{Si})$. With the same Mn:Fe ratio, the replacement of P by Si may result in a somewhat larger total moment than the replacement of P by As. The observed behavior of the total moment of the $\text{Mn}_{1.25}\text{Fe}_{0.70}\text{P}_{1-y}\text{Si}_y$ compounds is not in agreement with theoretical calculations which predicted an increase in the magnetic moment with increasing y [5].

7.4. Structural properties

Figure 7.5a displays the lattice parameters as a function of Si content at 150 and 500 K. We find that in the $\text{Mn}_{1.25}\text{Fe}_{0.70}\text{P}_{1-y}\text{Si}_y$ compounds, the a and c parameters change almost linearly with increasing Si content but in opposite sense, i.e., the a parameter increases while the c parameter decreases, leading to a decrease in c/a ratio. The slopes

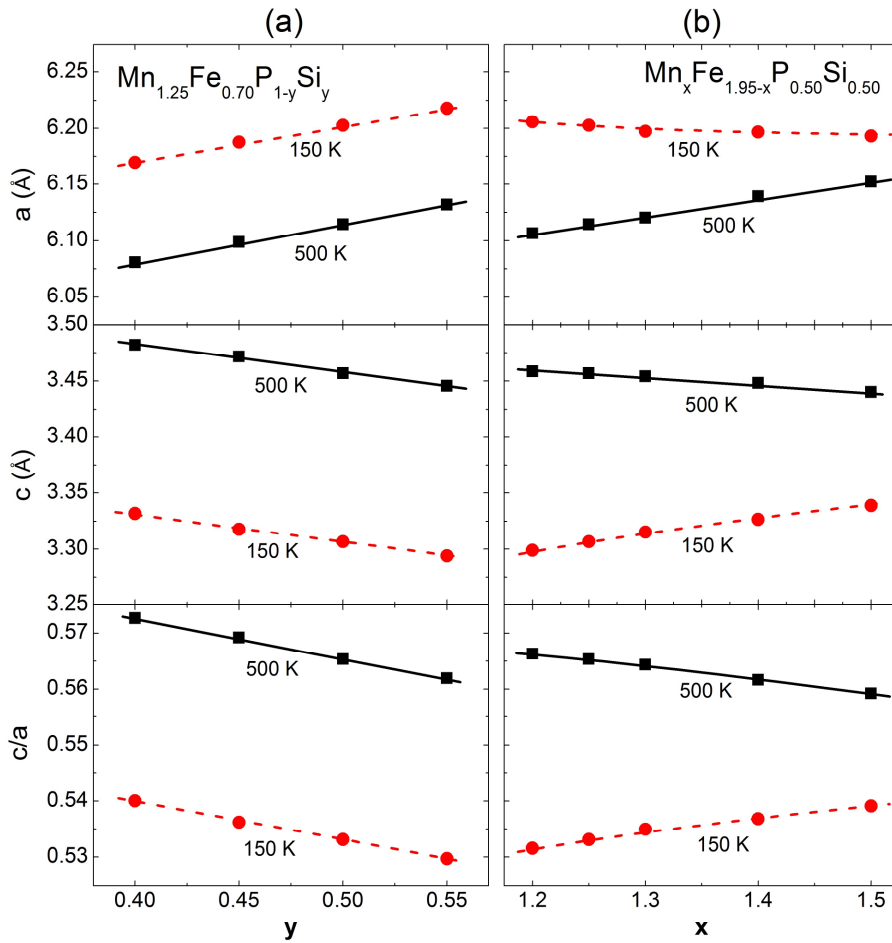


Figure 7.5. Lattice parameters as a function of composition for the (a) $\text{Mn}_{1.25}\text{Fe}_{0.70}\text{P}_{1-y}\text{Si}_y$ and (b) $\text{Mn}_x\text{Fe}_{1.95-x}\text{P}_{0.50}\text{Si}_{0.50}$ compounds at 150 K (ferromagnetic state) and 500 K (paramagnetic state).

of the lattice parameter versus Si content curves in the paramagnetic state are the same as those in the ferromagnetic state. However, this does not hold for Mn addition. Shown in Figure 7.5b are the lattice parameters as a function of Mn content for $\text{Mn}_x\text{Fe}_{1.95-x}\text{P}_{0.50}\text{Si}_{0.50}$ compounds at 150 and 500 K. It can be seen that the a (c) parameter increases (decreases) in the paramagnetic state but decreases (increases) in the ferromagnetic state with increasing Mn content. Hence, we can realize that magnetic order strongly affects the evolution of the lattice parameters when replacing

Fe with Mn. For the Si addition, the relative change of the lattice parameters in response to a change in Si content is the same in the ferro- and paramagnetic state. This observation is also found in Fe-rich Mn-Fe-P-Si compounds [18]. Hence, the differences of the lattice parameters at low and high temperatures are independent of Si content but depend on Mn:Fe ratio. For the Mn-rich hexagonal Mn-Fe-P-Si compounds, these differences are smaller if the Mn:Fe ratio is larger.

Recently, using first-principle theory for Si-doped Fe₂P, Delczeg-Czirjak *et. al.* [10] decomposed the change in the total magnetic exchange coupling upon doping into chemical and structural contributions. They showed that the structural contribution is important and the reduced c/a ratio caused by Si doping strengthens the Fe(3g)-Fe(3f) interlayer exchange coupling. This may still hold for the Mn_{1.25}Fe_{0.70}P_{1-y}Si_y compounds. The observed decrease of c/a may contribute to the increase in T_C due to increased Mn(3g)-Fe/Mn(3f) interlayer exchange coupling.

In the ferromagnetic state, since c/a increases with temperature (see Figures 6.7 and 6.8, Chapter 6), the Mn(3g)-Fe/Mn(3f) interlayer interactions would be reduced upon heating. Furthermore, the competition between moment formation and chemical bonding is proposed to be at the core of the first-order transition [5]. Therefore T_C depends not only on exchange coupling but also on chemical bonding. The determination of T_C based on theoretical calculations is then more complicated. With only contribution from exchange coupling, the calculated value of T_C may deviate from the experimental value. Delczeg-Czirjak *et. al.* [10] pointed out that compared with Fe₂P, 10 at% Si addition causes only an increase of 11 % in the total exchange coupling. This calculated value is much smaller than the experimental change of T_C .

7.5. Conclusions

In summary, the effects of P:Si ratio on the magnetic and structural properties in the Mn-Fe-P-Si compounds have been investigated. The replacement of P by Si brings the first-order transition close to the border with second-order transition, leading to a small hysteresis. We also indicated that the difference of the lattice parameters at low and high temperature and the total magnetic moment are independent of Si content. The

reduction of c/a caused by the Si addition is proposed to contribute to the increase in T_C via increased Mn(3g)-Fe/Mn(3f) interlayer exchange coupling. We suggest that for the determination of T_C chemical bonding also needs to be taken into account.

References

- [1] R. Wäppling, L. Häggström, T. Ericsson, S. Devanarayanan, E. Karlsson, B. Carlsson, and S. Rundqvist, *J. Solid State Chem.* **13**, 258 (1975).
- [2] H. Fujii, T. Hökabe, T. Kamigaichi, and T. Okamoto, *J. Phys. Soc. Jpn.* **43**, 41 (1977).
- [3] E. Brück, in *Handbook of Magnetic Materials*, edited by K. H. J. Buschow (Elsevier, Amsterdam, 2007), Vol. 17, pp. 235.
- [4] O. Tegus, E. Brück, K. H. J. Buschow, and F. R. de Boer, *Nature* **415**, 150 (2002).
- [5] N. H. Dung, Z. Q. Ou, L. Caron, L. Zhang, D. T. Cam Thanh, G. A. de Wijs, R. A. de Groot, K. H. J. Buschow, and E. Brück, *Adv. Energy Mater.* **1**, 1215 (2011).
- [6] N. H. Dung, L. Zhang, Z. Q. Ou, and E. Brück, *Appl. Phys. Lett.* **99**, 092511 (2011).
- [7] N. T. Trung, Z. Q. Ou, T. J. Gortenmulder, O. Tegus, K. H. J. Buschow, and E. Brück, *Appl. Phys. Lett.* **94**, 102513 (2009).
- [8] D. Liu, M. Yue, J. Zhang, T. M. McQueen, J. W. Lynn, X. Wang, Y. Chen, J. Li, R. J. Cava, X. Liu, Z. Altounian, and Q. Huang, *Phys. Rev. B* **79**, 014435 (2009).
- [9] P. Jernberg, A. A. Yousif, L. Häggström, and Y. Andersson, *J. Solid State Chem.* **53**, 313 (1984).
- [10] E. K. Delczeg-Czirjak, Z. GerCSI, L. Bergqvist, O. Eriksson, L. Szunyogh, P. Nordblad, B. Johansson, and L. Vitos, *Phys. Rev. B* **85**, 224435 (2012).
- [11] S. Nagase, H. Watanabe and T. Shinohara, *J. Phys. Soc. Jpn.* **34**, 908 (1973).
- [12] A. M. Tishin and Y. I. Spichkin, *The magnetocaloric effect and its applications* (Institute of Physics Publishing, Bristol, 2003).
- [13] O. Tegus, E. Brück, and W. Dagula, *Physica B* **319**, 174 (2002).
- [14] W. Dagula, O. Tegus, B. Fuquan, L. Zhang, P. Z. Si, M. Zhang, W. S. Zhang, E. Brück, F. R. de Boer, and K. H. J. Buschow, *IEEE Trans. Magn.* **41**, 2778 (2005).
- [15] O. Beckman and L. Lundgren, in *Handbook of Magnetic Materials*, edited by K. H. J. Buschow (Elsevier, Amsterdam, 1991), Vol. 6, pp. 181.
- [16] V. Hoglin, M. Hudl, M. Sahlberg, P. Nordblad, P. Beran, and Y. Andersson, *J. Solid State Chem.* **184**, 2434 (2011).

-
- [17] M. Hudl, L. Haggstrom, E. K. Delczeg-Czirjak, V. Hoglin, M. Sahlberg, L. Vitos, O. Eriksson, P. Nordblad, and Y. Andersson, *Appl. Phys. Lett.* **99**, 152502 (2011).
- [18] Z. Q. Ou, L. Zhang, N. H. Dung, L. van Eijck, M. Avdeev, A. Mulders, N. H. van Dijk, and E. Brück, *unpublished*.

Chapter 8

MAGNETO-ELASTIC COUPLING AND MAGNETOCALORIC EFFECT IN HEXAGONAL Mn-Fe-P-Si COMPOUNDS

8.1. Introduction

Magnetocaloric materials are the key to eco-friendly magnetic refrigeration technology [1-3]. Advanced magnetocaloric materials take advantage of a first-order magnetic transition because the first-order magnetic transition is often associated with a change in crystal lattice which enhances magnetocaloric effects. Therefore magnetocaloric materials often display magneto-elastic or magneto-structural transitions [4]. However, thermal or magnetic hysteresis, which is intrinsic to a first-order magnetic transition, is detrimental to the refrigeration-cycle efficiency [5]. Many efforts have been made to reduce the hysteresis of the magnetocaloric materials [1,3-7].

Magneto-elastic coupling in a solid may result in a change of shape or volume due to an applied magnetic field or a change in temperature. The effect is often the most pronounced if the state of the solid is close to a phase transition. However, the effect is small for most magnetic materials. Only certain materials possess a strong magneto-elastic coupling. These include some ferromagnetic shape memory [8], multiferroic [9] and magnetocaloric materials [10-12].

Fe₂P-based compounds display giant magnetocaloric effects [1,2,6,7]. It is well known that they often undergo a first-order magneto-elastic transition at which there are

sudden changes in the a and c parameters ($\Delta a/a$ and $\Delta c/c$, respectively) but the volume hardly changes at the transition temperature [1]. In Chapter 4, we report $(\text{Mn,Fe})_{1.95}(\text{P,Si})$ compounds with hexagonal Fe_2P -type structure as promising materials for room-temperature refrigeration applications because they display a giant magnetocaloric effect and a small hysteresis in a large temperature range around room temperature. Additionally, these compounds consist of abundant, cheap and non-toxic elements. Here we report on $\text{Mn}_x\text{Fe}_{1.95-x}\text{P}_{1-y}\text{Si}_y$ ($x = 1.20-1.30$, $y = 0.45-0.55$) compounds with emphasis on the correlation between the magnetic and structural properties. The magnetocaloric effects are discussed in relation to the magneto-elastic coupling. A preliminary comparison between Mn-Fe-P-X ($X = \text{As, Ge, Si}$) compounds is conducted to investigate the role of the p -electron element.

8.2. Experimental details

The $\text{Mn}_x\text{Fe}_{1.95-x}\text{P}_{0.50}\text{Si}_{0.50}$ ($x = 1.20-1.30$) and $\text{Mn}_{1.25}\text{Fe}_{0.70}\text{P}_{1-y}\text{Si}_y$ ($y = 0.45-0.55$) compounds were prepared as described in Chapter 3. Magnetic measurements were carried out using a SQUID magnetometer (Quantum Design MPMS 5XL) with the Reciprocating Sample Option (RSO) mode. The x-ray diffraction patterns were collected at various temperatures in zero field using a PANalytical X-pert Pro diffractometer with $\text{Cu K}\alpha$ radiation, a secondary-beam flat-crystal monochromator, a multichannel X'celerator detector and an Anton Paar TTK450 low temperature camera. Each x-ray pattern was recorded at a constant temperature and the following one was recorded at a higher temperature. Structure determination and refinement using FullProf [13] show that all the samples crystallize in the hexagonal Fe_2P -type structure (space group $P\bar{6}2m$).

8.3. Magneto-elastic coupling and hysteresis

From the x-ray patterns we derive the temperature dependence of the lattice parameters of the hexagonal unit cell as depicted in Figure 8.1. The most prominent feature in Figure 8.1 is the discontinuous jump in lattice parameters that shifts to lower and higher temperature with increasing x and y , respectively. At these transitions we

observe coexistence of two phases with the same hexagonal symmetry but different lattice parameters. All the samples show the same trend in the thermal evolution of the lattice parameters. Below the transition temperature (T_C),¹ the a parameter decreases while the c parameter increases with increasing temperature. This happens gradually near and below T_C and abruptly at the transition.

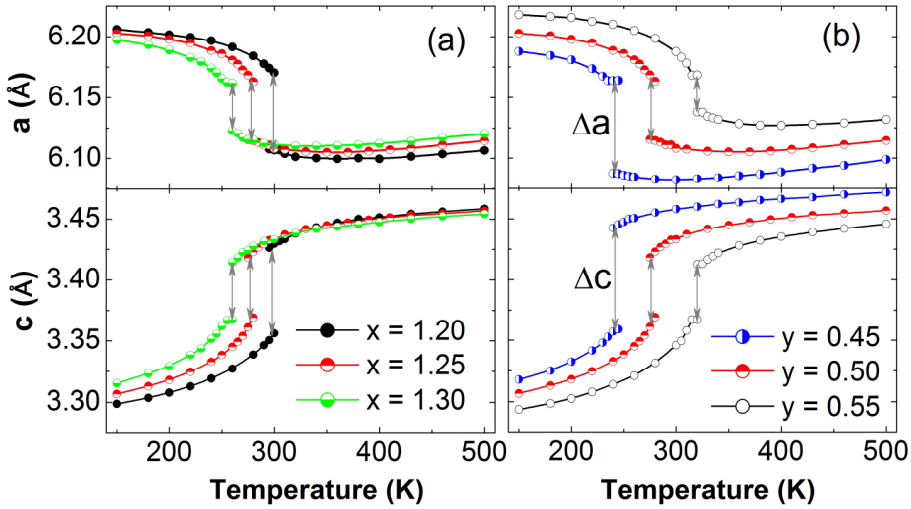


Figure 8.1. Lattice parameters a and c as a function of temperature derived from x-ray diffraction patterns measured in zero magnetic field upon heating for the (a) $\text{Mn}_x\text{Fe}_{1.95-x}\text{P}_{0.50}\text{Si}_{0.50}$ and (b) $\text{Mn}_{1.25}\text{Fe}_{0.70}\text{P}_{1-y}\text{Si}_y$ compounds. The symbol size is larger than the error bar.

Though the lattice parameters change drastically at the transition, only a small volume increase of about 0.1 % with increasing temperature was observed. That is because the a and c parameters change in opposite sense. Thus, Δa and Δc have opposite signs. Note that the magnitude of Δa and Δc decreases with increasing Mn and Si content (see Figure 8.1). For the $\text{Mn}_x\text{Fe}_{1.95-x}\text{P}_{0.50}\text{Si}_{0.50}$ compounds, the $|\Delta a/a|$ and $|\Delta c/c|$ change from 1.1 % and 2.2 % to 0.7 % and 1.5 %, respectively, when x increases from 1.20 to 1.30.

¹Transition temperature (T_C) is understood as zero-field T_C if the magnitude of the magnetic field is not mentioned.

For $\text{Mn}_{1.25}\text{Fe}_{0.70}\text{P}_{1-y}\text{Si}_y$ compounds, the $|\Delta a/a|$ and $|\Delta c/c|$ change from 1.3 % and 2.5 % to 0.5 % and 1.2 %, respectively, on increasing y from 0.45 to 0.55 (see Table 8.1).

Figure 8.2 shows the temperature dependence of the magnetization measured in a magnetic field of 1 T for the $\text{Mn}_x\text{Fe}_{1.95-x}\text{P}_{0.50}\text{Si}_{0.50}$ and $\text{Mn}_{1.25}\text{Fe}_{0.70}\text{P}_{1-y}\text{Si}_y$ compounds. Sharp ferro- to paramagnetic transitions are observed for these samples. The thermal hysteresis (ΔT_{hys}) reduces from 5 K down to 1 K on increasing x from 1.20 to 1.30, and from 7 K down to 1 K when y increases from 0.45 to 0.55. Comparing the data listed in Table 8.1 we find that the magnitude of the hysteresis can be correlated with the magnitude of the Δa and Δc steps. The larger the $|\Delta a/a|$ and $|\Delta c/c|$, the larger the hysteresis. It is well known that the hysteresis originates from the energy barrier of the first-order magnetic transition. Thus, the energy barrier is high when the lattice parameter difference between the ferro- and paramagnetic phases at T_C is large.

Table 8.1. Magnetic ordering temperature (T_C) in 1 T derived from the magnetization curves measured on heating, thermal hysteresis (ΔT_{hys}) derived from the magnetization curves measured in 1 T on cooling and heating, the maximal intrinsic value of the magnetic entropy change (ΔS_m) for $\Delta B = 0.5$ T, and the discontinuous changes of the lattice parameters $|\Delta a/a|$ and $|\Delta c/c|$ at the transition for the $\text{Mn}_x\text{Fe}_{1.95-x}\text{P}_{1-y}\text{Si}_y$ compounds. Note: the thermal hysteresis is not corrected for thermal lag of the equipment that results under the same conditions for Gd in a thermal hysteresis of 0.5 K.

Composition		T_C (K)	$ \Delta S_m $ ($\text{Jkg}^{-1}\text{K}^{-1}$)	ΔT_{hys} (K)	$ \Delta a/a $ (%)	$ \Delta c/c $ (%)
$y = 0.50$	$x = 1.20$	304	~ 31	5	1.1	2.2
	$x = 1.25$	285	~ 27	2	0.8	1.7
	$x = 1.30$	269	~ 21	1	0.7	1.5
$x = 1.25$	$y = 0.45$	246	~ 33	7	1.3	2.5
	$y = 0.50$	285	~ 27	2	0.8	1.7
	$y = 0.55$	323	~ 19	1	0.5	1.2

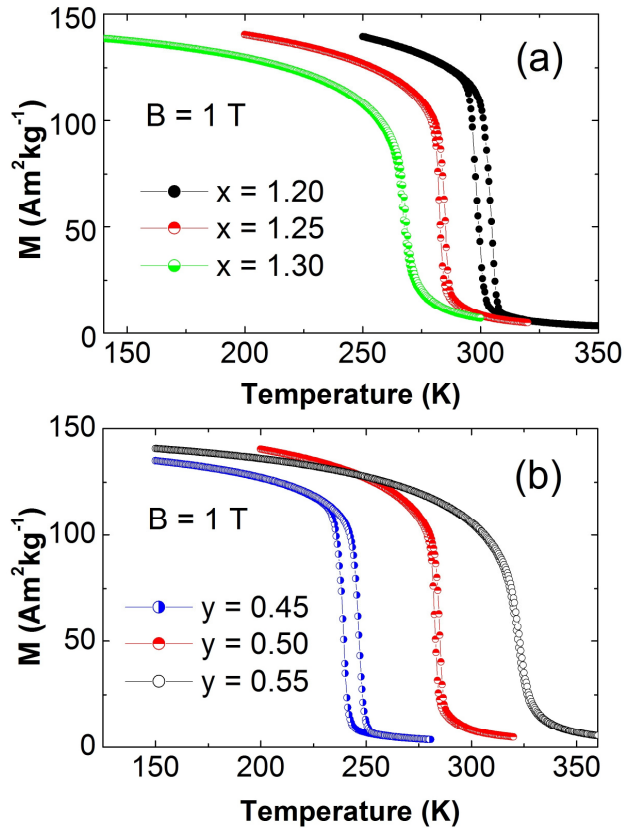


Figure 8.2. Temperature dependence of the magnetization measured in a magnetic field of 1 T upon cooling and heating for the (a) $\text{Mn}_x\text{Fe}_{1.95-x}\text{P}_{0.50}\text{Si}_{0.50}$ and (b) $\text{Mn}_{1.25}\text{Fe}_{0.70}\text{P}_{1-y}\text{Si}_y$ compounds.

8.4. Magneto-elastic coupling and magnetic entropy change

With strong magneto-elastic coupling, we expect to obtain a large magnetocaloric effect at the first-order magnetic transition. In this study, magnetic entropy change (ΔS_m) is derived from magnetic isotherms using the Maxwell relations [1]. Large $|\Delta S_m|$ can be achieved if the field-induced transition is complete, i.e., the whole sample is converted from one state to another. The ΔS_m observed will not reflect the intrinsic value of the ΔS_m of the compounds if the field-induced transition is incomplete. Thus, intrinsic $|\Delta S_m|$ obtained from complete field-induced transition is an important

parameter to evaluate and compare the size of the magnetocaloric effect of the compounds.

Figure 8.3a shows the magnetic isotherms measured in increasing field from the paramagnetic state for $x = 1.25$ and $y = 0.50$ as a representative sample. Each M - B curve was measured after the sample was zero-field cooled from the paramagnetic state at high temperature in order to avoid the coexistence of the ferro- and paramagnetic

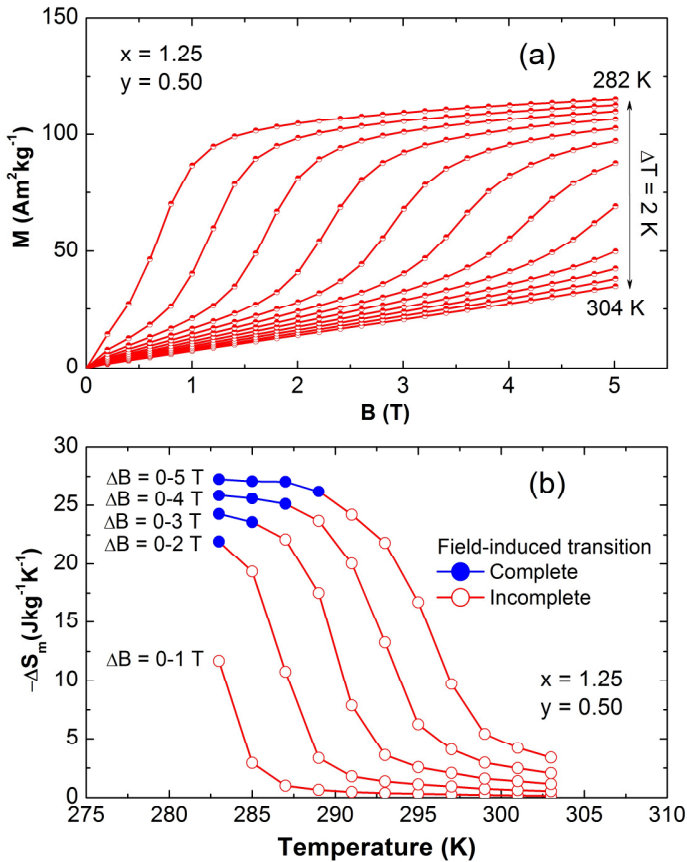


Figure 8.3. (a) Magnetic isotherms measured in increasing field from the paramagnetic state in the vicinity of the transition temperature and (b) temperature dependence of the magnetic entropy change derived from the magnetic isotherms for the $\text{Mn}_{1.25}\text{Fe}_{0.70}\text{P}_{0.50}\text{Si}_{0.50}$ compound ($x = 1.25$ and $y = 0.50$).

phases from the previous M - B measurement [14]. One can see that a low magnetic field is not sufficient to complete the field-induced transition. There is a critical magnetic field which drives the field-induced transition to completion [15]. The critical magnetic field tends to shift to higher values on increasing the measurement temperature. The values of ΔS_m as derived from the magnetic isotherms are shown in Figure 8.3b. Even though the field-induced transition is complete, the alignment of the magnetic moments may be influenced by thermal fluctuations. A high magnetic field tends to further align the magnetic moments. Thus, the intrinsic $|\Delta S_m|$ increases slowly with increasing magnetic field above the critical magnetic field. However, this increase in $|\Delta S_m|$ above the critical magnetic field is much less compared with that obtained from the field-induced transition. As can be seen from Figure 8.3a the field-induced transition becomes less pronounced for increasing temperature. Thus, the intrinsic $|\Delta S_m|$ will be larger at temperatures close to T_C (see Figure 8.3b).

Shown in Figure 8.4 is the magnetic field dependence of $|\Delta S_m|$ for the $\text{Mn}_x\text{Fe}_{1.95-x}\text{P}_{0.50}\text{Si}_{0.50}$ and $\text{Mn}_{1.25}\text{Fe}_{0.75}\text{P}_{1-y}\text{Si}_y$ compounds at temperatures near their T_C s. Obviously, field-induced transitions are complete with increasing field from 0 to 5 T for all the compounds. The $|\Delta S_m|$ for a field change of 0-5 T near the T_C s as seen in Figure 8.4 can be considered to be approximately the maximal intrinsic $|\Delta S_m|$ of the compounds under the same magnetic field change. We have clear indications that the maximal intrinsic $|\Delta S_m|$ is larger for the compound with lower x or y , pointing to the correlation of the size of the magnetocaloric effect with the $|\Delta a/a|$ and $|\Delta c/c|$ (see Table 8.1).

Very recently, Gschneidner *et al.* [15] proposed that the larger the volume change at the transition, the larger the $|\Delta S_m|$. For the Mn-Fe-P-Si compounds displaying a first-order magneto-elastic transition, there are changes in the lattice parameters at the transition but the volume hardly changes. Moreover, the changes in the lattice parameters give rise to redistribution of the valence electron and chemical bonding, and simultaneously cause a variation of the magnitude of the magnetic moments, exchange coupling and magnetic order. Thus, the correlation of the $|\Delta S_m|$ with the $|\Delta a/a|$ and $|\Delta c/c|$ rather than volume change is not surprising.

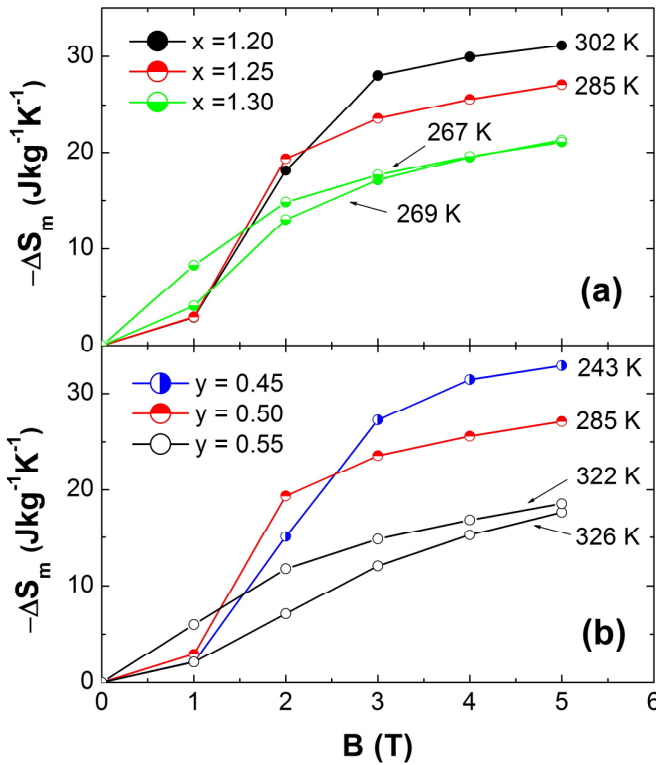


Figure 8.4. Magnetic entropy change as a function of magnetic field for the (a) $\text{Mn}_x\text{Fe}_{1.95-x}\text{P}_{0.50}\text{Si}_{0.50}$ and (b) $\text{Mn}_{1.25}\text{Fe}_{0.70}\text{P}_{1-y}\text{Si}_y$ compounds near the transition temperatures derived from the magnetic isotherms which were measured in increasing field from the paramagnetic state in the vicinity of the transition temperatures.

8.5. Critical magnetic field for field-induced transition

An incomplete field-induced transition gives a weak magnetocaloric effect because there is no phase transition for some part of sample. For magnetic refrigeration applications, the cooling power will be enhanced if complete field-induced transitions are exploited. Since magnetic refrigeration applications often use magnetic fields of less than 2 T produced from permanent magnet, they favor a low critical magnetic field in order to easily drive the field-induced transitions to completion. As mentioned above, the closer the temperature to T_C , the smaller the critical magnetic field. Thus, a

large magnetocaloric effect is always observed in the vicinity of T_C . In principle, the critical magnetic field is equal to zero for the field-induced transition at T_C and the maximal $|\Delta S_m|$ is also observed at T_C . However, if there is a distribution of T_{CS} , the critical magnetic field must be larger than a certain value in order to be able to drive the field-induced transition to completion (from para- to ferromagnetic phase) for the whole sample with different T_{CS} . The distribution of T_{CS} can arise from inhomogeneous composition. Besides, the sudden expansion and contraction of the crystal lattice can create constraints imposed by grain boundaries. Each grain is constrained by its neighbors, leading to the formation of a span of T_{CS} due to inhomogeneity of grain size and shape. The constraints are also obstacles for the first-order magnetic transition, resulting in an increase in the hysteresis. The distribution of T_{CS} leads to maximal intrinsic $|\Delta S_m|$ at the upper limit of the span of T_{CS} . Within the span of T_{CS} , the field-induced transitions are not complete because they start from the mixed ferro- and paramagnetic states. The ΔS_m derived from magnetic isotherms using the Maxwell relations should be calculated with great care within the span of T_{CS} [16].

The composition homogeneity can be improved by changes in preparation technique or heat treatment [17]. Introducing porosity is a possibility for reducing the constraints due to partial removal of the grain boundaries [18-20]. Porous materials should preferably consist of single-crystalline particles with uniform size distribution that will sharpen the transition and enhance the magnetocaloric effect [19]. The porous architecture also improves mechanical properties of the materials and leads to a considerable reduction in hysteresis. The hysteresis reduction has recently been observed by Lyubina *et al.* [19] in porous La(Fe,Si)₁₃ alloys. Sasso *et al.* [20] also found in Ni₅₅Mn₂₀Ga₂₅ metallic foams that the porous structure reduces the temperature span of the phase transition and increases the magnetocaloric effect.

In the present study, maximal $|\Delta S_m|$ for the $x = 1.30$ (see Figure 8.2a) and $y = 0.55$ (see Figure 8.2b) samples with very small hysteresis is estimated to be about $15 \text{ Jkg}^{-1}\text{K}^{-1}$ and $12 \text{ Jkg}^{-1}\text{K}^{-1}$ at 267 K and 322 K, respectively, for a field change of 0-2 T. The magnetic field of 2 T seems to be high enough to drive the field-induced transition to completion (see Figure 8.4). The magnetocaloric effect of these samples can still be

further enhanced to achieve high cooling power for a magnetic field change of less than 2 T that may be generated by a permanent magnet assembly [21].

8.6. Role of *p*-electron element

As was shown in Chapter 5, the magneto-elastic phase transition with large change in c/a results in a strong change in the position of the (300) and (002) diffraction peaks. Comparing the thermal evolution of these peaks may shed some light on the similarities and differences of MnFe(P,X) compounds.

Figure 8.5 shows x-ray diffraction patterns at different temperatures for MnFeP_{0.50}As_{0.50}, Mn_{1.20}Fe_{0.80}P_{0.75}Ge_{0.25} and Mn_{1.25}Fe_{0.70}P_{0.50}Si_{0.50} that all display a small hysteresis ($\Delta T_{\text{hys}} = 1\text{-}2$ K) and T_C near room temperature. The As- and Ge-containing compounds were prepared as described previously [6,22]. We find that the shift of the Bragg peaks (300) and (002) from high to low temperature for the Ge- and Si-containing compounds is stronger than that for the As-containing compound. Because the position of these peaks reflects the size of the lattice parameters, the observed peak shifts indicate that the differences of the lattice parameters at low and high temperature for the Ge- and Si-containing compounds are larger than those for the As-containing compound. For the compounds displaying a small hysteresis as seen in Figure 8.5, there are only small discontinuous changes of the lattice parameters at T_C . The Ge- and Si-containing compounds therefore exhibit large continuous changes of the lattice parameters at temperatures below and above T_C .

The Mn:Fe ratio of the As-containing compound is the smallest compared with the Ge- and Si-containing compounds. As shown in Chapter 7, the differences of the lattice parameters at high and low temperature would even be larger for the Si-containing compound if it had the same Mn:Fe ratio as the As-containing compound. Then, reducing the Si content could result in very large discontinuous changes of the lattice parameters at T_C far exceeding the changes in the As-containing compounds. Since the ΔT_{hys} and the entropy change for a field change are found to be correlated with the discontinuous changes of the lattice parameters, the above arguments explain why MnFe(P,Si) [23] can exhibit a very large ΔT_{hys} (up to 35 K) and, simultaneously, reach

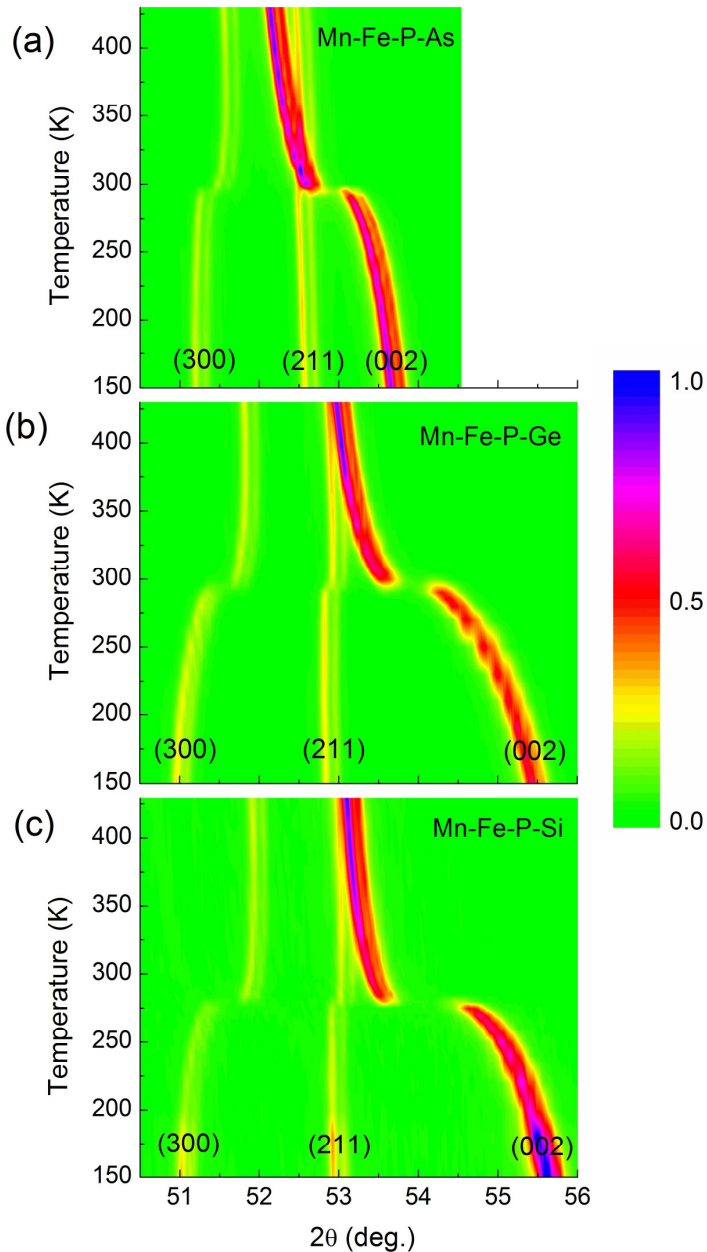


Figure 8.5. Contour plots of the x-ray diffraction patterns for (a) $\text{MnFeP}_{0.50}\text{As}_{0.50}$ ($\Delta T_{\text{hys}} = 1$ K), (b) $\text{Mn}_{1.20}\text{Fe}_{0.80}\text{P}_{0.75}\text{Ge}_{0.25}$ ($\Delta T_{\text{hys}} = 1$ K) and (c) $\text{Mn}_{1.25}\text{Fe}_{0.70}\text{P}_{0.50}\text{Si}_{0.50}$ ($\Delta T_{\text{hys}} = 2$ K) measured in zero field upon heating. Only a small range of 2θ is shown for clarity. The bar on the right represents the normalized intensity scale.

larger magnetocaloric effects than MnFe(P,As) [22]. Those arguments may still hold for the Ge-containing compound because MnFe(P,Ge) can also display a very large ΔT_{hys} (up to 20 K) [24].

The much larger effect found for Ge and Si strongly indicates that not the size of the p -electron atom but the number of valence electrons is the important parameter. Replacing P with elements with fewer valence electrons may induce strong modifications of the magnetic and structural properties, leading to a strong magneto-elastic coupling and a giant magnetocaloric effect.

8.7. Conclusions

In summary, a giant magneto-elastic coupling modified by changing chemical composition has been observed in the hexagonal Mn-Fe-P-Si compounds. The correlation of the hysteresis and the $|\Delta S_m|$ with the $|\Delta a/a|$ and $|\Delta c/c|$ is also evidence for the magneto-elastic coupling in which a large change of the lattice parameters strongly modifies the magnetic properties and vice versa. Reducing the hysteresis leads to a decrease in the $|\Delta S_m|$, but small hysteresis can be achieved without losing the giant magnetocaloric effect. A preliminary comparison between Mn-Fe-P-X (X = As, Ge, Si) compounds shows that Si and Ge can result in strong modifications of the magnetic and structural properties rather than As. Therefore, replacing P with elements with fewer valence electrons may lead to a strong magneto-elastic coupling and a giant magnetocaloric effect.

References

- [1] E. Brück, in *Handbook of Magnetic Materials*, edited by K. H. J. Buschow (Elsevier, Amsterdam, 2007), Vol. 17, pp. 235.
- [2] O. Tegus, E. Brück, K. H. J. Buschow, and F. R. de Boer, *Nature* **415**, 150 (2002).
- [3] K. A. Gschneidner, V. K. Pecharsky, and A. O. Tsokol, *Rep. Prog. Phys.* **68**, 1479 (2005).
- [4] N. H. Dung, L. Zhang, Z. Q. Ou, and E. Brück, *Appl. Phys. Lett.* **99**, 092511 (2011).
- [5] A. M. Tishin and Y. I. Spichkin, *The magnetocaloric effect and its applications* (Institute of Physics Publishing, Bristol, 2003).

- [6] N. T. Trung, Z. Q. Ou, T. J. Gortenmulder, O. Tegus, K. H. J. Buschow, and E. Brück, *Appl. Phys. Lett.* **94**, 102513 (2009).
- [7] N. H. Dung, Z. Q. Ou, L. Caron, L. Zhang, D. T. Cam Thanh, G. A. de Wijs, R. A. de Groot, K. H. J. Buschow, and E. Brück, *Adv. Energy Mater.* **1**, 1215 (2011).
- [8] A. N. Vasil'ev, A. D. Bozhko, V. V. Khovailo, I. E. Dikshtein, V. G. Shavrov, V. D. Buchelnikov, M. Matsumoto, S. Suzuki, T. Takagi, and J. Tani, *Phys. Rev. B* **59**, 1113 (1999).
- [9] S. Lee, A. Pirogov, M. Kang, K.-H. Jang, M. Yonemura, T. Kamiyama, S.-W. Cheong, F. Gozzo, N. Shin, H. Kimura, Y. Noda, and J.-G. Park, *Nature* **451**, 805 (2008).
- [10] A. Barcza, Z. Gercsi, K. S. Knight, and K. G. Sandeman, *Phys. Rev. Lett.* **104**, 247202 (2010).
- [11] A. K. Pathak, P. Basnyat, I. Dubenko, S. Stadler, and N. Ali, *J. Appl. Phys.* **106**, 063917 (2009).
- [12] N. H. Dung, L. Zhang, Z. Q. Ou, L. Zhao, L. van Eijck, A. Mulders, M. Avdeev, E. Suard, N. H. van Dijk, and E. Brück, *Phys. Rev. B* **86**, 045134 (2012).
- [13] See <http://www.ill.eu/sites/fullprof/index.html>
- [14] L. Caron, Z. Q. Ou, T. T. Nguyen, D. T. Cam Thanh, O. Tegus, and E. Brück, *J. Magn. Magn. Mater.* **321**, 3559 (2009).
- [15] K. A. Gschneidner, Y. Mudryk, and V. K. Pecharsky, *Scripta Mater.* **67**, 572 (2012).
- [16] G. J. Liu, R. Sun, J. Shen, B. Gao, H. W. Zhang, F. X. Hu, and B. G. Shen, *Appl. Phys. Lett.* **90**, 032507 (2007).
- [17] D. M. Liu, Q. Z. Huang, M. Yue, J. W. Lynn, L. J. Liu, Y. Chen, Z. H. Wu, and J. X. Zhang, *Phys. Rev. B* **80**, 174415 (2009).
- [18] M. Chmielus, X. X. Zhang, C. Witherspoon, D. C. Dunand, and P. Mullner, *Nat. Mater.* **8**, 863 (2009).
- [19] J. Lyubina, R. Schafer, N. Martin, L. Schultz, and O. Gutfleisch, *Adv. Mater.* **22**, 3735 (2010).
- [20] C. P. Sasso, P. Q. Zheng, V. Basso, P. Mullner, and D. C. Dunand, *Intermetallics* **19**, 952 (2011).
- [21] K. K. Nielsen, R. Bjoerk, J. B. Jensen, C. R. H Bahl, N. Pryds, A. Smith, A. Nordentoft, and J. Hattel, arXiv:0902.0812v1 [cond-mat.mtrl-sci] (2009).
- [22] O. Tegus, E. Brück, L. Zhang, W. Dagula, K. H. J. Buschow, and F. R. de Boer, *Physica B* **319**, 174 (2002).

-
- [23] D. T. C. Thanh, E. Brück, N. T. Trung, J. C. P. Klaasse, K. H. J. Buschow, Z. Q. Ou, O. Tegus, and L. Caron, *J. Appl. Phys.* **103**, 07B318 (2008).
- [24] N. T. Trung, *First-order phase transitions and giant magnetocaloric effect*, Delft University of Technology (2010), PhD thesis, Chapter 4.

SUMMARY

In this thesis, optimized magnetocaloric effects and related physical properties of hexagonal Mn-Fe-P-Si compounds are presented.

By varying the Mn:Fe and P:Si ratios, a giant magnetocaloric effect and a small thermal hysteresis in Mn-Fe-P-Si compounds of hexagonal Fe₂P-type structure have been achieved simultaneously. We demonstrate that the operating temperature can be controlled between 220 and 320 K by concurrently changing the Mn:Fe and P:Si ratios. The combination of several alloys with slightly different compositions in one active magnetic regenerator will allow for efficient magnetic refrigeration with large temperature span. The fact that we use materials that are not only globally-abundant and non-toxic but also able to be industrially-mass-produced via a simple powder-metallurgical method makes Mn-Fe-P-Si compounds particularly attractive. The discovery of these high-performance low-cost magnetic refrigerants paves the way for commercialization of magnetic refrigeration. (*Chapter 4*)

Varying the Mn:Fe ratio of the (Mn,Fe)_{1.95}P_{0.50}Si_{0.50} compounds makes a first-order magneto-elastic transition change into a first-order magneto-structural transition through a second-order isostructural magnetic transition. The preference of the hexagonal Fe₂P-type structure for the ferromagnetic order and a strong coupling between the crystal and magnetic structure have also been observed. Although the first-order magneto-structural transition produces a weak magnetocaloric effect, the existence of the first-order magneto-structural transition with the re-entrant hexagonal structure is very interesting for further study on exchange coupling in Fe₂P-based materials. Moreover, a small hysteresis and a giant magnetocaloric effect, which are

favorable for real magnetic refrigeration applications, can be achieved when the magnetic transition is controlled to be close to the border separating the first-order and second-order transition regimes. (*Chapter 5*)

Combining magnetic moments derived from low-temperature magnetization and neutron diffraction measurements, we show that the substitution of Fe with Mn on the 3*f* sites does not cause a change in the Mn(3*g*) magnetic moments but results in a linear decrease in the magnitude of the Fe/Mn(3*f*) magnetic moments. Consequently, the total moment is linearly reduced with increasing the Mn:Fe ratio. (*Chapter 6*)

A general physical picture of the evolution of the magnetic moments is given for the Mn-rich hexagonal Mn-Fe-P-Si compounds with first-order magneto-elastic transition. Using neutron diffraction, we observe a reduction of the magnetic moments with increasing temperature below the transition temperature. The sudden change in the interatomic distances at the point of transition validates our description of high/low-moment phase transition which leads to the deviation from the Rhodes-Wohlfarth plot. The formation and gradual development of the magnetic moment on the 3*f* sites upon cooling give rise to anomalous thermal expansion in the paramagnetic state. By exploiting high-temperature magnetic-susceptibility measurement, we demonstrate the difference of the magnitude of the magnetic moments at low and high temperatures. This work also reveals the role of short-range magnetic order in the development of the first-order magneto-elastic transition. These results support our proposal that the competition between the moments and chemical bonding is at the core of giant magnetocaloric effect displayed in the class of hexagonal Fe₂P-based materials with first-order magneto-elastic transition. (*Chapter 6*)

Concerning the effects of P:Si ratio on the magnetic and structural properties, the replacement of P by Si brings the first-order transition close to the border with second-order transition, leading to a small hysteresis. We also indicated that the difference of the lattice parameters at low and high temperature and the total magnetic moment are independent of Si content. The reduction of *c/a* caused by the Si addition is proposed to contribute to the increase in transition temperature via increased Mn(3*g*)-Fe/Mn(3*f*)

interlayer exchange coupling. We suggest that for the determination of the transition temperature chemical bonding also needs to be taken into account. (*Chapter 7*)

A giant magneto-elastic coupling modified by changing chemical composition was observed in the hexagonal Mn-Fe-P-Si compounds. The correlation of the hysteresis and the entropy change with the discontinuous change of the lattice parameters at the point of the first-order transition is also evidence for the magneto-elastic coupling in which a large change of the lattice parameters strongly modifies the magnetic properties and vice versa. Reducing the hysteresis leads to a decrease in the entropy change but small hysteresis can be achieved without losing the giant magnetocaloric effect. A preliminary comparison between Mn-Fe-P-X ($X = \text{As, Ge, Si}$) compounds shows that Si and Ge can result in strong modifications in magnetic and structural properties rather than As. Replacing P with elements with fewer valence electrons may lead to a strong magneto-elastic coupling and a giant magnetocaloric effect. (*Chapter 8*)

SAMENVATTING

In dit proefschrift worden geoptimaliseerde magnetocalorische effecten en daarmee verband houdende fysische eigenschappen van hexagonale Mn-Fe-P-Si verbindingen gepresenteerd.

Door de verhoudingen Mn:Fe en P:Si te variëren, zijn tegelijkertijd een reuze magnetocalorisch effect en een kleine thermische hysteresis in Mn-Fe-P-Si verbindingen met de hexagonale structuur van het Fe₂P-type bereikt. Wij tonen aan, dat de werktemperatuur ingesteld kan worden tussen 220 en 320 K door gelijktijdig de Mn:Fe en P:Si verhoudingen te variëren. Combinatie van verscheidene legeringen met enigszins verschillende samenstelling tot één actieve magnetische regenerator zal efficiënte magnetische koeling over een groot temperatuurbereik mogelijk maken. Het feit dat wij materialen gebruiken, die niet alleen wereldwijd overvloedig voorradig en niet giftig zijn maar ook grootschalig industrieel geproduceerd kunnen worden via een eenvoudige poeder-metallurgische methode maakt Mn-Fe-P-Si verbindingen bijzonder aantrekkelijk. De ontdekking van deze magnetische koelmiddelen met hoge prestatie en lage kosten paveit de weg naar commercialisering van magnetische koeling. *(Hoofdstuk 4)*

Variatie van de Mn:Fe verhouding in (Mn,Fe)_{1.95}P_{0.50}Si_{0.50} verbindingen verandert een eerste-orde magneto-elastische overgang in een eerste-orde magneto-structurele overgang via tweede-orde isostructurele magnetische overgang. Voorkeur van de hexagonale structuur van het Fe₂P-type voor ferromagnetische ordening en een sterke koppeling tussen de kristal- and magnetische structuur zijn eveneens waargenomen. Hoewel de eerste-orde magneto-structurele overgang een zwak magnetocalorisch effect

produceert, is het bestaan van de eerste-orde magneto-structurele overgang met de terugkerende hexagonale structuur erg interessant voor nadere studie van de exchange koppeling in materialen gebaseerd op Fe_2P . Bovendien kunnen een kleine hysteresis en een reuze magnetocalorisch effect, die gunstig zijn voor toepassing van magnetische koeling in de praktijk, bereikt worden, als de magnetische overgang dicht bij de grens tussen het eerste-orde en het tweede-orde overgangsregime wordt ingesteld. (*Hoofdstuk 5*)

Door de magnetische momenten afgeleid uit de magnetisatie bij lage temperatuur en metingen van neutronendiffractie te combineren, laten wij zien, dat de substitutie van Fe door Mn op de $3f$ sites geen verandering veroorzaakt in de Mn($3g$) magnetische momenten maar resulteert in een lineaire afname in de grootte van de Fe/Mn($3f$) magnetische momenten. Dientengevolge wordt het totale moment lineair gereduceerd met de Mn:Fe verhouding. (*Hoofdstuk 6*)

Een algemeen fysisch beeld van de evolutie van de magnetische momenten wordt gegeven voor de Mn-rijke hexagonale Mn-Fe-P-Si verbindingen met een eerste-orde magneto-elastische overgang. Met behulp van neutronendiffractie nemen wij een reductie waar van de magnetische momenten bij toenemende temperatuur beneden de overgangstemperatuur. De plotselinge verandering in de inter-atomaire afstanden op het overgangspunt bevestigt onze beschrijving van de faseovergang tussen laag en hoog magnetisch moment, die leidt tot de afwijking van de Rhodes-Wohlfarth plot. De vorming en de geleidelijke ontwikkeling van het magnetisch moment op de $3f$ sites bij koeling leidt tot een anomale thermische expansie in de paramagnetische toestand. Door gebruik te maken van de meting van de magnetische susceptibiliteit bij hoge temperatuur, tonen wij het verschil aan in de grootte van de magnetische momenten bij lage en hoge temperatuur. Dit werk onthult ook de rol van korte-drachts magnetische ordening in de ontwikkeling van de eerste-orde magneto-elastische overgang. Deze resultaten ondersteunen ons voorstel dat de competitie tussen de momenten en chemische binding de kern vormt van het reuze magnetocalorisch effect, zoals vertoond in de klasse van hexagonale materialen op Fe_2P -basis met een eerste-orde magneto-elastische overgang. (*Hoofdstuk 6*)

Wat betreft de effecten van de P:Si verhouding op de magnetische en structuureigenschappen, brengt de vervanging van P door Si de eerste-orde overgang dicht bij de grens met de tweede-orde overgang, wat leidt tot een kleine hysteresis. Wij vinden ook dat het verschil tussen de roosterparameters bij lage and hoge temperatuur en het totale magnetisch moment niet afhankelijk zijn van de hoeveelheid Si. De verkleining van de verhouding c/a , veroorzaakt door de toevoeging van Si wordt voorgesteld als bijdrage tot de verhoging van de overgangstemperatuur via een toename van de exchange koppeling tussen de Mn(3g) en Fe/Mn(3f) lagen. Wij suggereren dat chemische binding ook in rekening gebracht moet worden bij de bepaling van de overgangstemperatuur. (*Hoofdstuk 7*)

Een reuze magneto-elastische koppeling gemodificeerd door verandering in chemische samenstelling werd waargenomen in hexagonale Mn-Fe-P-Si verbindingen. De correlatie van de hysteresis en de entropieverandering met de discontinue verandering van de roosterparameters op het punt van de eerste-orde overgang is ook een bewijs voor de magneto-elastische koppeling, waar een grote verandering van de roosterparameters de magnetische eigenschappen sterk wijzigt en vice versa. Reduceren van de hysteresis leidt tot een afname in de entropieverandering, maar een kleine hysteresis kan bereikt worden zonder het reuze magnetocalorisch effect te verliezen. Een voorlopige vergelijking tussen Mn-Fe-P-X (X = As, Ge, Si) verbindingen laat zien dat Si and Ge, eerder dan As, kunnen resulteren in sterke wijzigingen in magnetische and structuur- eigenschappen. Substitutie van P door elementen met minder valentie-electronen kan leiden tot een sterke magneto-elastische koppeling en een reuze magnetocalorisch effect. (*Hoofdstuk 8*)

LIST OF PUBLICATIONS

Publications related to the work presented in this thesis:

1. **N. H. Dung**, Z. Q. Ou, L. Caron, L. Zhang, D. T. Cam Thanh, G. A. de Wijs, R. A. de Groot, K. H. J. Buschow, and E. Brück
Mixed magnetism for refrigeration and energy conversion
Adv. Energy Mater. **1**, 1215 (2011) (Chapters 2 and 4)
2. **N. H. Dung**, L. Zhang, Z. Q. Ou, and E. Brück
From first-order magneto-elastic to magneto-structural transition in $(\text{Mn,Fe})_{1.95}\text{P}_{0.50}\text{Si}_{0.50}$ compounds
Appl. Phys. Lett. **99**, 092511 (2011) (Chapter 5)
3. **N. H. Dung**, L. Zhang, Z. Q. Ou, L. Zhao, L. van Eijck, A. Mulders, M. Avdeev, E. Suard, N. H. van Dijk, and E. Brück
High/low-moment phase transition in hexagonal Mn-Fe-P-Si compounds
Phys. Rev. B **86**, 045134 (2012) (Chapter 6)
4. **N. H. Dung**, L. Zhang, Z. Q. Ou, N. T. Trung, and E. Brück
Effects of P:Si ratio on the magnetic and structural properties of hexagonal Mn-Fe-P-Si compounds
In preparation (Chapters 7 and 8)
5. **N. H. Dung**, L. Zhang, Z. Q. Ou, and E. Brück
Magneto-elastic coupling and magnetocaloric effect in hexagonal Mn-Fe-P-Si compounds
Scripta Mater. **67**, 975 (2012) (Chapter 8)

Other publications

1. Z. Q. Ou, L. Zhang, **N. H. Dung**, L. van Eijck, M. Avdeev, A. Mulders, N. H. van Dijk, and E. Brück
Neutron diffraction study on the magnetic structure of $(\text{Mn,Fe})_{1.95}\text{P}_{1-x}\text{Si}_x$ compounds
In preparation
2. L. Caron, M. Hudl, V. Höglin, **N. H. Dung**, C. P. Gomez, M. Sahlberg, E. Brück, Y. Andersson, and P. Nordblad
Magnetocrystalline anisotropy and the magnetocaloric effect in Fe_2P
To be submitted
3. Z. Q. Ou, L. Caron, **N. H. Dung**, L. Zhang, and E. Brück
Interstitial boron in $\text{MnFe}(\text{P,As})$ giant-magnetocaloric alloy
Res. Phys. **2**, 110 (2012)
4. **N. H. Dung**, N. P. Thuy, N. A. Tuan, N. T. Long, and N. N. Phuoc
Out-of-plane exchange bias and magnetic anisotropy in MnPd/Co multilayers
J. Magn. Magn. Mater. **320**, 3334 (2008)

Patent

1. Reesink Bennie, Brueck Ekkehard, **Nguyen Huu Dung**, and Zhang Lian
Magnetocaloric materials
US patent, No. 20110167837 (2011)

CURRICULUM VITAE

Nguyễn Hữu Dũng (pronounced *Zung*) was born in 1983 in Thai Binh, Vietnam. He studied in a Honors program of Hanoi National University of Education and received his BSc degree in Physics in 2005.



In the same year, he followed a Master program at the International Training Institute for Materials Science (ITIMS), Hanoi University of Technology where he started working on magnetic materials and magnetism under the supervision of the late Prof. Nguyễn Phú Thùỵ. He got his MSc degree in Materials Science in 2007.

In late 2008, he was employed by the Dutch Foundation for Fundamental Research on Matter (FOM) as a PhD student. He has spent 4 years of PhD working on magnetocaloric materials under the guidance of Prof. Ekkes Brück at Delft University of Technology. His PhD project aimed at searching for and optimizing novel magnetocaloric materials in bulk form for refrigeration applications at room temperature. The outstanding results from his PhD research are presented in this thesis and in a number of publications.

Recently, he has secured a post-doc position in the Micro and Nano Magnetism group at the Institut Néel of CNRS Grenoble (starting January 2013). He will work with Dr. Nora Dempsey on developing magnetocaloric materials in thin-film form, in the framework of a new EU project.



ISBN/EAN: 978-94-6186-081-1